



UNIVERSITY OF  
HOHENHEIM

Faculty of Agricultural Sciences  
Institute of Agricultural Engineering  
Technology in Crop Production (440d)

**Prof. Dr. Hans W. Griepentrog**

## **Modelling and optimisation of no-till seeder dynamics for precise seeding depth**

Dissertation

Submitted in fulfilment of the regulations to acquire the degree

“Doktor der Agrarwissenschaften”

(Dr. sc. agr. in Agricultural Sciences)

to the

Faculty of Agricultural Sciences

Submitted by: **M.Sc. Galibjon M. Sharipov**

Born in: Uzbekistan

Year of publication: 2019

This thesis was accepted as a doctoral thesis (Dissertation) in fulfillment of the regulations to acquire the degree “Doktor der Agrarwissenschaften” (Dr.sc.agr. in Agricultural Sciences) by the Faculty of Agricultural Sciences at University of Hohenheim on 24.09.2018.

Date of oral examination: 14. December 2018

### **Examination Committee**

Head of the Committee: Prof. Dr. Jörn Bennewitz  
Reviewer and 1st Examiner: Prof. Dr. Hans W. Griepentrog  
Co-reviewer: Assoc. Prof. Dr. Sulaymon Eshkabilov  
2nd Examiner: Prof. Dr.-Ing. Stefan Böttinger  
3rd Examiner: Prof. Dr. Enno Bahrs

TIMUR project coordinator: Assoc. Prof. Dr. Alim Pulatov

All rights reserved. The use of texts and pictures, even in part, without the consent of the author is punishable under copyright law. This applies especially to reproduction, translation, microfilming and storage, and processing in electronic systems.

© 2019

Self-publishing: Galibjon M. Sharipov  
Source of supply: Institute of Agricultural Engineering of  
the University of Hohenheim  
Garbenstraße 9, 70599 Stuttgart

## Acknowledgments

Completion of this doctoral dissertation was possible with the valuable support and help of several organizations and individuals who I would like to express my sincere gratitude to.

First and foremost, I would like to express my sincere gratitude to Prof. Dr. Hans. W. Griepentrog for accepting me as a doctoral student in the first place and giving me the opportunity to work under his supervision on such an appealing research topic. He was always willing to provide enthusiastic assistance and solutions to the problems throughout the project. His brilliant guidance on both academic and technical matters has been very crucial for the success of the project.

Second, I am hugely indebted to my colleague Dr. Dimitris S. Paraforos for his invaluable co-supervision from the beginning to the end of the project. He was always present to provide his inestimable help in conducting experiments, processing data and representing the results. I sincerely thank him for his time and efforts during the process of paper writing. Furthermore, I would like to express my gratitude to Prof. Dr.-Ing. Stefan Böttinger from the University of Hohenheim for accepting to be in the examining committee of my dissertation and for his valuable comments.

I would like to gratefully acknowledge the financial support of Erasmus Mundus Action 2 TIMUR (Training of Individuals through Mobility to EU from the Uzbek Republic) and I am thankful to the coordinators of the project, Alim Pulatov, Ewa Wietsma and Anna Voitenko for their support and good collaborations. Furthermore, it was a pleasure to collaborate with the AMAZONEN-WERKE H. Dreyer GmbH & Co.KG. In particular, I am grateful to Dr. R. Resch and Ch. Gall for providing the seeding machine and assisting during the field experiments.

My sincere thanks also go to other fellow doctoral students and senior colleagues at the section of Technology in Crop Production for their support, motivation, and providing a stimulating and fun-filled environment. Furthermore, the contribution of our section's secretary Karin Haack and Helga Floto and technicians Cristian Schwarze and Gianluca Bersi is gratefully acknowledged. I would also like to extend my thanks my dear friends at IT Training centre in Tashkent.

Last but not the least; I would like to thank my parents and sisters for their endless support, encouragement and guidance. My dear parents, thank you for believing in me and supporting me throughout my work. I am also deeply thankful to my wife, Manzura and my adorable daughter, Dilnura and my son, Otajon for their enduring support, patience and love. They encouraged and motivated me to get all the endeavours possible.

Galibjon Sharipov

Stuttgart-Hohenheim, February 2019

# Contents

<b>1</b>	<b>Introduction</b> .....	1
1.1	Problem definition and working quality of no-till seeders.....	1
1.2	Seeder performance as seeding depth and dynamic response.....	3
1.3	Optimisation of seeder performance for better seed placement.....	3
1.4	Aim and objectives.....	4
1.5	Appended papers.....	5
	References.....	6
<b>2</b>	<b>Dynamic performance of a no-till seeding assembly</b> .....	9
2.1	Introduction .....	11
2.2	Materials and Methods .....	13
2.2.1	Instrumentation and data acquisition.....	13
2.2.2	Validation of the profile sensing system .....	15
2.2.3	Experiments.....	16
2.3	Theory .....	20
2.3.1	Strain to force .....	20
2.3.2	Field surface profile determination.....	22
2.3.3	Correlation between the seeding depth variation and the developed forces.....	23
2.4	Results and discussion.....	24
2.4.1	Validation of the profile sensing system .....	24
2.4.2	Surface profiles with seed positions and the developed forces .....	25
2.4.3	Seeding depth variation .....	26
2.4.4	The effect of forces on the seeding depth variation.....	28
2.5	Conclusions .....	30
	Acknowledgement .....	31
	References.....	31
<b>3</b>	<b>Modelling and simulation of the dynamic performance of a no-till seeding assembly with a semi-active damper</b> .....	35
3.1	Introduction .....	36
3.2	Materials and Methods .....	38
3.2.1	Equipment and Sensors .....	38
3.2.2	Experiments.....	39



3.3	Modelling and control .....	40
3.3.1	Coulter assembly dynamics model .....	40
3.3.2	Validation of the coulter assembly dynamics developed model.....	42
3.3.3	Modelling of the semi-active MR damper system.....	45
3.3.4	Control design for the semi-active MR damper system .....	46
3.3.5	Simulation of the semi-active MR damper models .....	48
3.3.6	Performance criteria.....	50
3.4	Results and discussion .....	50
3.4.1	Assessment of the simulation model validity .....	50
3.4.2	Performance of the semi-active MR damper with the applied hysteresis models .....	52
3.5	Conclusions .....	56
	Acknowledgement .....	56
	References.....	57
<b>4</b>	<b>Implementation of a magnetorheological damper on a no-till seeding assembly for optimising seeding depth .....</b>	<b>59</b>
4.1	Introduction .....	61
4.2	Materials and Methods .....	63
4.2.1	Developed no-till seeding prototype.....	63
4.2.2	Semi-active MR damper specifications .....	65
4.2.3	Validation of the surface profile sensing system .....	66
4.2.4	Experiments .....	66
4.3	Theory.....	69
4.3.1	Determination of forces and surface profiles.....	69
4.3.2	Dynamics assessment criteria .....	72
4.4	Results and discussion .....	72
4.4.1	Profile sensing system validation .....	72
4.4.2	Performance of the seeding assemblies .....	73
4.4.3	Assessment of improvements in dynamics.....	78
4.4.4	Estimation of seeding depth variations.....	80
4.5	Conclusions .....	81
	Acknowledgements.....	82
	References.....	82
<b>5</b>	<b>General discussion .....</b>	<b>85</b>
5.1	Working quality of a no-till seeder .....	85
5.2	Simulating the dynamic response of a no-till seeder .....	86

5.3 The effect of the optimised seeder dynamics on seeding depth .....	87
5.4 Outlook .....	88
<b>Summary</b> .....	91
<b>Zusammenfassung</b> .....	93
<b>Curriculum Vitae</b> .....	95
<b>Author's declaration</b> .....	97

# CHAPTER 1

## Introduction

### 1.1 Problem definition and working quality of no-till seeders

No tillage or no-till seeding, as an essential aspect of conservation farming that has been gaining the greatest interest of farmers since the middle of 19<sup>th</sup> century (Derpsch et al., 2010), is a soil cultivation system in which seeds are deposited directly into untilled soil (Gattinger et al., 2011). In no-till seeding, a proper seeding depth is a very important factor that affects seed germination and seedling emergence and hence the seeding rate. As the seeding depth increases so does the energy the seed requires to reach the covered soil surface and, thus delaying and even reducing emergence rate. Conversely, a shallow depth cannot provide the necessary soil moisture for seeds to germinate. Both factors ultimately reduce proper crop growth and in general yields (Özmerzi et al., 2002).

Maintaining a consistent seeding depth is one of the most demanding tasks that no-till seeders must cope with (Baker et al., 2006). This task is very challenging due to the following reasons:

- Untilled soils are more compacted than tilled soils. This requires higher downforce in order to keep the seeding assembly on the ground for achieving the target seeding depth. However, the excessive downforce results in a higher variation of the seeding depth (Morrison, 1987) due to variations in hard soil resistance.
- Untilled soils show more surface undulations. This causes less cushioning and more bouncing effect in the vertical movement of the seeding assembly, especially at higher operating speeds.
- The existence of crop residues and stubble on untilled soil surface increases the difficulty in achieving a desired response of the seeding assembly to the untilled soil surface.

- High driving speeds during seeding due to timeliness of completing the seeding operation and reducing labour costs.

If the seeding assembly performance relies only on the downforce to penetrate the untilled soil, place the seed and pack it, then the seeding depth will vary as much as the variation in soil resistance and strength (Nielsen et al., 2016). Based on manufacturer's recommendations, both the downforce applied to the seeding assembly and the seeding depth are manually set once by the operator (Weatherly and Bowers, 1997; Nielsen et al., 2018) and these are kept constant during seeding operation. However, there is a necessity to consider the field heterogeneity, in terms of surface undulations and mass of crop residue, and variations in soil resistance, while performing seeding operation in order to achieve better seed placement.

The need to conduct research on optimising no-till seeder performance for better seed placement can be seen by the limited number of previously carried out studies that are found in the literature. The advent of no tillage inspired Morrison and Abrams (1972) to carry out thorough research on assessing the performance of no-till seeders and optimising their dynamics for better seeding depth. In their earliest study, they investigated a variety of no-till seeder performance regarding seeding depth and its effects on seed germination and plant emergence. Later, they proceeded with improving the dynamics of those seeders by optimising components like gauge wheels, seeding mechanism and coulters (Morrison and Abrams, 1978; Morrison, 1978), and by developing control techniques for seeding mechanisms (Morrison and Gerik, 1985; Morrison, 1988). Collins (1996) showed that seeding depth was highly affected by seeder dynamics characterised by the soil reaction forces (Loghin et al., 2012). In a recent work by Hasimu and Chen (2014) the effects of soil disturbance and the penetration forces arising at the soil-opener interface on seeding depth variation were examined in a soil bin.

Seeding depth is usually evaluated by measuring the length of seedlings between the seed and the soil surface (hypocotyl) and calculating mean and standard deviation; this is called ground truth seeding depth (Tessier et al., 1991; Burce et al., 2011). The challenge in this methodology is to assess accurately the correspondence between the seeder vertical motion dynamics and its performance, due to existence of stubble and crop residues as well as changes in soil surface until the seeds emerged. Many researchers have used this hypocotyl methodology as a reference in order to validate their proposed methodologies for measuring seeding depth (Suomi and Oksanen, 2015; Nielsen et al., 2018). In the present work, a new methodology for obtaining the absolute geo-referenced seeding depth was employed utilising the surface profile measured from the impact point of the packer wheel (Paraforos et al., 2016) and the georeferenced seed' positions.

## 1.2 Seeder performance as seeding depth and dynamic response

Performance of no-till seeder, in terms of seeding depth, is strongly affected by the dynamic response of the seeder to the soil condition, which is mostly introduced by the draught and vertical forces due to the coulter-soil interaction. Those forces and vertical movements of the seeding assembly, which are not fully regulated during an operation, cause an instability in the dynamic response of the seeder to the heterogeneous soil condition (Abo Al-Kheer et al., 2011; Loghin et al., 2012). The total resultant forces acting on the seeding assembly are usually defined by the vertical and horizontal forces (Chen et al., 2013), but also depend on how many components are involved in the soil-tool interaction. In case the seeding assembly contains a packer wheel as well, the ground impact forces should be necessarily considered when modelling the motion dynamics of the seeding assembly (Mouazen et al., 2004).

The amount of the disturbed soil and the draft and vertical forces acting on the opener significantly vary depending on the design and type of the openers (Baker et al., 2006). The opener width and rake angle are also considered as key characteristics of the openers considerably effecting on the seeding assembly dynamic behaviour (Collins and Fowler, 1996). Comparative studies carried out by Chaudhuri. (2001) shows that a hoe (tine) type openers creates more soil disturbance compared to other types of openers like single or doublé disc, chisel and shoe. However, the hoe type openers outperform the other types of openers, in terms of low soil reaction forces (draught and vertical) due to small rake angles.

A study of seeding machine dynamics and modelling of its motion behaviour dates from the late 1960's. Lawrance (1969) concluded that excessive vertical oscillations of a semi-mounted seeding implement resulted in undesired seeding depth, occurred due to the dynamic response of the implement to soil condition. More advanced research on defining the relationship between the dynamic response of the no-till seeder, surface undulations and depth variation was carried out by Mouazen et al. (2004), Saeys et al. (2004) and Zhao et al. (2013). Furthermore, the performance of a seeding machine relevant to the soil surface irregularities and operation speed is standardised by ISO standard 7256-2 (ISO, 1984). The ISO standard also specifies the testing methods of seeding machine dynamics for seed placement. With the aim to achieve consistency in the seeding depth, the seeder vertical motion dynamics and its responses to soil conditions should be examined.

## 1.3 Optimisation of seeder performance for better seed placement

Since the inadequate response of the seeder motion dynamics to harsh soil condition and to high driving speed is a crucial factor of extreme variations in the desired seeding depth, optimising the dynamics of no-till seeder for better performance is of high importance for seeding machine developers. Many techniques for optimising the dynamic response of no-till seeders and controlling the seed placement mechanism have been introduced in order to improve the accuracy in seeding depth (Loghin et al., 2012; Nielsen et al., 2018). One of the common methods is to regulate the applied downforce on the entire seeding assembly (Karayel and Šarauškus, 2011; Rui et al., 2016), however, in this method, advanced control cannot be achieved due to the non-linearity in compressing/depressing component (spring or rubber) (Gratton et al., 2003) and the complexity of the assembly design.

Defining the nature of the interaction between the soil and one single seeding assembly, can offer the means to optimise the entire seeder dynamics (Burce et al., 2013). The resulted forces from the interaction and the vertical displacements of the seeding assembly can be regulated by developing a control system that can dampen those forces resulting in optimised vertical movements. However, in-field experimental data from real-life measurements, which describe the dynamic behaviour of the seeding assembly and its responses to soil condition, like vertical accelerations, displacements, tilting and the forces of soil-engaging component, are unknown. These parameters should be obtained in order to be able to describe the relationship between the dynamics of the seeder and heterogeneous field condition. The soil conditions such as surface undulations, soil resistance and crop residue mass should also be acquired to define the seeder dynamic responses. With these data, the developers will be able to assess the dynamics of the seeder together with the corresponding seeding depth variation, and monitor the occurrence of the variation in the seeding depth. By simulating the dynamic response of the seeder to untilled soil condition (Shahgoli et al., 2010) using measured data as input, a control system for the seeding mechanism can be developed to reduce the vertical coulter dynamics and hence to offer higher evenness in the seeding depth.

#### **1.4 Aim and objectives**

The aim of this work is to optimise a no-till seeder dynamics in terms of vertical motion stability for better seed placement under realistic high capacity performance. In order to fulfil this aim, the following objectives should be accomplished:

- Field experiments with data acquisition for:
  - Seeder dynamics (relevant forces, vertical displacements and tilting).
  - Soil surface profile.

- Evenness of seeding depth.
- Evaluation of seeder dynamic performance (forces, displacements etc.) and working quality (seeding depth).
- Modelling and simulation of no-till seeder motion dynamics with a damping control system:
  - Modelling of the unmodified seeder motion behaviour.
  - Specifications of the damping control system for the actual seeding assembly.
  - Simulation of seeder motion dynamics with the specified damping control system.
- Development and implementation of the damping control system on the seeding assembly.
- Assessing of the modified seeder dynamic performances and the working quality.

## 1.5 Appended papers

The dissertation is based on the following papers:

- A. Sharipov, G.M., Paraforos, D.S., Pulatov, A., Griepentrog, H.W., (2017). Dynamic performance of a no-till seeding assembly. *Biosyst. Eng.* 158, 64–75. doi:10.1016/j.biosystemseng.2017.03.016.
- B. Sharipov, G.M., Paraforos, D.S., Griepentrog, H.W., (2017). Modelling and simulation of the dynamic performance of a no-till seeding assembly with a semi-active damper. *Comput. Electron. Agric.* 139, 187–197. doi:10.1016/j.compag.2017.05.010
- C. Sharipov, G.M., Paraforos, D.S., Griepentrog, H.W., 2018. Implementation of a magnetorheological damper on a no-till seeding assembly for optimising seeding depth. *Comput. Electron. Agric.* 150, 465–475. doi:10.1016/j.compag.2018.05.024

In Paper A, the developed sensor-frame for measuring the seeder dynamics together with the corresponding field surface profile and the new methodology for acquiring seed positions in absolute geo-referenced coordinates were represented. In this paper, the frequency content of the seeder dynamics and seeding depth variation was correlated to define the reason for the extreme variations in seeding depth. The mathematical modelling of the vertical motion dynamics of the no-till seeding assembly with the packer wheel as a passive system and with the semi-active magnetorheological (MR) damper system, and the simulation based on measured data were presented in Paper B. This paper also evaluated the improvement of the seeder dynamics resulting in better seed placements. In Paper C, a no-till seeder prototype was constructed consisting of an automatic seed dose mechanism and two seeding assemblies with and without a semi-active MR damper. The optimum parameters for the semi-active MR damper, for the seeding assembly to achieve its best performance, were

defined, and the performance of the seeder prototype in terms of seeding depth variation and the dynamics of both seeding assemblies (damped and undamped) was evaluated.

## References

- Abo Al-Kheer, A., Eid, M., Aoues, Y., El-Hami, A., Kharmanda, M.G., Mouazen, A.M., 2011. Theoretical analysis of the spatial variability in tillage forces for fatigue analysis of tillage machines. *J. Terramechanics* 48, 285–295. doi:10.1016/j.jterra.2011.05.002
- B. Collins, D.F., 1996. Effect of soil characteristics, seeding depth, operating speed, and opener design on draft force during direct seeding. *Soil Tillage Res.* 39, 199–211. doi:10.1016/S0167-1987(96)01062-8
- Baker, C.J., Saxton, K.E., Ritchie, W.R., Chamen, W.C.T., Reicosky, D.C., Ribeiro, F., Justice, S.E., Hobbs, P.R., Justice, F.R.S.E., 2006. No-tillage seeding in conservation agriculture, No-Tillage Seeding: *Science and Practice*. doi:10.1079/9781845931162.0000
- Burce, M.E., Kataoka, T., Okamoto, H., Shibata, Y., 2011. Precise Seed Placement Control System for Various Terrain Surfaces. *ASABE 7004*.
- Burce, M.E.C., Kataoka, T., Okamoto, H., 2013. Seeding Depth Regulation Controlled by Independent Furrow Openers for Zero Tillage Systems - Part 2: Control System of Independent Furrow Openers. *Eng. Agric. Environ. Food* 6, 13–19. doi:http://dx.doi.org/10.1016/S1881-8366(13)80012-2
- Chen, Y., Munkholm, L.J., Nyord, T., 2013. A discrete element model for soil–sweep interaction in three different soils. *Soil Tillage Res.* 126, 34–41. doi:10.1016/j.still.2012.08.008
- Chaudhuri, D., 2001. Performance Evaluation of Various Types of Furrow Openers on Seed Drills—a Review. *J. Agric. Eng. Res.* 79, 125–137. doi:10.1006/jaer.2000.0688
- Derpsch, R., Friedrich, T., Kassam, A., Hongwen, L., 2010. Current status of adoption of no-till farming in the world and some of its main benefits. *Int. J. Agric. Biol. Eng.* 3, 1–25. doi:10.3965/j.issn.1934-6344.2010.01.001-025
- Gattinger, A., Jawtusich, J., Müller, A., Mäder, P., 2011. No-till agriculture – a climate smart solution? *Misereor* 24.
- Gratton, J., Chen, Y., Tessier, S., 2003. Design of a spring-loaded downforce system for a no-till seed opener. *Can. Biosyst. Eng.* 45.
- Hasimu, A., Chen, Y., 2014. Soil disturbance and draft force of selected seed openers. *Soil Tillage Res.* 140, 48–54. doi:10.1016/j.still.2014.02.011
- ISO, 1984. “ISO 7256/2: Sowing equipment-Test methods- Seed drills for sowing in lines” 16.



- Karayel, D., Šarauskis, E., 2011. EFFECT OF DOWNFORCE ON THE PERFORMANCE OF NO-TILL DISC FURROW OPENERS FOR CLAY-LOAM AND LOAMY SOILS. *Agric. Eng. Res. Pap.* 43, 16–24.
- Lawrance, N.S., 1969. A method of Analyzing Dynamic Responses of A Semi-mounted Farm Implement. *The Ohio State University*.
- Loghin, F., Ene, T.A., Mocanu, V., Căpătină, I., 2012. Dynamic Modeling of Technical System Tractor - Seed Drill. *Agric. Food Eng.* 5 (54), 155–160.
- Morrison, J.E., 1988. Hydraulic Downpressure System Performance for Conservation Planting Machines 31, 19–23.
- Morrison, J.E., 1987. Interactive Planter Depth Control and Pneumatic Downpressure System. *Power Mach. Div. ASAE*.
- Morrison, J.E., 1978. No-Tillage Experimental Planter Performance and Depth Regulation Evaluation 3–6.
- Morrison, J.E., Abrams, C.F., 1978. Furrow opener and apparatus for no tillage planters. USA4090456.
- Morrison, J.E., Gerik, T.J., 1985. Planter Depth Control : II . Empirical Testing and Plant Responses. *Trans. ASAE* 28 (6), 1744–1748.
- Morrison J. E, Abrams C. F, 1972. Selecting no-tillage planters by need (*No. AEN-2*).
- Mouazen, a. M., Anthonis, J., Saeys, W., Ramon, H., 2004. An Automatic Depth Control System for Online Measurement of Spatial Variation in Soil Compaction, Part 1: Sensor Design for Measurement of Frame Height Variation from Soil Surface. *Biosyst. Eng.* 89, 139–150. doi:10.1016/j.biosystemseng.2004.06.005
- Nielsen, S.K., Munkholm, L.J., Lamandé, M., Nørremark, M., Edwards, G.T.C., Green, O., 2018. Seed drill depth control system for precision seeding. *Comput. Electron. Agric.* 144, 174–180. doi:10.1016/j.compag.2017.12.008
- Nielsen, S.K., Norremark, M., Green, O., 2016. Sensor and control for consistent seed drill coulter depth. *Comput. Electron. Agric.* 127, 690–698. doi:10.1016/j.compag.2016.07.029
- Özmerzi, A., Karayel, D., Topakci, M., 2002. Effect of Sowing Depth on Precision Seeder Uniformity. *Biosyst. Eng.* 82, 227–230. doi:10.1006/bioe.2002.0057
- Paraforos, D.S., Griepentrog, H.W., Vougioukas, S.G., 2016. Country road and field surface profiles acquisition, modelling and synthetic realisation for evaluating fatigue life of agricultural machinery. *J. Terramechanics* 63, 1–12. doi:10.1016/j.jterra.2015.10.001
- Rui, Z., Tao, C., Dandan, H., Dongxing, Z., Kehong, L., Xiaowei, Y., Yunxia, W., Xiantao, H., Li, Y., 2016. Design of depth-control planting unit with single-side gauge wheel for no-till maize

- precision planter. *Int J Agric Biol Eng* Open Access <http://www.ijabe.org> 9. doi:10.3965/j.ijabe.20160906.2394
- Saeys, W., Mouazen, a. M., Anthonis, J., Ramon, H., 2004. An Automatic Depth Control System for Online Measurement of Spatial Variation in Soil Compaction, Part 2: Modelling of the Depth Control System. *Biosyst. Eng.* 89, 267–280. doi:10.1016/j.biosystemseng.2004.06.009
- Shahgoli, G., Fielke, J., Saunders, C., Desbiolles, J., 2010. Simulation of the dynamic behaviour of a tractor-oscillating subsoiler system. *Biosyst. Eng.* 106, 147–155. doi:10.1016/j.biosystemseng.2010.03.002
- Suomi, P., Oksanen, T., 2015. Automatic working depth control for seed drill using ISO 11783 remote control messages. *Comput. Electron. Agric.* 116, 30–35. doi:10.1016/j.compag.2015.05.016
- Tessier, S., Hyde, G.M., Papendick, R.I., Saxton, K.E., 1991. No-till seeders effects on seed zone properties and wheat emergence. *Power Mach. Div. ASAE* 34, 733–739.
- Weatherly, E.T., Bowers, C.G., 1997. Automatic depth control of a seed planter based on soil drying front sensing. *Power Mach. Div. ASAE* 40, 295–305.
- Zhao, T., Zhao, Y., Nitta, Y., Yagioka, A., Komatsuzaki, M., 2013. Performance of a no-tillage seeder with different cover crop species and residue management for sweet sorghum for sustainable biofuel production. *Eng. Agric. Environ. Food* 6, 152–159. doi:10.1016/S1881-8366(13)80002-X

## CHAPTER 2

### Paper A

## Dynamic performance of a no-till seeding assembly<sup>1</sup>

Galibjon Sharipov, Dimitris S. Paraforos, Alim Pulatov, Hans W. Griepentrog

### Abstract

Precise seeding depth plays an important role in achieving reliable germination rate and even plant emergence. In no-till seeding, this aim is more challenging due to the inappropriate response of the machine dynamics to harsh soil conditions, such as compacted soil undulations and stubble. In this paper, a sensor-frame was mounted on a no-till seeder, to measure the field surface profiles during seeding operation. Its accuracy was validated by acquiring the profile of trapezoidal bumps with known dimensions resulting in a root mean squared (RMS) error of 7.3 and 8.7 mm for travelling speed of 2 km h<sup>-1</sup> and 10 km h<sup>-1</sup>, respectively. Strain gauges were used to measure the soil reaction forces, on one of the seeding assemblies during seeding operation at travelling speed of 10 km h<sup>-1</sup>. After seeding wheat (*triticum aestivum* L.), the geo-referenced position of each single seed was measured using a total station, to calculate the seeding depth. The correlation between the seeding depth variation and the developed forces showed that the frequencies of 11.8 Hz and 17.8 Hz of the vertical forces, which corresponded to a wavelength of 0.21 m and 0.14 m, respectively, were responsible for the high variation in seeding depth. For the profile impact forces, these values were equal to 10.7 Hz and 20.6 Hz. The corresponding wavelengths were equal to 0.23 m and 0.12 m. The peak value of seeding depth was detected at a frequency of 8.3 Hz with 0.3 m wavelength for both vertical and impact profile forces.

---

<sup>1</sup> The publication of Chapter 2 is done with the consent of the Elsevier Verlag. The original publication was in: Journal of Biosystems Engineering, Vol. 158, pp. 64 – 75. It can be found under the following link: <http://doi.org/10.1016/j.biosystemseng.2017.03.016>

**Keywords:** no-till seeder, seeding depth, soil surface profile, soil reaction forces

**Nomenclature**

$a$  horizontal distance between the attached point of strain gauges (assembly arm) and the action line of profile impact forces, m

$b$  horizontal distance between the attached point of strain gauges (assembly arm) and the action line of vertical forces, m

$c$  horizontal distance between the attached point of strain gauges (wheel shank) and the action line of profile impact forces, m

$d$  vertical distance between the attached point of strain gauges (chisel coulter of the assembly) and the action line of draft forces, m

$e$  vertical distance between the attached point of strain gauges (assembly arm) and the action line of draft forces, m

$E$  Young's modulus,  $\text{N m}^{-2}$

$F_d$  draft forces on the coulter, N

$F_v$  vertical forces on the coulter, N

$F_{sp}$  profile impact forces on the wheel, N

$g$  horizontal distance between the attached point of strain gauges (chisel coulter of the assembly) and the action line of profile impact forces, m

$h_j$  height of rectangular area at the attached point of strain gauges, m

$l_j$  width of rectangular area at the attached point of strain gauges, m

$k$  vertical distance between the attached point of strain gauges (wheel shank) and the action line of draft forces, m

$m$  horizontal distance between the attached point of strain gauges (wheel shank) and the action line of vertical forces, m

$M_j$  summation moments of forces at point  $j$  where strain gauges attached, N m

$n$  horizontal distance between the attached point of strain gauges (chisel coulter of the assembly) and the action line of vertical forces, m

$P_{FF}$  power spectrum density (PSD) function of the chosen force,  $\text{m N}^2$

$P_{Var}$  PSD function of seeding depth variation,  $\text{m}^3$

$P_{F,Var}$  cross spectrum density of the selected two data sets,  $\text{m}^4 \text{N}^2$

$R_{wheel}$  radius of the wheel, m

$T_p^a$  transformation matrix from the prism coordinate system to the seeding assembly coordinate system

$T_a^{pr}$  transformation matrix from the seeding assembly coordinate system to the ground impact point

$x_a, y_a, z_a$  coordinate system of the seeding assembly

$x_p, y_p, z_p$  coordinate system of the prism

$x_{pr}, y_{pr}, z_{pr}$  coordinate system of the ground impact point

$z_{el}$  measured elevation profile, m

$z_b$  measured bump profile, m

$W_{s,j}$  cross-sectional area at point  $j$ ,  $m^3$

$\alpha$  constant angle between the plate and the packer wheel shank, deg

$\gamma_{F,Var}$  coherence value

$\varepsilon_j$  measured strain at point  $j$

$\theta_1$  pitch angle of the seeding assembly, deg

$\theta_2$  pitch angle of the seeder main frame, deg

$\xi$  distance from the prism to the laser pointer, m

$q$  length of the plate, m

$\sigma_j$  stress at point  $j$ , Pa

$\chi$  distance detected by the laser pointer on the plate, m

$\psi$  length of the wheel shank, m

## 2.1 Introduction

No-till seeding demands a machine that interacts appropriately with harsh soil conditions like compacted soil and plant residues, with the purpose of placing seeds at the optimum depth, which will result in reliable seed germination and even plant emergence (Collins & Fowler, 1996). The seeds should not be too close to the soil surface, in order to avoid seed drying, but also not too deep because then the stored seed nutrients would be inadequate for germination (Özmerzi, Karayel, & Topakci, 2002). Since the seeding depth variation is considerably affected by the machine dynamic response to soil surface undulations, a significant improvement in direct seeding could be achieved by controlling seeding mechanism, regulating the impact of the compacted surface undulations, and optimising the machine dynamics.

The seeding depth does not only depend on the coulter model (Suomi & Oksanen, 2015), but also on the soil type, soil conditions, etc. Therefore, understanding the nature of the soil-machine

interaction, in terms of machine dynamic response to soil conditions, is crucial to define the reasons of extreme seeding depth variation (Liu, Chen, & Kushwaha, 2010). This interaction can be characterised by the resulting forces from the soil-tool interface (Chen, Munkholm, & Nyord, 2013). In addition, soil profile undulations and soil resistance, affected by soil physical properties, can be described by the soil reaction forces on the furrow opener, which in turn, influence the mean seeding depth across the seeder width (Fountas et al., 2013). The reaction forces on a furrow opener (e.g. a chisel coulter) can be expressed with its horizontal and vertical components (Abo Al-Kheer et al., 2011) and the responses of profile undulations to machine dynamics could be introduced by the developed forces (Loghin, Ene, Mocanu, & Căpătină, 2012). In this study, the total forces acting on the seeding assembly were determined by the vertical, horizontal, and profile impact forces, since the assembly contains an additional packer wheel for adjusting the seeding depth and for compacting the soil.

The furrow opener depth, which also specifies the seeding depth, is not constant even under laboratory conditions (Karayel & Özmerzi, 2008). Even when the seeding depth is manually adjusted by the operator, it is difficult for the machine to keep a precise depth during field operation, as the demand for operational efficiency is maximised with higher driving speeds. The recommended driving speed for seeding machines from many manufacturers is 8-10 km h<sup>-1</sup>. Nevertheless, the relatively higher travelling speed shows that the mechanical system, in terms of coulter assembly, is not able to behave as proposed and to follow the fine contour of the field. As a result, the seeding depth varies along the driving line (Suomi & Oksanen, 2015).

Many researches were conducted over the last decades with the aim to reduce the variation of the vertical seed distribution, considering the vertical response of the machine due to soil conditions. An early research by Lawrance (1969) showed that the excessive vertical oscillations of the furrow opening component, which described the motion behaviour of the seed depositing apparatus, were due to the dynamic response of the machine to soil undulations. An assessment regarding the influence of soil surface irregularities on the performance of no-till seeding machines was introduced by Morrison and Gerik (1985). For seed depth characterisation on a standard soil seedbed with well-defined characteristics, like composition and moisture content, a standardised procedure by ISO standard 7256-1 exists (ISO, 1984a). The performance of seeding machines, taking into account the effect of seed type, the slope of the ground, the soil surface condition, and the forward speed, is standardised by ISO standard 7256-2 (ISO, 1984b). However, the conditions that are mentioned in ISO 7256-1 and 7256-2 are not achievable under all field tests. In addition, these standards do not state any ranges regarding the acceptable seeding depth variation (Garrido, Kimberly, Deepa, & Board, 2011). Derpsch et al. (2014) stated that the seed placement, soil conditions, the configuration

of the seeder and operation speed, are the important questions of today's research in no-tillage cultivation.

Several studies focused on the experimental comparison of different no-till seeders performance under laboratory conditions (Chaudhuri, 2001) and in-field conditions (Allen, 1988; Doan, Chen, & Irvine, 2005). However, limited studies have been carried out on assessing only an individual seeding assembly of no-till seeders, under in-field condition. Most of these studies have been conducted using a very common technique for measuring ground truth seeding depth, i.e. measuring the distance of each seed to the soil surface some weeks after seeding from the emerged seedlings. Modern sensors with a high accuracy, such as robotic total stations, whose accuracy has been tested under in-field conditions (Paraforos, Griepentrog, Geipel, & Stehle, 2015; Garrido et al., 2015), could provide the actual soil profile that is followed by the packer wheel in real time. This has the advantage that synchronised measurements related to the developed forces on the machine could be analysed to reveal the reason for seeding depth variation.

Recent field experiment performed by Sharipov, Paraforos, and Griepentrog (2016) showed that undulations of the soil surface highly affect machine's performance. In addition, the dynamic behaviour of the seeder that is described by forces, accelerations and tilting, affects the seeding depth, since the dynamic response of the machine is highly influenced by the draft and vertical forces, and the operation speed. Therefore, there is the necessity to accurately measure the seeding depth along with the corresponding forces. A project was set up to optimise a no-till seeder, in terms of vertical motion stability, for reducing the variation of seeding depth under realistic high-capacity performance. With the aim to assess the working quality of the machine, this paper focuses on defining the critical frequencies of the vertical and profile forces that cause seeding depth variation, by correlating the forces with the corresponding surface profile and the geo-referenced seed positions. A sensor-frame for measuring soil surface profiles in absolute geo-referenced coordinates and a new methodology for measuring seeding depth by geo-referencing every seed position should be developed. This should be considered as the first step towards the performance optimisation of a no-till seeder.

## **2.2 Materials and Methods**

### **2.2.1 Instrumentation and data acquisition**

A 12-row no-till seeder with 25 cm inter-row distance (AMAZONEN-Werke H. Dreyer GmbH & Co. KG, Hasbergen, Germany) and a 6210R 156.6 kW tractor (John Deere, Moline, Illinois, USA) were employed, to perform the field experiments. A metal sensor-frame that carried all the necessary sensors was mounted on the main frame of the seeder (Figure 2.1), to measure the field surface profiles and the machine dynamics parameters, i.e. accelerations, displacements, and tilting information. Multiple sensors were placed on both the sensor-frame and one of the seeding assemblies. An SPS930 total station (Trimble, Sunnyvale, USA) provided the in-field absolute geo-referenced position of the seeder by tracking a Trimble MT900 machine control prism target fixed on the developed sensor-frame. A DT50 laser range finder (SICK AG, Waldkirch, Germany) detected the distance from the sensor-frame to a metal plate mounted on the seeding assembly. Two VN-100 inertial measurement units (IMUs) (VectorNav, Dallas, USA), one on the sensor-frame, and a second one fixed to the plate were used to gather real-time tilt information (roll-pitch-yaw) of the main frame and the seeding assembly, respectively. Three linear 350 Ohm DY41-1.5 strain gauges (HBM GmbH, Darmstadt, Germany), with two parallel measuring grids, were attached at equivalent critical points on the seeding assembly, in order to record the vertical and surface profile impact loads.

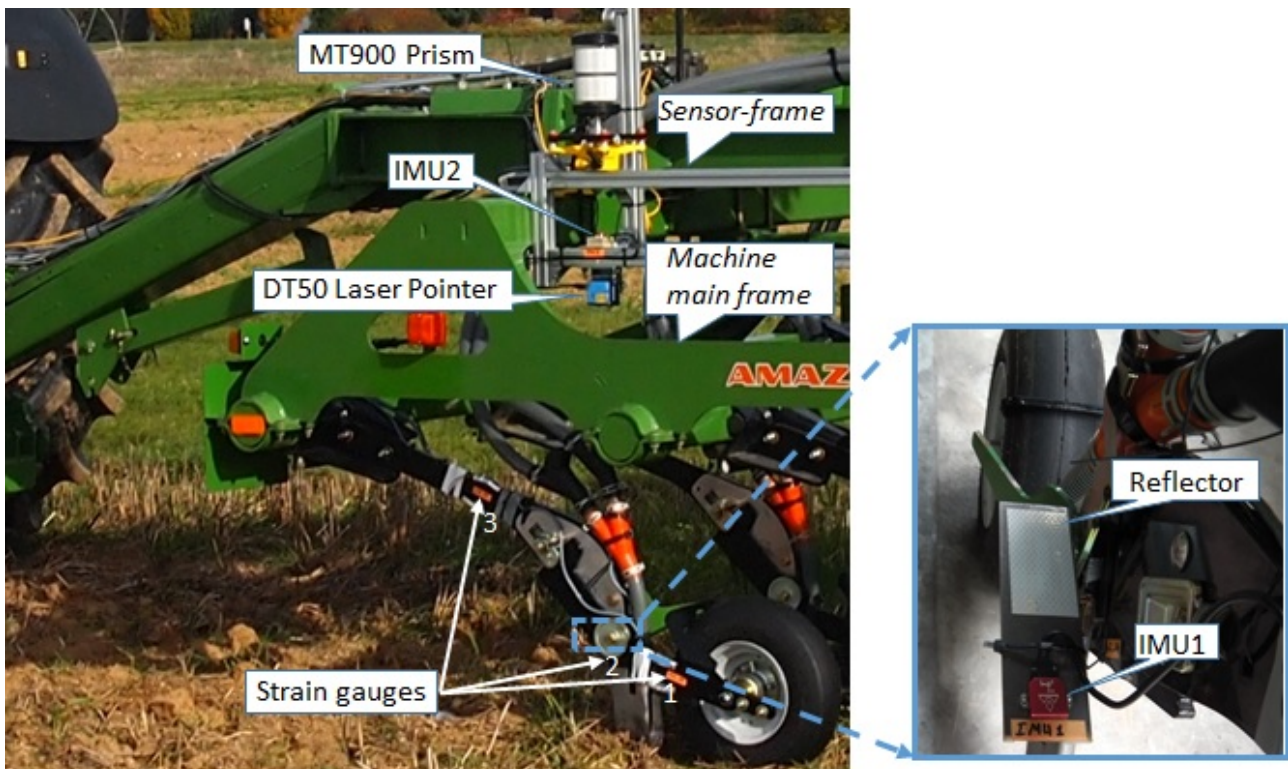


Figure 2.1. Sensor-frame mounted on the main frame of the no-till seeder for measuring field surface profiles, and the positions of the attached strain gauges for acquiring the developed forces during seeding.



The developed software in Microsoft Visual Studio C# 2010 (Paraforos, Griepentrog, & Vougioukas, 2016) for recording and storing the data from the total station, the laser pointer and the two IMUs, had a multi-thread architecture, thus making possible a parallel data acquisition. To store the data from the strain gauges, a QuantumX-MX840B (HBM GmbH, Darmstadt, Germany) data acquisition system with eight channels was used. Three channels were utilised in a full bridge configuration, one for each of the three strain gauges. The CatmanEasy AP software (HBM GmbH, Darmstadt, Germany) had a data sampling rate of 300 Hz. A built-in Butterworth low-pass filter with a cut-off frequency of 50 Hz was applied at every utilised channel, in order to reduce high-frequency noise. All sensor data were stored with a timestamp, for synchronisation purposes during post-processing.

### **2.2.2 Validation of the profile sensing system**

The developed sensor-frame was tested by measuring trapezoidal bumps, to verify the correctness of the calculations and to assess the accuracy of the measured profile (Figure 2.2). Measuring the profile of trapezoidal bumps is a widely used methodology for validating profile measuring systems (Ngwangwa, Heyns, Breytenbach, & Els, 2014; Paraforos et al., 2016). The profiles of the trapezoidal bumps were also measured using the total station, to have their dimensions in the same coordinate system as the measured profiles. The acquired data from the total station were compared with the known descriptive dimensions of the used trapezoidal bumps. The bumps were firmly attached on the surface using a metal pin, to avoid sliding motion when the wheel of the seeding assembly was traversing them.



Figure 2.2. Measuring the profile of a trapezoidal bump.

The accuracy of the profile measuring sensor-frame was evaluated along the length of the trapezoidal bumps, based on the Root-Mean-Squared (RMS) error between the elevation profile and the trapezoidal bumps profile. The RMS error was calculated using the following equation:

$$RMS_{error} = \sqrt{\frac{\sum_{i=1}^n (z_{el,i} - z_{b,i})^2}{n}} \quad (2.1)$$

where  $z_{el,i}$  is the elevation profile and  $z_{b,i}$  is the bump profile for the  $i$ th point, and  $n$  is the number of the measured points for each profile.

## 2.2.3 Experiments

### 2.2.3.1 Field characteristics

All field experiments were carried out at the agricultural field “Heidfeldhof” of the University of Hohenheim (48°42′39.28″N, 9°11′47.19″E). The soil at the field was slightly stagnic luvisol with 9.4% sand, 68.1% silt, and 22.6% clay (Högy, Poll, Marhan, Kandeler, & Fangmeier, 2013). The field was cultivated the previous year with wheat (*triticum aestivum* L.). The measured stubble density was 177 plant-stems per m<sup>2</sup> with an average height of 15 cm. Soil samples were taken at nine points of

the field with 0.1 m depth to define an average bulk density and gravimetric moisture of the soil. The average bulk density and moisture content were  $1.18 \text{ g cm}^{-3}$  and 17 %, respectively.

### 2.2.3.2 Surface profiles and machine dynamics during seeding operation

Field experiments seeding wheat (*triticum aestivum* L.) were performed to obtain surface profiles, forces and machine dynamic parameters, like vertical accelerations and displacements, under stubble field condition. For all dynamic measurements, the speed of the tractor was set constant at  $10 \text{ km h}^{-1}$  while the target seeding depth was adjusted at 50 mm, as these were the recommended settings by the manufacturer. Three sections with 10 m length each were selected to be examined, as presented in Figure 2.3. Two of these repetitions belonged to the same row (red coloured Lines A1, A2), while the third one was part of another seeded row (Line C). In these three rows, after performing the seeding operation, a measurement was set up to geo-reference the position of every single seed and thus, to calculate seeding depth. For validating purposes, the seeding depth was also measured from the seedlings along the green Line B of Figure 2.3.

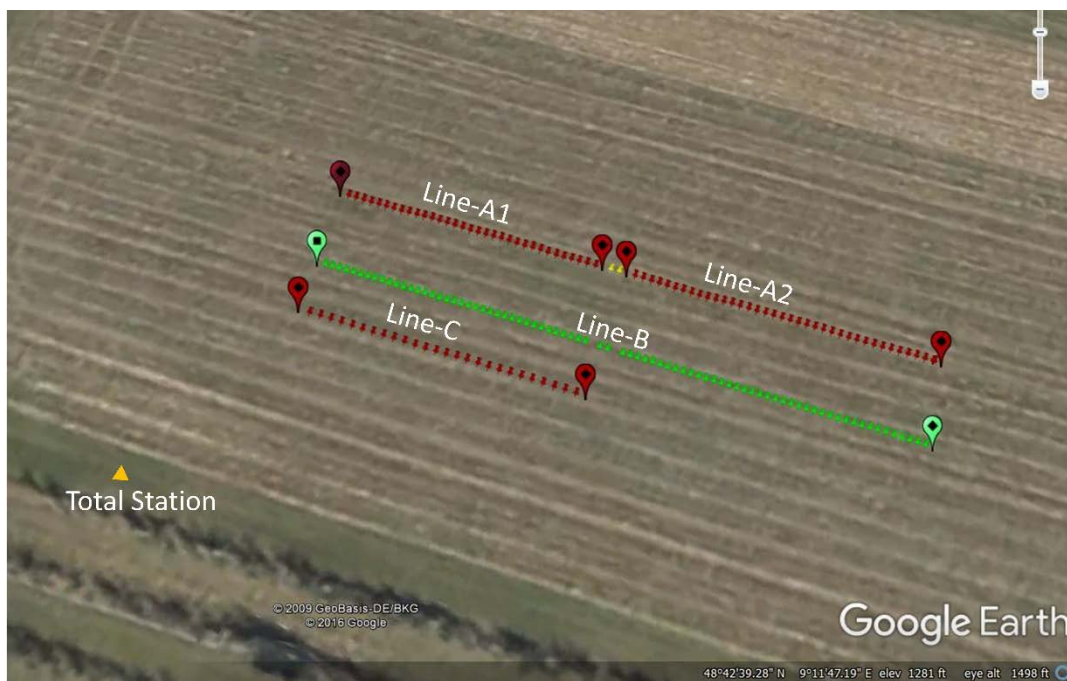


Figure 2.3. Satellite image of the field where the measurements were performed. Lines A1, A2 and C indicate the paths of the examined seeding assembly where the position of seeds was geo-referenced. The ground truth seeding depths from seedlings were measured in Line B. The position of the total station is also indicated (▲).

The 300 Hz sampling rate of the strain gauges data allowed to calculate the vertical forces and the surface impact forces every around 9 mm. The laser pointer acquired data with a 62 Hz sampling rate, which made possible to obtain the surface elevation every 44 mm. The IMUs and the total station provided data with a sampling rate of 50 Hz and 20 Hz, respectively. Due to the different sampling rates of the sensors, non-concurrent data resulted from the measurement. Therefore, the measurement values in synchronised time instances were calculated using the linear interpolation method based on their individual timestamps.

### 2.2.3.3 *Geo-referenced measurement of seed positions*

Before performing the seeding operation, the seeding dose mechanism of the seeder was calibrated according to the manufacturer instruction with a seeding rate of 30 kg ha<sup>-1</sup>, which corresponded to 70.62 seeds per m<sup>2</sup>. Considering the inter-row distance of the seeder, the seed rate was equal to approximately 18 seeds per metre. The three 10 m furrows (Figure 2.3, Lines A1, A2, and C) were carefully opened by hand without disturbing the seeds position on the seedbed, to reveal 176 seeds in each of the first two furrows and 169 seeds in the third furrow. Next, the total station using the MT1000-G prism and a 2 m pole provided every seed 3D position in the same coordinate system as the acquired surface profile (Figure 2.4).



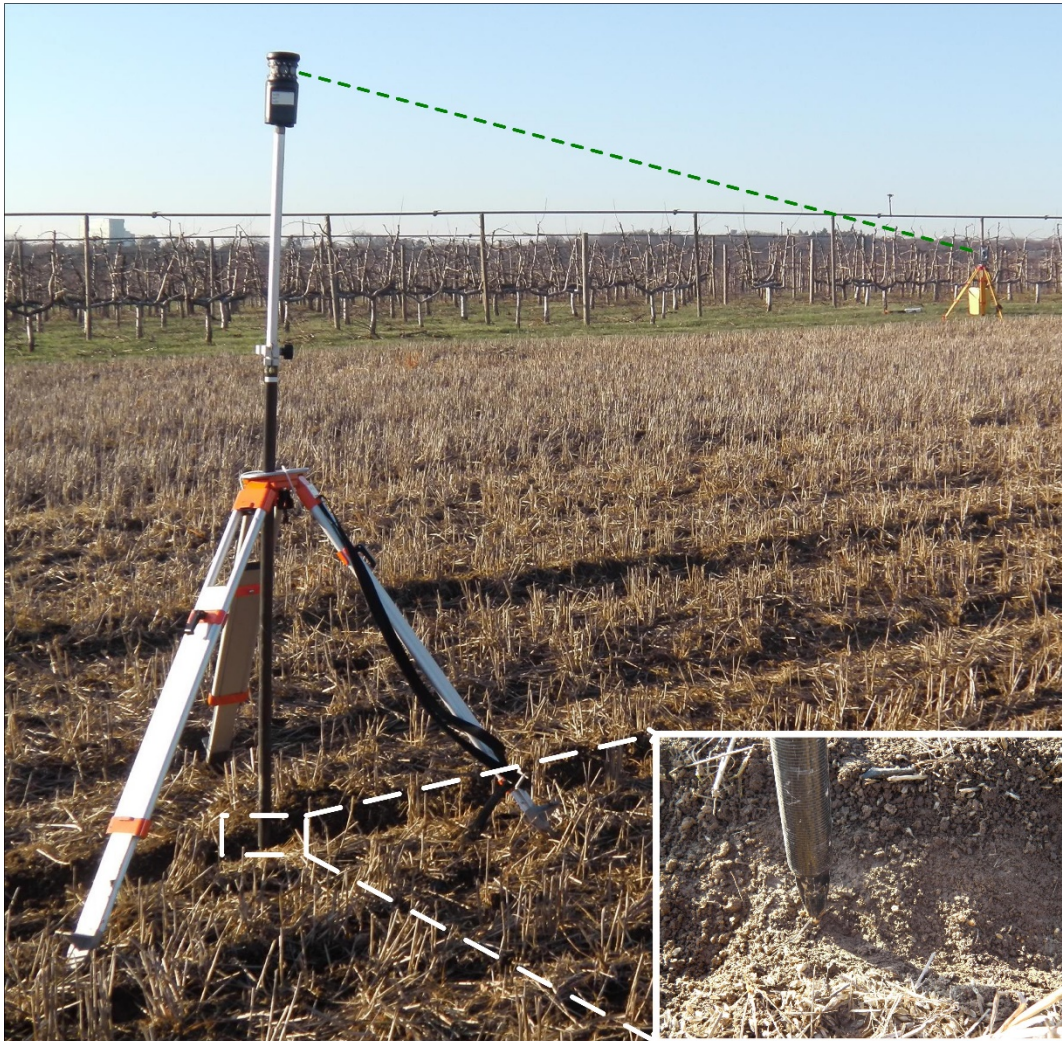


Figure 2.4. Measuring geo-referenced seed positions.

#### 2.2.3.4 Seeding depth measurement from seedlings

The most common technique to obtain the ground truth seeding depth is by measuring the length of the seedlings between the seeds and the soil surface (Burce, Kataoka, Okamoto, & Shibata, 2011; Suomi & Oksanen, 2015). To evaluate the correctness of the introduced methodology for obtaining geo-referenced seeding depth, the results were compared with the ground truth depth measurement from seedlings. All plants from Line B of Figure 2.3 were uprooted, and the ground truth depth was measured as can be seen in Figure 2.5. In total 248 seedlings were measured. Although a higher number was expected within this length, it was limited due to the reduced field emergence. The aim to carry out the measurement of the ground truth depth from seedlings in Line B was to avoid the error, which would occur if the ground truth depth were measured in Lines A1, A2, and C since the surface profile would be different after excavating the furrow and covering it back with soil. This would result in changes of the ground truth seeding depth.



Figure 2.5. The ground truth seeding depth measurement from seedlings.

## 2.3 Theory

### 2.3.1 Strain to force

A combination of strains ( $\varepsilon_1$ ,  $\varepsilon_2$ ,  $\varepsilon_3$ ) was recorded at the three corresponding points of the seeding assembly (Figure 2.6) and was used to calculate the vertical forces ( $F_v$ ), draft forces ( $F_d$ ) and the profile impact forces ( $F_{sp}$ ).



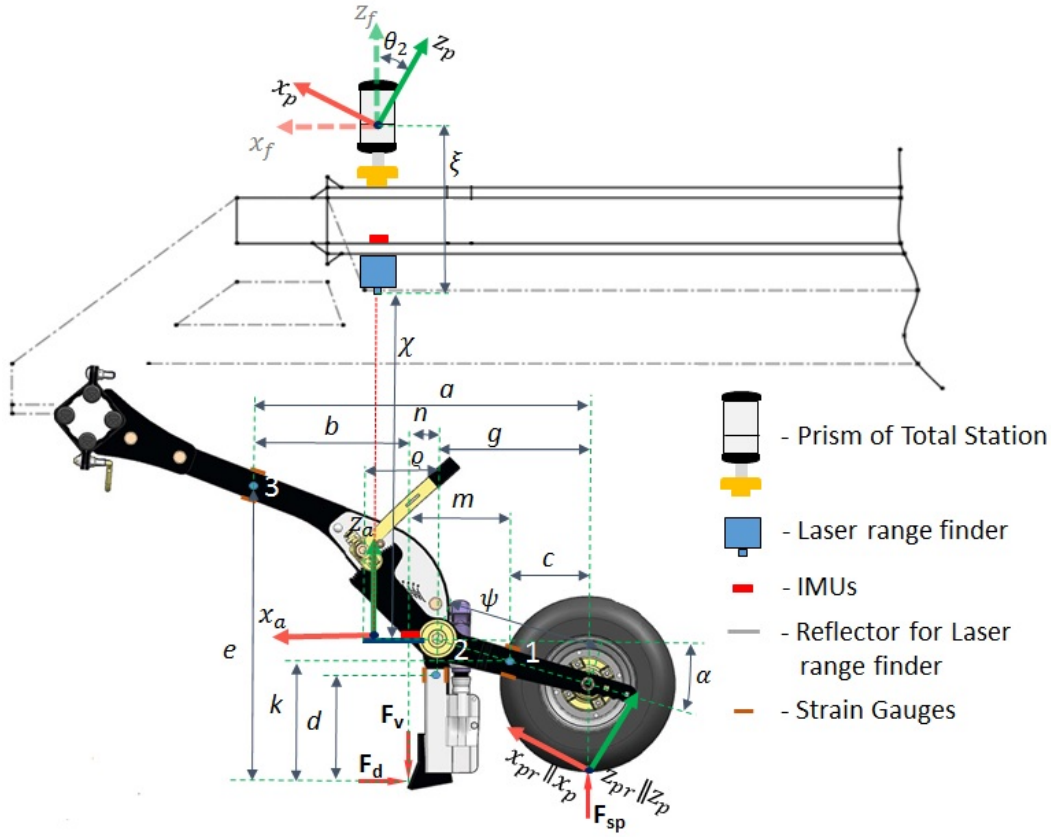


Figure 2.6. Sketch of the seeding assembly and the seeder main frame with the transformation dimensions and the arm of the forces moments.

Summation moments of the forces at point 1 ( $M_1$ ), point 2 ( $M_2$ ) and point 3 ( $M_3$ ) (Vable, 2012) were derived to calculate the relationship between strains and forces as follows:

$$\begin{bmatrix} M_1 \\ M_2 \\ M_3 \end{bmatrix} = \begin{bmatrix} k & m & c \\ d & n & g \\ e & -b & a \end{bmatrix} \cdot \begin{bmatrix} F_d \\ F_v \\ F_{sp} \end{bmatrix} \quad (2.2)$$

where  $a, b, c, d, e, g, k, m, n$  are the measured dimensions of the moments arm, represented in Figure 2.6. On the other hand, by combining the equilibrium expressions for stress calculation  $\sigma_j = M_j/W_{s,j}$  and  $\sigma_j = \varepsilon_j \cdot E$  ( $j = 1,2,3$ ), the moments can be also determined by the following equations:

$$\begin{bmatrix} M_1 \\ M_2 \\ M_3 \end{bmatrix} = E \cdot \begin{bmatrix} \varepsilon_1 \cdot W_{s,1} \\ \varepsilon_2 \cdot W_{s,2} \\ \varepsilon_3 \cdot W_{s,3} \end{bmatrix} \quad (2.3)$$

where  $E = 210 \cdot 10^9 \text{ N m}^{-2}$  is the Young's modulus for steel and  $W_{s,j} = l_j \cdot h_j^2/6$  is the sectional modulus for the rectangular cross-section area where the strain gauges were attached on. By replacing the left hand side of Eq. (2.2) with the right hand side of Eq. (2.3), the following equation was yielded:

$$\frac{1}{E} \cdot \begin{bmatrix} m/W_{s,1} & k/W_{s,1} & c/W_{s,1} \\ d/W_{s,2} & n/W_{s,2} & g/W_{s,2} \\ b/W_{s,3} & -e/W_{s,3} & a/W_{s,3} \end{bmatrix} \cdot \begin{bmatrix} F_d \\ F_v \\ F_{sp} \end{bmatrix} = \begin{bmatrix} \varepsilon_1 \\ \varepsilon_2 \\ \varepsilon_3 \end{bmatrix} \quad (2.4)$$

### 2.3.2 Field surface profile determination

The necessary rotations and translations from the machine control prism target, tracked by the total station, to the ground impact point of the packer wheel were implemented, to obtain the surface profiles in geo-referenced coordinates. Due to the static position of the total station, during the dynamic measurement, its position was selected as the origin of the coordinate system and the machine control prism target was selected as the reference point. Since only the vertical position of the seeding assembly, relatively to the surface profile, was the focus of the study, all rotations and translations were performed in the vertical  $xz$  –plane.

The dynamic tilt information provided by the IMUs and the vertical displacements of the seeding assembly as they were detected from the laser pointer, made possible to calculate the parallel profile at the ground impact point of the packer wheel (Figure 2.6). Initially, the provided pitch ( $\theta_2$ ) from IMU-2, which was attached on the sensor-frame, and the vertical displacement ( $\chi$ ) detected by the laser pointer, were used to convert the position from the coordinate system of the machine control prism target ( $x_p, y_p, z_p$ ) to the coordinate system of the assembly ( $x_a, y_a, z_a$ ):

$$[x_a \ y_a \ z_a \ 1]^T = [T_p^a] \times [x_p \ y_p \ z_p \ 1]^T \quad (2.5)$$

where  $T_p^a$  is the transformation matrix from the coordinate system of the prism target to the coordinate system of the seeding assembly. This required a rotation  $Rot(y_p, \theta_2)$  over the  $y_p$ -axis with an angle  $\theta_2$ , to convert the position to the coordinate system of the main frame of the seeder ( $x_f, y_f, z_f$ ), and then a translation  $Trans(z_f, -\xi - \chi)$  over the  $z_f$ -axis for a distance equal to  $(-\xi - \chi)$

$$\begin{aligned} T_p^a &= Rot(y_p, \theta_2) \cdot Trans(z_f, -\xi - \chi) = \\ &= \begin{bmatrix} \cos \theta_2 & 0 & \sin \theta_2 & 0 \\ 0 & 1 & 0 & 0 \\ -\sin \theta_2 & 0 & \cos \theta_2 & 0 \\ 0 & 0 & 0 & 1 \end{bmatrix} \cdot \begin{bmatrix} 1 & 0 & 0 & 0 \\ 0 & 1 & 0 & 0 \\ 0 & 0 & 1 & -\xi - \chi \\ 0 & 0 & 0 & 1 \end{bmatrix} \end{aligned} \quad (2.6)$$

Finally, the assembly coordinate system was shifted locally to the ground impact point ( $x_{pr}, y_{pr}, z_{pr}$ ) of the packer wheel using the following equation:

$$[x_{pr} \ y_{pr} \ z_{pr} \ 1]^T = [T_a^{pr}] \times [x_a \ y_a \ z_a \ 1]^T \quad (2.7)$$



where  $T_a^{pr}$  is the transformation matrix produced by the translations using the known dimensions  $\rho$ ,  $\psi$ , and  $R_{wheel}$ , of the assembly, the rotations with the pitch information from both IMU-2 ( $\theta_2$ ) and IMU-1 ( $\theta_1$ ), and the constant angle ( $\alpha$ ) between the plate and the packer wheel shank. The sequence of all required rotations and translations can be seen in the following equation:

$$T_a^{pr} = Rot(y_a, -\theta_2) \cdot Rot(y_a, \theta_1) \cdot Trans(x_a, -\rho) \cdot Rot(y_a, \alpha) \cdot Trans(x_a, -\psi) \cdot Rot(y_a, -\alpha) \cdot Trans(z_a, -R_{wheel}) \cdot Rot(y_a, -\theta_1) \quad (2.8)$$

By substituting in Eq. (2.8) all corresponding rotations and translations yields:

$$T_a^{pr} = \begin{bmatrix} \cos(-\theta_2) & 0 & \sin(-\theta_2) & 0 \\ 0 & 1 & 0 & 0 \\ -\sin(-\theta_2) & 0 & \cos(-\theta_2) & 0 \\ 0 & 0 & 0 & 1 \end{bmatrix} \cdot \begin{bmatrix} \cos \theta_1 & 0 & \sin \theta_1 & 0 \\ 0 & 1 & 0 & 0 \\ -\sin \theta_1 & 0 & \cos \theta_1 & 0 \\ 0 & 0 & 0 & 1 \end{bmatrix} \cdot \begin{bmatrix} 1 & 0 & 0 & -\rho \\ 0 & 1 & 0 & 0 \\ 0 & 0 & 1 & 0 \\ 0 & 0 & 0 & 1 \end{bmatrix} \cdot \begin{bmatrix} \cos \alpha & 0 & \sin \alpha & 0 \\ 0 & 1 & 0 & 0 \\ -\sin \alpha & 0 & \cos \alpha & 0 \\ 0 & 0 & 0 & 1 \end{bmatrix} \cdot \begin{bmatrix} 1 & 0 & 0 & -\psi \\ 0 & 1 & 0 & 0 \\ 0 & 0 & 1 & 0 \\ 0 & 0 & 0 & 1 \end{bmatrix} \cdot \begin{bmatrix} \cos(-\alpha) & 0 & \sin(-\alpha) & 0 \\ 0 & 1 & 0 & 0 \\ -\sin(-\alpha) & 0 & \cos(-\alpha) & 0 \\ 0 & 0 & 0 & 1 \end{bmatrix} \cdot \begin{bmatrix} 1 & 0 & 0 & 0 \\ 0 & 1 & 0 & 0 \\ 0 & 0 & 1 & -R_{wheel} \\ 0 & 0 & 0 & 1 \end{bmatrix} \cdot \begin{bmatrix} \cos(-\theta_1) & 0 & \sin(-\theta_1) & 0 \\ 0 & 1 & 0 & 0 \\ -\sin(-\theta_1) & 0 & \cos(-\theta_1) & 0 \\ 0 & 0 & 0 & 1 \end{bmatrix} \quad (2.9)$$

### 2.3.3 Correlation between the seeding depth variation and the developed forces

Due to the wide range of frequencies of the force signal wavelengths, it would be partially infeasible to describe the relation between the forces and the seeding depth variation in the spatial domain. In this case, a correlation between the forces and the seeding depth variation, by analysing the spectrum of their irregular wavelengths in the frequency domain, would be the best means of demonstrating their relationship.

The correlation of the forces and the seeding depth variation can be performed if both data sets exist in the time domain because the correlation uses the power spectral density (PSD) to calculate the coherence function, which describes the matching frequency content between two data sets (Hawari, Haitham & Murray, 2006). Therefore, the data of the seeding depth variation were converted into time domain using the constant travelling speed of the tractor and then were interpolated with the time stamps of the force data existing in the time domain. To build the frequency content of those data, MATLAB's *pwelch* function for Welch's estimation was used to calculate the PSD from the measured forces and the seeding depth variation. Subsequently, the PSDs of each data set was employed to calculate the coherence ( $0 \leq \gamma \leq 1$ ) using the following equation:

$$\gamma_{F,Var}(f) = \frac{|P_{F,Var}(f)|^2}{P_{FF}(f) \cdot P_{Var}(f)} \quad (2.10)$$

where the  $P_{FF}$  and  $P_{Var}$  are the PSD function of the forces and the depth variation, respectively, and  $P_{F,Var}$  is the cross spectrum density of those two data sets. The coherence value of 1 meant excellent correlation between the forces and seeding depth variation. Conversely, a value of 0 indicated no correlation at all. In our analyses, the threshold for coherence value was equal to 0.6, since the most of the spatial frequencies in all data sets were up to 10 cycle  $m^{-1}$  (Hilton, John, & Field, 2011).

## 2.4 Results and discussion

### 2.4.1 Validation of the profile sensing system

With the aim to evaluate the influence of the travelling speed on the error resulting from measuring the surface profiles, the elevation profile measurements on the trapezoidal bumps were performed with two different speeds: a slower travelling speed of 2  $km\ h^{-1}$  and the traveling speed of 10  $km\ h^{-1}$  with which the field experiments were also performed. The elevation profiles from traversing the trapezoidal bumps were obtained by applying Eq. (2.5) and Eq. (2.7). In Figure 2.7, the profile of the trapezoidal bumps and the obtained profiles for the two different travelling speeds are illustrated.

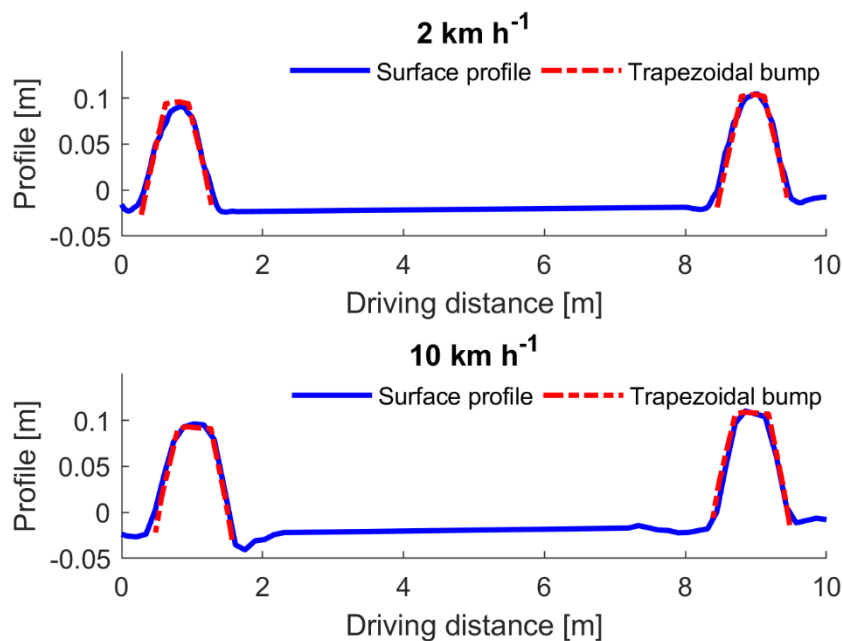


Figure 2.7. Elevation profiles traversing the trapezoidal bumps with a travelling speed of (a) 2  $km\ h^{-1}$  and (b) 10  $km\ h^{-1}$ .

Using Eq. (2.1), the RMS error between the elevation profile and the bump profile was evaluated. The RMS error was 7.3 mm and 8.7 mm, and the maximum absolute error was 9.4 mm and 14.7 mm for the travelling speed of 2 km h<sup>-1</sup> and 10 km h<sup>-1</sup>, respectively. Based on the resulted errors, it can be concluded that the methodology is able to estimate the field surface profile with the afore-given discrepancies. Taking into account the size of the seeding assembly tyres, the resulted accuracy of the system was considered adequate for measuring the surface profile.

#### **2.4.2 Surface profiles with seed positions and the developed forces**

The geo-referenced seed positions together with the corresponding surface profile of the selected three lines of 10 m (parts with the red colour of Line A1, A2 and C in Figure 2.3) are presented in Figure 2.8a1, a2 and a3. The combinations of the geo-referenced seed positions and the profile determined using Eq. (2.7) for each selected lines, which were employed to calculate the absolute seeding depth, are illustrated in Figure 2.8b1, b2 and b3. The corresponding vertical forces and the profile impact forces were extracted from the measured strain using Eq. (2.4), and can be seen in Figure 2.8c1, c2, c3 and d1, d2, d3, respectively.

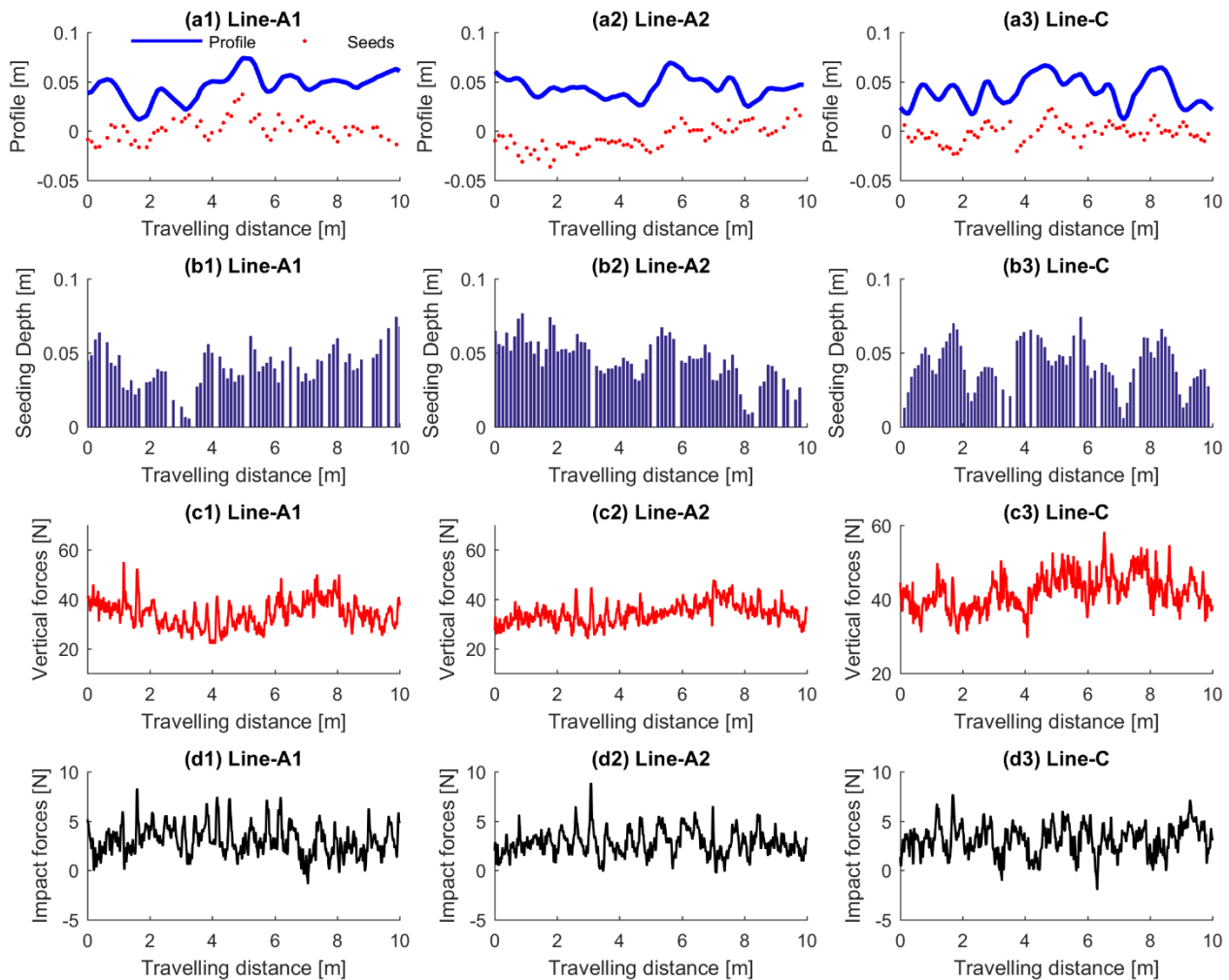


Figure 2.8. (a1, a2 and a3) Seed positions with the corresponding surface profile, (b1, b2 and b3) absolute seeding depth and the corresponding (c1, c2 and c3) vertical and (d1, d2 and d3) impact forces.

### 2.4.3 Seeding depth variation

The frequency histograms of the seeding depth measurements by measuring the seedlings (ground truth) and by using the total station (three repetitions) are presented in Figure 2.9a, b, c and d, respectively. The summary statistics of all tests are presented in Table 2.1. The comparison analyses indicated that the maximum value of ground truth seeding depth was bigger with a difference of 2.6 mm, 0.2 mm and 2.7 mm than the georeferenced seeding depth in Lines A1, A2 and C, respectively. However, these differences were higher when comparing the minimum values with 2.3 mm, 5.1 mm and 4.1 mm, respectively. The mean value of the ground truth seeding depth was higher than the mean values for the geo-referenced seeding depth. Comparing these four values with the target seeding depth of 50 mm, a difference of 3.8 mm, 6 mm, 5.8 mm and 6.3 mm can be noticed for Lines B, A1,

A2, and C, respectively. The differences between the standard deviations of the ground truth seeding depth and the georeferenced seeding depth were 0.7 mm, 0.1 mm and 1.2 mm. This means that in both measurements, the variation of the seeding depth was evenly close to its mean value. In addition, the 95<sup>th</sup> percentile of the geo-referenced seeding depth samples for all tests were smaller than that of the ground truth seeding depth samples, as expected. Suomi et al. (2015) used the ground truth seeding depth from seedlings, to compare it with seeding depth measurements from a controlled system of a seeder. The differences between the mean values, standard deviations and maximum values for target seeding depth of 50 mm were equal to 2.2 mm, 6.4 mm and 15 mm, respectively. Our comparison analyses indicated a discrepancy of 2.3 mm between mean values, 0.2 mm between standard deviation and 2.1 mm between maximum values.

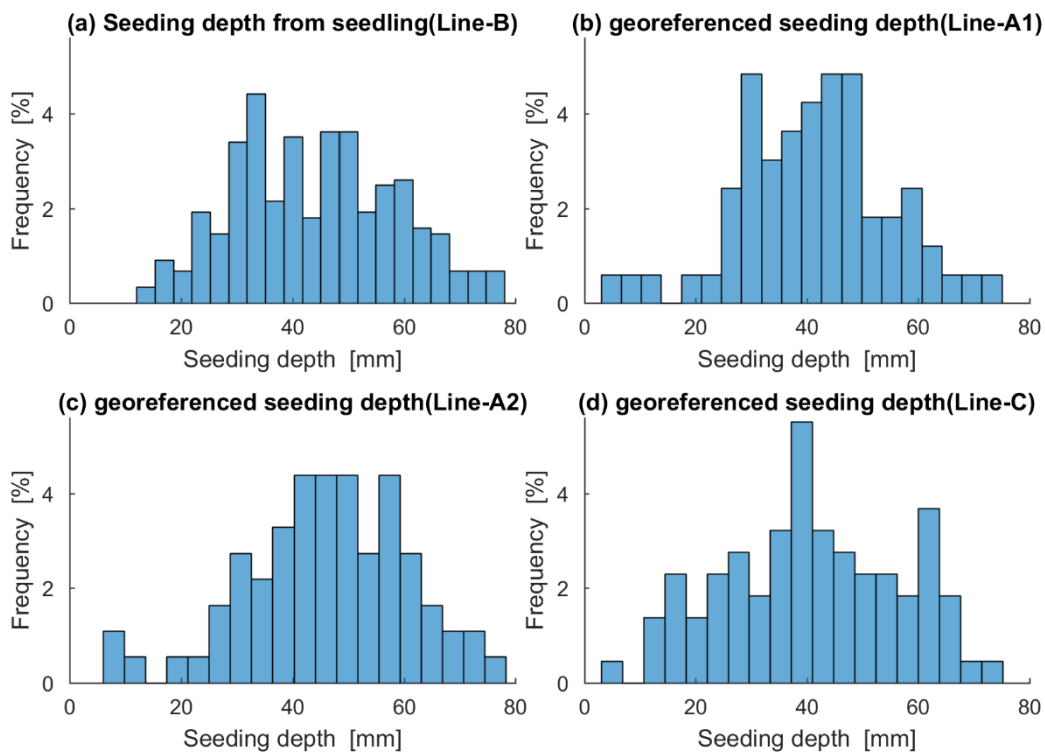


Figure 2.9. Frequency histograms of the seeding depth measured from (a) seedlings in Line-B and from (b, c and d) geo-referenced seed positions and surface profiles in Line A1, A2 and C.

**Table 2.1** Statistics of the field experiments

Dataset	Number of samples	Mean value	Standard deviation	95 <sup>th</sup> percentile	Maximum value [mm]	Minimum value [mm]
Seedlings (Line B)	248	46.2	14.5	68.7	77	14
Georeferenced (Line A1)	176	44	13.8	64.4	74.4	11.7
Georeferenced (Line A2)	176	44.2	14.6	68.3	76.8	8.9
Georeferenced (Line C)	169	43.7	15.7	65.6	74.3	9.9

The histograms for the variation of the ground truth seeding depth and the georeferenced seeding depth in Line C were best fitted by the Weibull distribution with shape parameter equal to 3.37 and 2.86, and scale parameter equal to 0.049 and 0.042, respectively. The histograms of the georeferenced seeding depth variation in Line A1 and A2 were best fitted by the Logistic and the Rician distribution, respectively. The location and scale parameters were equal to 0.41 and 0.007 for the Logistic distribution and 0.046 and 0.014 for the Rician distribution. The utilisation of the one sample Kolmogorov-Smirnov test on each dataset of the seeding depth measurements indicated that for each dataset the null hypotheses was rejected as none of them was normally distributed. Since the data were not following a normal distribution, the Kruskal-Wallis non-parametric method was used to test whether the datasets originated from the identical population. The results of this analysis proved that all data originated from the same population and none of the datasets of the georeferenced seeding depth variation was significantly different from the ground truth seeding depth variation.

#### 2.4.4 The effect of forces on the seeding depth variation

The relation between the forces and the variation of seeding depth was introduced by correlating spatial frequency contents of each dataset using the coherence function of Eq. (2.10). The PSD and the coherence function for all datasets of the georeferenced seeding depth variation and the corresponding vertical forces are presented in Figure 2.10. Two corresponding peaks were detected at the spatial frequencies of 4.8 and 7.2 cycle  $m^{-1}$  (Figure 2.10a1, a2 and a3) in all datasets, which corresponded to a wavelength of 0.21 and 0.14 m, respectively. All the resulting coherence values were higher than the threshold value of 0.6 (Figure 2.10b1, b2 and b3). In Figure 2.11a1, a2 and a3 it is indicated that the corresponding peaks between the PSD of the seeding depth variation and the profile impact forces for all three data sets, existed at 4.35 and 8.2 cycle  $m^{-1}$ , which are equal to a 0.23 and 0.12 m wavelength, respectively. This resulted in higher coherence value for all three

datasets than the threshold value (Figure 2.11b1, b2 and b3) except that one was equal to 0.48 at the frequency of 4.35 for the dataset from Line-A2. In addition, a peak at a spatial frequency of 3.34 cycle  $m^{-1}$  was observed in all PSDs and the correlation was higher than the threshold coherence value of 0.6.

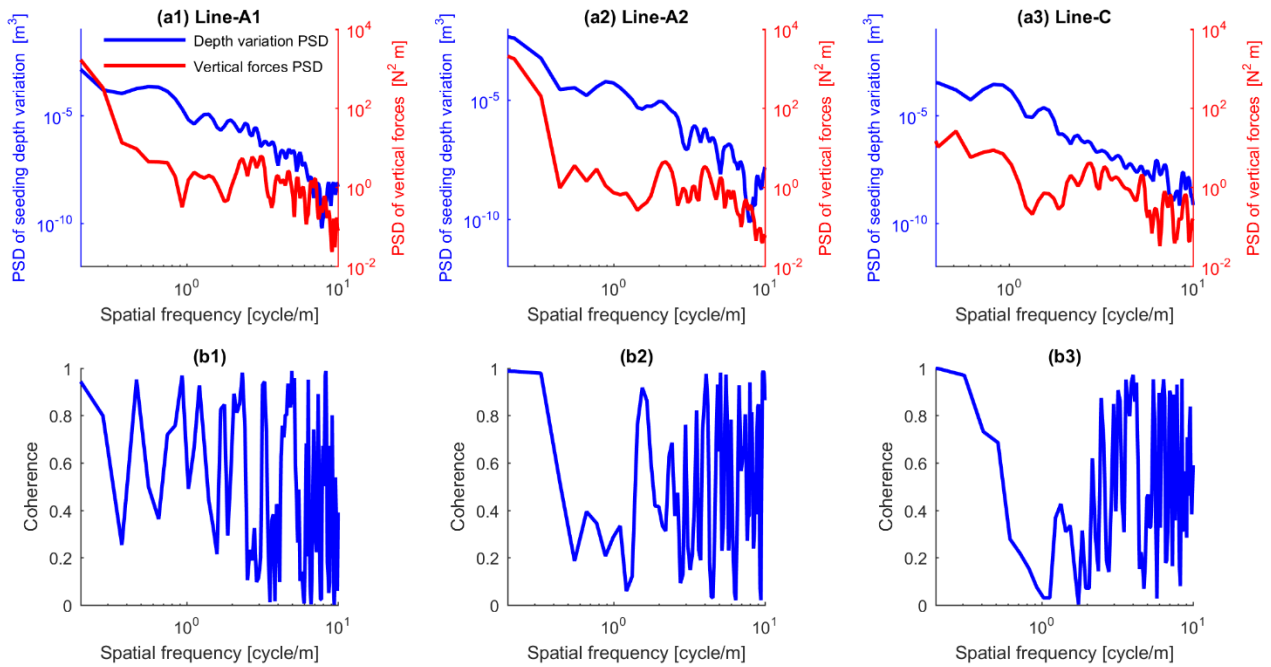


Figure 2.10. (a1, a2 and a3) PSD of the seeding depth variation and vertical forces and (b1, b2 and b3) the corresponding coherence function.

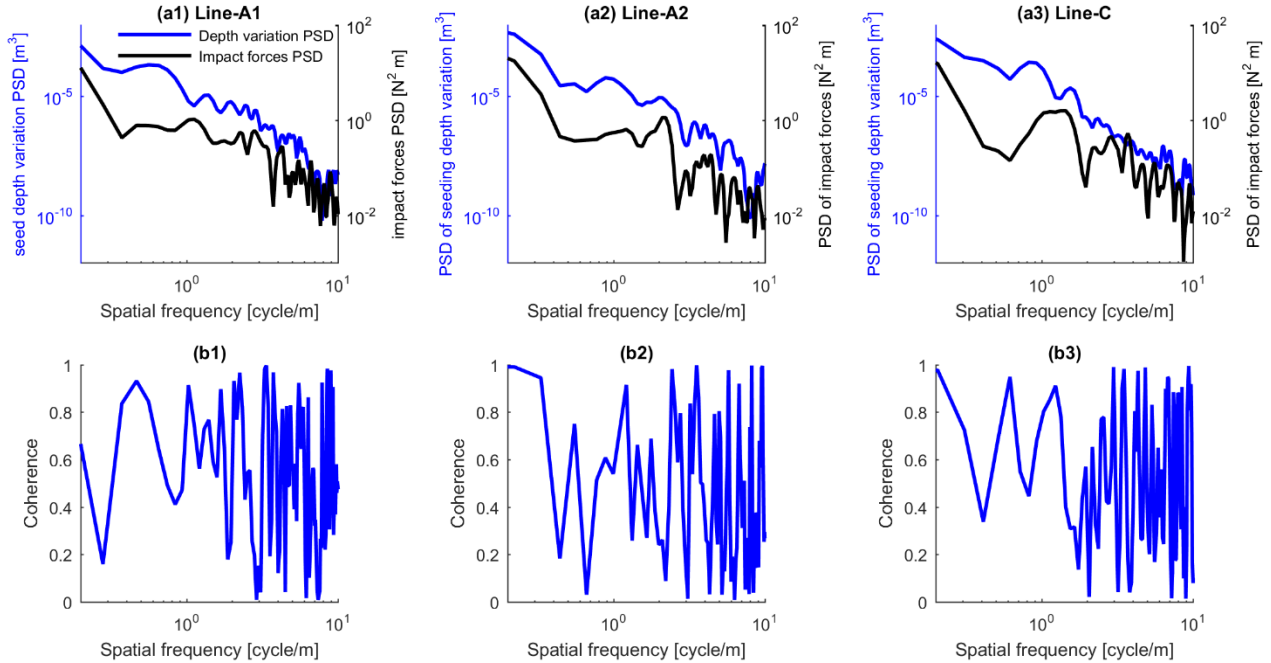


Figure 2.11. (a1, a2 and a3) PSD of the seeding depth variation and impact forces and (b1, b2 and b3) the corresponding coherence function.

The analyses of the coherence function depicted a high correlation between seeding depth and forces at many spatial frequency points up to  $10 \text{ cycle m}^{-1}$ . However, the above-described particular frequencies of the forces must be taken into consideration while optimising the seeding assembly dynamics for better seed placements. For this reason, the frequencies of the forces causing seeding depth variation were calculated using the true operation speed resulted from the geo-referenced positions of the machine and the time of field operation at the chosen distance. The vertical forces that caused high variation in seeding depth had a frequency of 11.8 Hz and 17.8 Hz. This figure was equal to 10.7 Hz and 20.6 Hz for the profile impact forces. The peak value of seeding depth was detected at a frequency of 8.3 Hz for both vertical and impact profile forces.

## 2.5 Conclusions

The developed sensor-frame allowed to obtain field surface profiles during seeding operation in absolute geo-referenced coordinates with sufficient accuracy. A new methodology for measuring seed positions in absolute geo-referenced coordinates was proposed to assess the seeding depth variation. The comparison analysis of verifying the correctness of the methodology indicate that the introduced methodology adequately results in measuring the seeding depth. In comparison with the latter, the proposed methodology has the following advantages:

- 3D geo-referenced coordinates of every single seed allow assessing the seeding depth variation as well as seed-to-seed distance more accurately since they are not dependent on the seedling emergence but on the actual seed position.
- The measurement can be performed directly after seeding operation and therefore the results of the measurements are not affected by any surface profile changes.
- Geo-referenced coordinates of seed positions in combination with geo-referenced surface profile and machine dynamics parameters, offer the possibility to define the reason of seeding depth variation.

Using the introduced methodology, the frequency content analyses of vertical and profile impact forces and seeding depth variation were performed and the critical frequencies, where extreme seeding depth variation occurred, were defined. The defined force frequencies would be a salient parameter in modelling the seeding assembly dynamics, simulating its performance, and finally implementing a mechanism able to reduce the effect of these frequencies for optimised seed placement in no-till cultivation.



## Acknowledgement

The financial support of GA nr 213-2723/001–001–EM Action2 TIMUR (Training of Individuals through Mobility to EU from the Uzbek Republic) project is gratefully acknowledged. The authors would like to thank C. Schwarze and G. Bersi for their technical assistance in setting up the sensor system and performing the experiments. We are also immensely grateful to Ch. Gall from AMAZONEN-WERKE H.Dreyer GmbH & Co.KG for providing the machine and assisting during the field experiments.

The project is conducted at the Max-Eyth Endowed Chair (Instrumentation & Test Engineering) at Hohenheim University (Stuttgart, Germany), which is partly grant funded by the Deutsche Landwirtschafts-Gesellschaft (DLG) e.V.

## References

- Abo Al-Kheer, A., Eid, M., Aoues, Y., El-Hami, A., Kharmanda, M. G., & Mouazen, A. M. (2011). Theoretical analysis of the spatial variability in tillage forces for fatigue analysis of tillage machines. *Journal of Terramechanics*, 48(4), 285–295. <https://doi.org/10.1016/j.jterra.2011.05.002>
- Allen, R. R. (1988). Performance of Three Wheat Seeders in Conservation Tillage Residue. *Applied Engineering in Agriculture*, 4(3), 191–196.
- Burce, M. E., Kataoka, T., Okamoto, H., & Shibata, Y. (2011). Precise Seed Placement Control System for Various Terrain Surfaces. *ASABE*, 7004(11).
- Chaudhuri, D. (2001). Performance Evaluation of Various Types of Furrow Openers on Seed Drills—a Review. *Journal of Agricultural Engineering Research*, 79(2), 125–137. <https://doi.org/10.1006/jaer.2000.0688>
- Chen, Y., Munkholm, L. J., & Nyord, T. (2013). A discrete element model for soil–sweep interaction in three different soils. *Soil and Tillage Research*, 126, 34–41. <https://doi.org/10.1016/j.still.2012.08.008>
- Collins, B. A., & Fowler, D. B. (1996). Effect of soil characteristics, seeding depth, operating speed, and opener design on draft force during direct seeding. *Soil and Tillage Research*, 39(3–4), 199–211. [https://doi.org/10.1016/S0167-1987\(96\)01062-8](https://doi.org/10.1016/S0167-1987(96)01062-8)
- Derpsch, R., Franzluebbers, A. J., Duiker, S. W., Reicosky, D. C., Koeller, K., Friedrich, T., ... Weiss, K. (2014). Why do we need to standardize no-tillage research? *Soil and Tillage Research*, 137,

- 16–22. <https://doi.org/10.1016/j.still.2013.10.002>
- Doan, V., Chen, Y., & Irvine, B. (2005). Effect of residue type on the performance of no-till seeder openers. *Canadian Biosystems Engineering*, *47*, 29–35.
- Flow, G. F. C. M. (2009). Operating manual, (November).
- Fountas, S., Paraforos, D., Cavalaris, C., Karamoutis, C., Gemtos, T. A., Abu-Khalaf, N., & Tagarakis, A. (2013). A five-point penetrometer with GPS for measuring soil compaction variability. *Computers and Electronics in Agriculture*, *96*, 109–116. <https://doi.org/10.1016/j.compag.2013.04.018>
- Garrido, M., Kimberly, M., Deepa, G., & Board, E. (2011). Evaluating the need for an active depth-control system in direct seeding in Portugal. In *8th European Conference on Precision Agriculture* (pp. 1–5). <https://doi.org/10.1007/s13398-014-0173-7.2>
- Garrido, M., Paraforos, D., Reiser, D., Vázquez Arellano, M., Griepentrog, H., & Valero, C. (2015). 3D Maize Plant Reconstruction Based on Georeferenced Overlapping LiDAR Point Clouds. *Remote Sensing*, *7*(12), 17077–17096. <https://doi.org/10.3390/rs71215870>
- Hawari, Haitham and Murray, M. H. (2006). Correlating track forces and track profile. In *Proceedings Conference on Railway Engineering CORE2006* (Vol. 54, pp. 259–266). Melbourne, Australia. [https://doi.org/10.1016/S0261-5177\(02\)00005-5](https://doi.org/10.1016/S0261-5177(02)00005-5)
- Hilton, J., John, N., & Field, L. (2011). Estimation of signal coherence threshold and concealed spectral lines applied to detection of turbofan engine combustion noise. *The Journal of the Acoustical Society of America*, *129*(5). <https://doi.org/10.1121/1.3546097>
- Högy, P., Poll, C., Marhan, S., Kandeler, E., & Fangmeier, A. (2013). Impacts of temperature increase and change in precipitation pattern on crop yield and yield quality of barley. *Food Chemistry*, *136*(3–4), 1470–1477. <https://doi.org/10.1016/j.foodchem.2012.09.056>
- ISO. (1984a). “ISO 7256/1: Sowing equipment-Test methods- Single seed drills (precision drills),” 18.
- ISO. (1984b). “ISO 7256/2: Sowing equipment-Test methods- Seed drills for sowing in lines,” 16.
- Karayel, D., & Özmerzi, A. (2008). Evaluation of three depth-control components on seed placement accuracy and emergence for a precision planter. *Applied Engineering in Agriculture*, *24*(3), 271–276.
- Lawrance, N. S. (1969). *A method of Analyzing Dynamic Responses of A Semi-mounted Farm Implement*. The Ohio State University.
- Liu, J., Chen, Y., & Kushwaha, R. L. (2010). Effect of tillage speed and straw length on soil and straw movement by a sweep. *Soil and Tillage Research*, *109*(1), 9–17. <https://doi.org/10.1016/j.still.2010.03.014>

- Loghin, F., Ene, T. A., Mocanu, V., & Căpătină, I. (2012). Dynamic Modeling of Technical System Tractor - Seed Drill. *Bulletin of the Transylvania University of Brasov, Series II. Forestry, Wood Industry, Agricultural Food Engineering*, 5 (54)(1), 155–160.
- Morrison, J. E., & Gerik, T. J. (1985). Planter Depth Control: II . Empirical Testing and Plant Responses. *TRANSACTIONS of the ASAE*, 28 (6), 1744–1748.
- Ngwangwa, H. M., Heyns, P. S., Breytenbach, H. G. a., & Els, P. S. (2014). Reconstruction of road defects and road roughness classification using Artificial Neural Networks simulation and vehicle dynamic responses: Application to experimental data. *Journal of Terramechanics*, 53, 1–18. <https://doi.org/10.1016/j.jterra.2014.03.002>
- Özmerzi, A., Karayel, D., & Topakci, M. (2002). Effect of Sowing Depth on Precision Seeder Uniformity. *Biosystems Engineering*, 82(2), 227–230. <https://doi.org/10.1006/bioe.2002.0057>
- Paraforos, D. S., Griepentrog, H. W., Geipel, J., & Stehle, T. (2015). Fused inertial measurement unit and real time kinematic-global navigation satellite system data assessment based on robotic total station information for in-field dynamic positioning. In *Precision Agriculture 2015* (pp. 275–282). Israel.
- Paraforos, D. S., Griepentrog, H. W., & Vougioukas, S. G. (2016). Country road and field surface profiles acquisition, modelling and synthetic realisation for evaluating fatigue life of agricultural machinery. *Journal of Terramechanics*, 63, 1–12. <https://doi.org/10.1016/j.jterra.2015.10.001>
- Sharipov, G., Paraforos, D., & Griepentrog, H. W. (2016). Modeling and optimization of a no-till direct seeding machine. In *Lecture Notes in Informatics (LNI), Proceedings - Series of the Gesellschaft für Informatik (GI)* (pp. 193–196). Osnabrück.
- Suomi, P., & Oksanen, T. (2015). Automatic working depth control for seed drill using ISO 11783 remote control messages. *Computers and Electronics in Agriculture*, 116, 30–35. <https://doi.org/10.1016/j.compag.2015.05.016>
- Vable, M. (2012). *Mechanics of Materials*. Michigan Technology University.



# CHAPTER 3

## Paper B

### **Modelling and simulation of the dynamic performance of a no-till seeding assembly with a semi-active damper<sup>2</sup>**

Galibjon M. Sharipov\*, Dimitris S. Paraforos, Hans W. Griepentrog

#### **Abstract**

In no-till seeding, one of the biggest challenges to achieve a reliable seed germination and an even plant field emergence is an extreme variation in the desired seeding depth. This is caused by the inadequate response of the seeder motion dynamics to harsh soil conditions and to high operating speeds. In order to assess and optimise the dynamic response of a no-till seeder, mathematical models were developed for simulating the vertical motion of a coulter assembly. The models included the dynamics of the coulter assembly, with the packer wheel as a passive system, and a semi-active MR (magnetorheological) damper system, which was considered to be located in-between the coulter and the packer wheel. The developed model of the coulter assembly dynamics was validated based on a correlation between the simulated and the measured impact forces and pitch angles. A root-mean-squared (RMS) error resulted from the correlation have increased from 6.84% at the lower speed of 10 km h<sup>-1</sup> to 14.5% at the higher speed of 15 km h<sup>-1</sup> for the impact forces, from 8.1% at the lower speed of 10 km h<sup>-1</sup> to 13.1% at the higher speed of 15 km h<sup>-1</sup> for the pitch angle.

Conversely, there was a fall in the correlation coefficient from 0.699 to 0.681 for the impact forces and from 0.942 to 0.684 for the pitch angle between the lower speed of 10 km h<sup>-1</sup> and the higher speed of 15 km h<sup>-1</sup>, respectively. Furthermore, all three applied hysteresis models, such as

---

<sup>2</sup> The publication of Chapter 3 is done with the consent of the Elsevier Verlag. The original publication was in: Journal of Computer and Electronics in Agriculture, Vol. 139, pp. 187 – 197. It can be found under the following link: <http://doi.org/10.1016/j.compag.2017.05.010>

Bingham, Dahl and Bounc-Wen model, for the semi-active MR damper system behaviour demonstrated significant improvements over the passive system model. Among the models, the Bouc-Wen model produced more adequacy of the MR damper behaviour with the highest reduction of 54.1%, 63.3% and 41.2% in the amplitude of the impact forces and 52.3%, 58.2% and 38.1% in the amplitude of the pitch angles at the speeds of 10 km h<sup>-1</sup>, 12 km h<sup>-1</sup> and 15 km h<sup>-1</sup>, respectively.

**Keywords:** coulter assembly dynamics, semi-active MR damper performance, impact forces and pitch angles

### 3.1 Introduction

During no-till seeding operation, the inappropriate dynamic response of the seeder to soil condition, which is mostly represented by the draught and vertical force components, considerably affects its performance in terms of uneven seeding depth. The latter causes inconsistency in seed germination and crop emergence. The variability of coulter dynamic response to heterogeneous soil conditions is due to forces and vertical displacements that are not completely controlled during an operation (Abo Al-Kheer et al., 2011). The forces arising at the interface, where the coulter interacts with the soil, can describe the motion behaviour of the coulter assembly (Hasimu and Chen, 2014). The coulter assembly mainly consists of the coulter arm and tine, where the draught and vertical forces arise, and the packer wheel, which is affected by the profile impact forces (Sharipov et al., 2017). Considering these forces in controlling the seeding mechanism, regulating the impact of the compacted surface undulations, and optimising the dynamics, the performance of the seeder can be significantly improved. Thus, modelling and simulation of the seeder's dynamic response with a semi-active damper system would be a first salient step to foresee the reduction of the forces amplitude.

Many types of research on simulating and controlling the dynamics of farm machinery have been carried out during the last decades. A mathematical model of a semi-mounted seeding implement and the simulation of its dynamic response to surface undulations was introduced by Lawrance (1969). His research revealed that the vertical excessive oscillations of the furrow-opening component, which described the motion behaviour of the seed depositing apparatus, were due to the dynamic response of the machine to soil undulations. To develop an automatic depth control system of a seeder, its dynamic response was modelled and simulated under laboratory condition by Weatherly and Bowers (1997). By introducing a simulation model of an oscillating subsoiler dynamic behaviour, Shahgoli

et al. (2010) demonstrated the effect of the field profile and stiffness and damping of subsoiler tyres, on the vertical motion behaviour of the machine.

Early studies related to improved seeding depth control via hydraulic and air suspension systems (Morrison & Gerik, 1985; Morrison, 1987) showed that surface undulations, crop residues and soil strength are the most contributing factors to the undesired behaviour of seeder's vertical motion, which results in high seeding depth variation. Burce et al. (2013) evaluated the performance of a zero tillage seeder by implementing an active control system on independent furrow openers. Suomi and Oksanen (2015) presented an automatic control system to assess the performance of a seed drill with disc coulters. Furthermore, a passive suspension and chassis have been examined in simulating and optimising agriculture machine dynamics (Ismoilov et al., 2015). However, limited studies have been conducted on developing a simulation and control model of vertical motion behaviour of a no-till direct seeder with semi-active suspension using the corresponding actual surface profile and measured forces.

The type of the semi-active suspension system that consists of a hydraulic cylinder, magnetic coils and magnetorheological (MR) fluids (damper) offers simplicity in design and control. In addition, the semi-active MR dampers operate with relatively very low power input and produce high yield stress up to 100 kPa. The operation is very stable in a wide range of temperature (40–150 °C). Moreover, the passive damping system provides a level of safety when the magnetic field of the MR damper fails during functional operation (Şahin et al., 2010). Therefore, the semi-active MR dampers have gained a wide recognition in different fields of applications like automotive suspension and vibration control. Nonetheless, none of the semi-active MR dampers applications can be found in no-till seeder that aim to cope with the response of seeder dynamics to harsh soil conditions.

Sharipov et al. (2017) demonstrated that the seeder's performance is highly affected by the dynamic response of the seeder to harsh soil conditions. Up-to-date sensors like robotic total stations, inertial measurement units, and laser pointers, whose accuracy has been thoroughly assessed using an industrial robotic arm (Paraforos et al., 2017), made it possible to correctly assess the performance of the seeder in terms of georeferenced seeding depth with the corresponding seeder dynamics. The analysis of the correlation between the measured forces and the seeding depth variation showed the necessity to develop a system that can reduce the amplitude of the forces causing the extreme seeding depth variation. Thus, the first step forward would be a simulation of the dynamics of the seeder with a semi-active damper system.

The aim of this paper is to develop a mathematical and simulations model for the vertical motion behaviour of the coulter assembly together with the packer wheel as a passively controlled system. The produced forces of the developed model should be compared with the measured ones using data

from realistic no-till seeding conditions. In order to improve the dynamic performance of the seeder coulter assembly, this paper moves one step further by simulating the implementation of a semi-active MR damper system using as inputs the measured experimental data. The improvement in terms of reduction in the amplitude of the impact forces compared to the produced damped forces is a critical factor on choosing the appropriate method for controlling the semi-active MR damper system. This can be regarded as a first step on developing mechanisms that reduce seeding depth variation in no-till seeding applications.

## 3.2 Materials and Methods

### 3.2.1 Equipment and Sensors

A no-till direct seeder (AMAZONEN-Werke H. Dreyer GmbH & Co. KG, Hasbergen, Germany) carrying 12 coulter assemblies with a 25 cm inter-row distance and a 6210R 156.6 kW tractor (John Deere, Moline, Illinois, USA) were used in this study. The examined coulter assembly together with the packer wheel was attached to a square rod of the main frame (Figure 3.1). To determine the surface profile on the ground impact point of the packer wheel, the main-frame of the seeder was georeferenced using position data acquired by an SPS930 total station (Trimble, Sunnyvale, USA). The displacement of the coulter assembly compared to the main frame was detected by a DT50 laser range finder (SICK AG, Waldkirch, Germany). Two VN-100 inertial measurement units (IMUs) (VectorNav, Dallas, USA), one on the sensor-frame, and a second one on the coulter assembly, provided the real-time tilt information (roll-pitch-yaw). The vertical and surface profile impact loads were recorded using three linear 350 Ohm DY41-1.5 strain gauges (HBM GmbH, Darmstadt, Germany) in a full-bridge configuration, attached at the critical points on the coulter assembly. The 300 Hz sampling rate of the strain gauges data allowed to calculate the vertical forces and the surface impact forces every around 9 mm. The laser pointer acquired data with a 62 Hz sampling rate, which made possible to obtain the surface elevation every 44 mm. The IMUs and the total station provided data with a sampling rate of 50 Hz and 20 Hz, respectively. More details about the sensors, the data acquisition system and the validation of the developed sensor-frame can be found in Sharipov et al. (2017).





Figure 3.1. The configuration of the utilised no-till direct seeder.

### 3.2.2 Experiments

All field experiments were carried out at the agricultural field “Heidfeldhof” of the University of Hohenheim ( $48^{\circ}42'39.28''\text{N}$ ,  $9^{\circ}11'47.19''\text{E}$ ). Sensor data were acquired to obtain the surface profiles and the machine dynamic parameters (vertical, draught and profile impact forces arising at the interaction points of the coulter tine and packer wheel with the soil), tilting, vertical accelerations and displacements, during seeding wheat (*Triticum aestivum* L.). Three sections with a length of 20 m each (Figure 3.2, Lines – A, B, C) were selected within three different rows, to examine the dynamics of the coulter assembly. The travelling speed of the tractor was set constant for each selected section:  $10\text{ km h}^{-1}$  for Line-A,  $12\text{ km h}^{-1}$  for Line-B, and  $15\text{ km h}^{-1}$  for Line-C.



Figure 3.2. Satellite image of the field where the dynamic measurements were performed under the travelling speeds of  $10 \text{ km h}^{-1}$  (Line-A),  $12 \text{ km h}^{-1}$  (Line-B), and  $15 \text{ km h}^{-1}$  (Line-C). The position of the total station is also indicated ( $\blacktriangle$ ).

### 3.3 Modelling and control

#### 3.3.1 Coulter assembly dynamics model

The coulter assembly, together with the square rod of the seeder mainframe, can be introduced as a damped swinging arm mechanism due to the rubber packer wheel that is considered as a passively controlled damped and spring system (Figure 3.3). An equation of motion for a damped swinging arm mechanism in terms of mechanical vibrations and control dynamics has been introduced in the literature (Inman, 2014; Saeys et al., 2004). The motion behaviour of the packer wheel can be characterised by the profile impact forces  $F_{sp}$  resulted from the soil-tire interaction. To reduce modelling complexity and due to the non-tilled soil conditions it was assumed that the packer wheel followed the surface profile contour without any soil sinkage. Any possible errors coming from this assumption were evaluated in a previous work by the authors by validating the profile acquisition system, and was found to be acceptable (Sharipov et al., 2017). The profile impact forces can be defined by the deformation and damping properties of the packer wheel. Therefore, the stiffness forces  $F_{st}$  and damping forces  $F_{wd}$  acting on the tyre, and the vertical surface profile  $x_p$  can express the profile impact forces as follows:

$$F_{sp} = F_{st} + F_{wd} = K_w(x_p - L_a\theta) + C_w(\dot{x}_p - L_a\dot{\theta}) \quad (3.1)$$

where  $\theta$  is the pitch angle of the coultter assembly motion;  $L_a$  is the distance between the assembly fixing point on the square rod and the wheel axle [m];  $K_w$  is the stiffness of the tyre [ $\text{N m}^{-1}$ ] and  $C_w$  is the damping coefficient of the tyre [ $\text{N s m}^{-1}$ ].

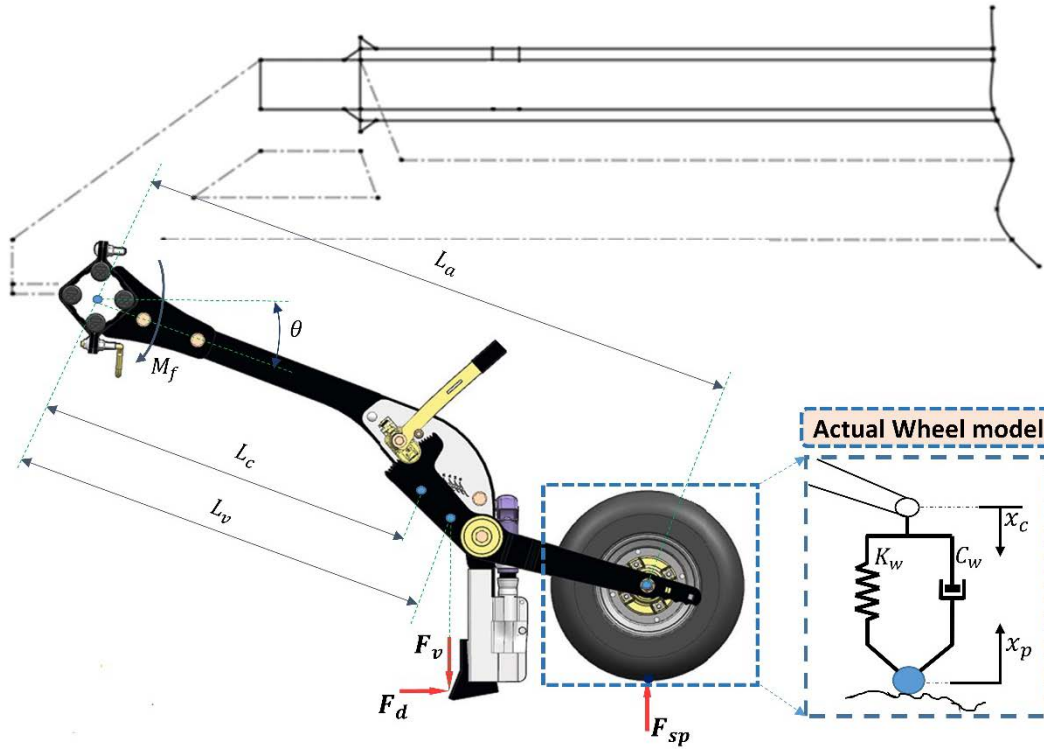


Figure 3.3. Sketch of the coultter assembly and the modelled packer wheel as a passively controlled damping and spring system.

The vertical stiffness and damping coefficient of the attached tire (4.80-8 NHS, a non-high way tire with 4.80 in width and 8 in rim diameter) were calculated from the following formula (Lines and Murphy, 1991; Shahgoli et al., 2010):

$$K_w = 172 - 1.77 R + 5.6 A + 0.34 W R P \quad (3.2)$$

$$C_w = C_o + 70 P \quad (3.3)$$

where  $R$  is the rim diameter [in];  $W$  is the tire section width [in];  $A$  is the exploited age tire [years];  $P$  is the inflation pressure [kPa] set during the field experiment; and  $C_o$  is the vertical damping of the tyre at zero inflation pressure [ $\text{kN s m}^{-1}$ ].

Considering the fact that the horizontal forces have a minor effect on the vertical motion behaviour of the coultter assembly, the draught forces  $F_d$  were neglected when modelling the vertical motion dynamics of the coultter assembly. By taking into account the moment of the vertical forces on the coultter  $F_v$ , the moment of the applied force from the square rod of the main frame at the fixed point of the coultter assembly  $M_f$ , and the above-expressed profile impact forces  $F_{sp}$ , the equation of the entire coultter assembly motion can be described as follows:

$$\left(m_w + \frac{m_c}{4}\right)L_a^2\ddot{\theta} = F_{sp}L_a - ((m_w + m_c)gL_c + F_vL_v)\theta - M_f \quad (3.4)$$

where  $m_c$  and  $m_w$  are the mass of the coultter assembly and the packer wheel, respectively [kg];  $L_c$  is the distance between the coultter fixing point on the main frame and the centre of mass [m]; and  $L_v$  is the distance between the coultter fixing point on the main frame and the point that the vertical forces are acting on the coultter [m].

### 3.3.2 Validation of the coultter assembly dynamics developed model

The equations (3.1)-(3.4) were programmed using MATLAB and Simulink to simulate the profile impact forces on the packer wheel (passive suspension system) and the pitch angle of the assembly vertical motion. All numerical values of the coultter assembly model parameters are presented in Table 3.1. The correlation between the simulated and the measured values was assessed by evaluating the (root-mean-squared) RMS error expressed in percentage. The RMS error in percentage indicates the errors in the absolute fitting of the simulated data to the measured data. A smaller percentage of RMS errors shows a higher correlation between those two data sets and vice versa. Considering the disregarded lateral forces in modelling and the errors in tire modelling, the RMS error values that are less than 25% are considered acceptable (Ngwangwa and Heyns, 2014). The errors can be formulated by the following equations:

$$\varepsilon_{rms} = \frac{|Y_{rms}^m - Y_{rms}^s|}{Y_{rms}^m} \times 100\% \quad (3.5)$$

where  $Y_{rms}^m = \sqrt{\sum_{i=1}^N (y_m(t)^2)/N}$ ;  $Y_{rms}^s = \sqrt{\sum_{i=1}^N (y_s(t)^2)/N}$ ;  $y_m(t)$  and  $y_s(t)$  are the measured and simulated data, respectively, within the time  $t$  spent traveling the specified distances;  $N$  is the total number of samples in the measured and simulated data.

**Table 3.1.** Coulter assembly model parameters.

Parameter name	Notation	Value	Unit
Coulter mass (sprung mass)	$m_c$	31	[kg]
Packer wheel mass (unsprung mass)	$m_w$	4	[kg]
Stiffness of the tire	$K_w$	17132	[N m <sup>-1</sup> ]
Damping coefficient of the tire	$C_w$	911	[N s m <sup>-1</sup> ]

The simulation used as input the determined field surface profiles (Figure 3.4a1, a2 and a3) and the vertical forces (Figure 3.4b1, b2 and b3) in time domain that were measured in the three field experiments of Figure 3.2. Therefore, the field surface profile and the vertical forces were converted from the distance domain to the time domain considering the true speed of the operation. The true speed of the seeder for each selected sections was defined based on the recording time and the coordinates of the coulter assembly during the operation captured by the total station. The necessary coordinate transformations from the machine control prism target, tracked by the total station, to the ground impact point of the packer wheel were implemented, to obtain the surface profiles in geo-referenced coordinates. A combination of strains recorded at the three corresponding points of the seeding assembly using strain gauges was engaged to calculate the vertical forces. More information about the determination of the field surface profile and the vertical forces can be found in Sharipov et al., (2017).

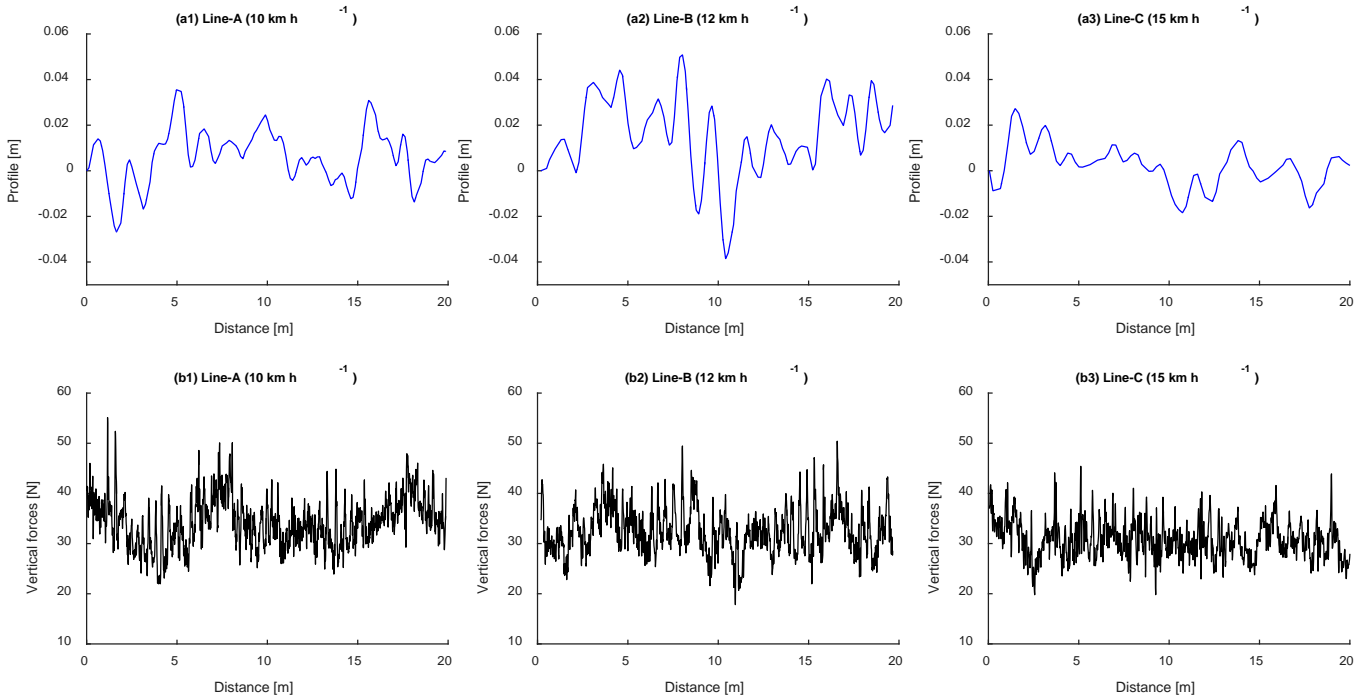


Figure 3.4. Measured surface profiles (a1) 10 km h<sup>-1</sup>, (a2) 12 km h<sup>-1</sup> and (a3) 15 km h<sup>-1</sup> and the corresponding measured vertical forces (b1, b2 and b3).

The fitting accuracy between the simulated and the measured data was also described by the correlation coefficient. The value of the correlation coefficient ranges between -1 and 1. A greater absolute value of the correlation coefficient expresses a stronger relationship between the two data sets. Conversely, a value closer to 0 shows a weaker relationship. In our case, values higher than 0.6 were considered as practically acceptable (Ngwangwa & Heyns, 2014; Sharipov et al., 2017). The correlation coefficient  $R$  was determined by the following formula:

$$R = 1 - \left( \frac{1}{N-1} \sum_{i=1}^N \left( \frac{y_m(t) - \overline{y_m(t)}}{\sigma_{y_m}} \right) \left( \frac{y_s(t) - \overline{y_s(t)}}{\sigma_{y_s}} \right) \right)^2 \quad (3.6)$$

where  $\overline{y_m(t)}$  and  $\sigma_{y_m}$  are the mean value and standard deviation of  $y_m(t)$ , respectively, and  $\overline{y_s(t)}$  and  $\sigma_{y_s}$  are the mean value and standard deviation of  $y_s(t)$ , respectively.

Since the profile impact force was selected as an important parameter in optimising the dynamics of the coulter assembly, it was necessary to check if the simulated and measured forces had a similar frequency content. Therefore, a correlation based on coherence analysis between the measured and simulated forces in the frequency domain was carried out. The Power Spectrum Density (PSD) of each data set were employed to correlate the measured and simulated forces using a function called coherence. The coherence value ranges between 0 and 1. A value of 1 means excellent correlation while a value of 0 indicates no correlation at all. In our analyses, the threshold for coherence value

that indicated sufficient correlation was equal to 0.5. The coherence value of 0.5, which denotes a 50 % overlap, results in the upper 95 % confidence interval of matching between two independent datasets (Hilton et al., 2011).

### 3.3.3 Modelling of the semi-active MR damper system

The examined coultter assembly is composed of a coultter, a wheel shank and a packer wheel. To develop a mathematical model of the coultter assembly with the semi-active MR damper system, a mass-spring-damper model was used. The semi-active MR damper was considered to be located between the wheel shank and the packer wheel, as shown in Figure 3.5. The model has the mass of the packer wheel as an unsprung mass  $m_w$ , and the mass of the coultter together with the wheel shank as a sprung mass  $m_c$ . In this case, the deformation and damping force of the packer wheel can be described by the displacements and the velocity of the unsprung mass, respectively. The profile impact forces  $F_{sp}$  were expressed by the following formula:

$$F_{sp} = K_w(x_p - x_w) + C_w(\dot{x}_p - \dot{x}_w) \quad (3.7)$$

where  $x_w$ ,  $\dot{x}_w$  are the vertical displacement and velocity of packer wheel, in [m] and [m s<sup>-1</sup>], respectively.

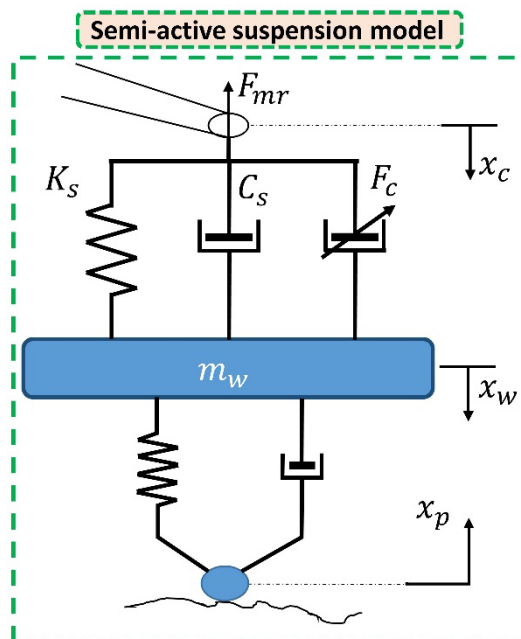


Figure 3.5. Representative view of the semi-active MR damper system design.

In this model, it is apparent that the affecting force to the coultter assembly is the damping force  $F_{mr}$  resulting from the semi-active suspension system. Therefore, by substituting  $F_{sp}$  for  $F_{mr}$  in Eq. (3.4), the equations for motion behaviour of the coultter assembly, including a semi-active MR damper system, can be rewritten as follows:

$$\left(m_w + \frac{m_c}{4}\right)L_a^2\ddot{\theta} = F_{mr}L_a - ((m_w + m_c)gL_c + F_vL_v)\theta - M_f \quad (3.8)$$

$$m_w\ddot{x}_w + C_s(\dot{x}_w - L_a\dot{\theta}) + K_s(x_w - L_a\theta) + C_w\dot{x}_w + K_w x_w = F_{sp} - F_{mr} \quad (3.9)$$

where  $\ddot{x}_w$  is the vertical acceleration of the packer wheel [ $\text{m s}^{-2}$ ];  $K_s$  and  $C_s$  are the stiffness and damping coefficient of the semi-active suspension passive components, in [ $\text{N m}^{-1}$ ] and [ $\text{N s m}^{-1}$ ], respectively.

### 3.3.4 Control design for the semi-active MR damper system

In semi-active suspension systems, skyhook control is known as the most used and simplest control strategy (Guglielmino et al., 2008). This strategy shows that the damper force from the MR damper is controlled by switching between two damping values in terms of maximum and minimum. The determination of whether the MR damper is to be adjusted to a logical high (if the damped force is positive or zero) or a logical low damping state (otherwise), depends on the product of the relative velocity of the coultter assembly ( $\dot{x}_c$ ) and the packer wheel ( $\dot{x}_w$ ). This strategy can be summarised as:

$$F_{mr} = \begin{cases} F_{mr} & \text{if } \xi_r \geq 0 \\ 0 & \text{if } \xi_r < 0 \end{cases} \quad (3.10)$$

where  $\xi_r = \dot{x}_c(\dot{x}_c - \dot{x}_w)$  is the relative velocity relation between of the coultter assembly against the packer wheel.

Considering three different parametric models, namely Bingham, Dahl, and Bouc-Wen (presented in Figure 3.6a, b and c, respectively) that address the hysteresis and nonlinear behaviour of the MR dampers, equivalent control strategies were developed based on the skyhook control logic (Figure 3.7). These three models were chosen to investigate the nonlinear behavior of the MR damper due to their outperformances compared to the performance of other existing models (Eshkabilov, 2016; Şahin et al., 2010). The control strategy was based on the feedback of the vertical displacements of the coultter and the difference between the desired command force and the produced damping force from the MR damper. However, in our case of simulating the performance of the MR damper, a set



of constant supply voltage was used to feed the MR damper and therefore the desired command force was neglected in the simulation. Nevertheless, the implementation of the described control strategy should involve real-time control of the MR damper by varying the control voltage.

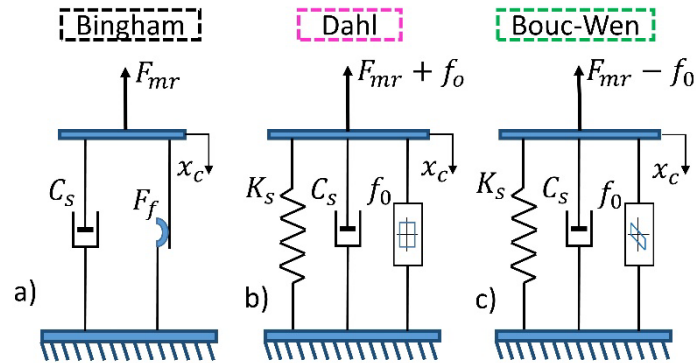


Figure 3.6. Schematic view of the (a) Bingham, (b) Dahl and (c) Bouc-Wen model.

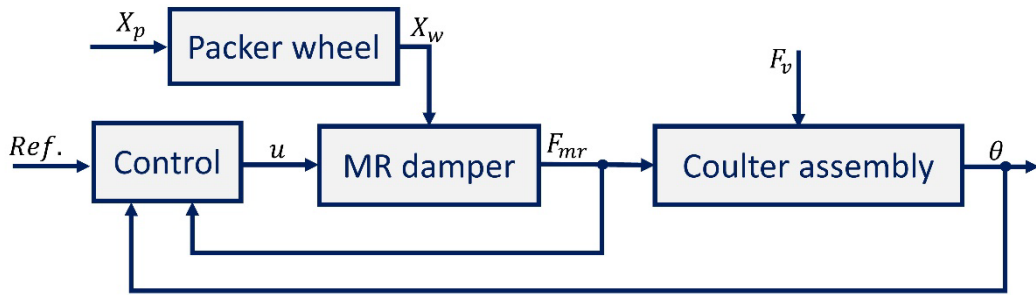


Figure 3.7. Block diagram of the semi-active suspension control.

### 3.3.4.1 Bingham model

The idealisation of the MR dampers that use similarities in the rheological behaviour of the MR fluids can be introduced by the Bingham model (Sapiński and Filuś, 2003). Figure 6a presents a schematic view of the Bingham model. According to this model, the piston velocity  $\dot{x}_c$  and the damping force  $F_{mr}$  can be expressed as:

$$F_{mr} = F_f \operatorname{sgn}(\dot{x}_c) + C_s \dot{x}_c + K_s x_c + f_0 \quad (3.11)$$

where  $F_f$  is the frictional force resulted from the Coulomb friction element placed parallel to the viscous damper; and  $f_0$  is the offset force due to the presence of the accumulation in the magnetic field. In the Bingham model, the active control force  $F_c$  corresponds to the damping force  $F_{mr}$  produced by the response of the displacement and velocity of the sprung mass controlled by the *signum* function.

### 3.3.4.2 Dahl model

The Dahl model characterises the force-velocity relationship by considering quasi-static bonds in the origin of friction (Dahl, 1968). Figure 3.6b illustrates how the hysteresis can be captured using this model. The Dahl model consists of the following equations:

$$F_{mr} = K_s x_c + (C_{sa} + C_{sb} u) \dot{x}_c + (K_{sa} + K_{sb} u) w \quad (3.12)$$

$$\dot{w} = \rho (\dot{x}_c - |\dot{x}_c| w) \quad (3.13)$$

where  $F_{mr}$  is the resulted force from the MR damper;  $u$  is the control voltage;  $w$  is the hysteresis coefficient or the internal state variable;  $K_s$  is the stiffness of the spring;  $K_{sa}$  is the stiffness set for hysteresis loop;  $K_{sb}$  is the stiffness affected by the control voltage;  $C_{sa}$  is the damping coefficient set for hysteresis loop;  $C_{sb}$  is the damping coefficient affected by the control voltage;  $\rho$  are the control parameters for the hysteresis loop shape and size. Unlike the Bingham model, the damping force  $F_{mr}$  is produced by taking into account the difference between the actual and the absolute values of the sprung mass (the mass of the couler) velocity.

### 3.3.4.3 Bouc-Wen model

The Bouc-Wen model is one of the recent models that has been very common in modelling the hysteric behaviour of the MR dampers (Şahin et al., 2010). The schematic representation of this model was depicted in Figure 3.6c. The damping force in the Bouc-Wen model is described by the following expressions:

$$F_{mr} = C_s(u) \dot{x}_c + K_s(u) x_c + \alpha z + f_0 \quad (3.14)$$

where the internal state variable  $z$  is governed by:

$$\dot{z} = \gamma z |x_c| |z|^{n-1} - \beta x_c |z|^n + A x_c \quad (3.15)$$

where  $\gamma$ ,  $\beta$  and  $A$  are the control parameters for the internal state variable that can vary from a sinusoidal to a quasi-rectangular function of time;  $f_0$  is the force due to the accumulator that considers the pre-yield stress of the damper;  $\alpha$  is the parameter that defines the influence of the model on the active control force;  $K_s(u)$  and  $C_s(u)$  are the stiffness and damping coefficients, respectively, with respect to the control voltage. As similar to the other two models for the hysteresis behavior of the MR damper, the active control force is equal to the damping force coming from the model.

### 3.3.5 Simulation of the semi-active MR damper models

The mathematical equations from (3.7) to (3.15) for the semi-active MR damper models were implemented and simulated in MATLAB and Simulink. The same field surface profiles and the vertical forces of Figure 3.4 were used as inputs for assessing the performance of the semi-active MR damper models. All numerical values of the coulter assembly model and the hysteresis models (Bingham, Dahl and Bouc-Wen) parameters, which were found by trial and error (Eshkabilov, 2016; Rashid et al., 2011), are given in Table 3.2. The passive components of the MR damper were defined by tuning the simulation model since the properties of these components were recommended to be defined by engaging an empirical formulation that uses experimental data (Braz-Cesar and Barros, 2010). The damped forces, which are produced by the semi-active MR damper system and the resulted pitch angles of the coulter assembly, were compared against the simulated ones of the passively controlled system.

**Table 3.2.** Parameters of the three parametric models.

Model	Parameter name	Notation	Value	Unit
Bingham	Passive component stiffness of the MR damper system	$K_c$	30000	[N m <sup>-1</sup> ]
	Passive component damping coefficient of the MR damper system	$C_c$	5200	[N s m <sup>-1</sup> ]
	Frictional force	$F_f$	4	[N]
	Offset force	$f_0$	10	[N]
Dahl	Stiffness for hysteresis loop	$K_{sa}$	250	[N m <sup>-1</sup> ]
	Stiffness affected by the control voltage	$K_{sb}$	800	[N m <sup>-1</sup> ]
	Damping coefficient for hysteresis loop	$C_{sa}$	175	[N s m <sup>-1</sup> ]
	Damping coefficient affected by the control voltage	$C_{sb}$	80	[N s m <sup>-1</sup> ]
	Hysteresis coefficient	$w$	5	[-]
	Control voltage	$u$	3	[V]
	Control parameters for the hysteresis loop shape	$\rho$	25	
Bouc-Wen	Control parameter	$\gamma$	1	[-]
	Control parameter	$\beta$	737	[-]
	Control parameter	$A$	5	[-]

Parameter defining the influence of the model on the active control force	$\alpha$	91	
Control voltage	$u$	5	[V]

### 3.3.6 Performance criteria

In order to make a comparative evaluation of the various hysteresis models applied for the control of the semi-active MR damper, performance criteria such as mean squared deviation (MSD) and mean deviation percentage (MDP) were analysed, since the graphical representation would not be sufficient to quantitatively describe the performance evaluation of each model. The MSD measured the average of the squares of the deviations that were the differences between the simulated parameter of the passively controlled system and the models for the semi-actively controlled system. Meanwhile, the MDP estimated the reduction percentage, i.e. the decrease of the amplitude of the simulated parameter of the models for the semi-actively controlled system as compared to that of the passive one. The expressions of the MSD and MDP were defined as

$$MSD = \frac{1}{N} \sum_{j=1}^N (A_{sp,j} - A_{mr,j})^2 \quad (3.16)$$

$$MDP = \frac{1}{N} \sum_{j=1}^N \left| \frac{A_{sp,j} - A_{mr,j}}{A_{sp,j}} \right| \times 100\% \quad (3.17)$$

where  $A_{sp,j}$  is the simulated pitch angles and forces when the packer wheel is considered as passive system and  $A_{mr,j}$  is those simulated dynamic parameters of the coultter assembly with the semi-active system for time instance  $j$ .

## 3.4 Results and discussion

### 3.4.1 Assessment of the simulation model validity

Figure 3.8 presents the measured and simulated time-series of the pitch angles and profile impact forces. The calculated RMS error percentage (Eq. 3.5) and the correlation coefficient (Eq. 3.6) are also presented at the title of each plot. The best correlation between the simulated and the measured impact forces with 6.84% of RMSE and 0.699 of correlation coefficient was observed at the lower travelling speed of 10 km h<sup>-1</sup> (Figure 3.8a1). These figures were equal to 8.1% and 0.942 for the

correlation between the simulated and measured pitch angles (Figure 3.8b1). On the contrary, the lowest correlation with 14.5% of RMSE and 0.681 of the correlation coefficient for the profile impact forces (Figure 3.8a3) and 13.1% of RMSE and 0.684 of the correlation coefficient for the pitches (Figure 3.8b3) occurred at the higher travelling speed of 15 km h<sup>-1</sup>. For the speed of 12 km h<sup>-1</sup> the RMSE and the correlation coefficient were equal to 12.3% and 0.614 for the impact forces (Figure 3.8a2), and 11% and 0.891 for the pitch angles (Figure 3.8b2), respectively, which also showed less correlation than that of 10 km h<sup>-1</sup>. The correlation analyses depicted that both the impact forces and pitch angles at all three speeds had their RMS errors ranging below 15%, which was significantly lower than the threshold of 25%. It was observed that the correlation between the simulated and the measured impact forces and pitch angles significantly decreased as the travelling speed of the seeder increased. This was due to the sampling rate of the sensor system that detected less data points within the selected sections as the speed increased. However, the correlation coefficient for both impact forces and pitch angles at all three speeds were above 0.6. Based on these results, the correctness of the modelling and simulation performances can be considered acceptable.

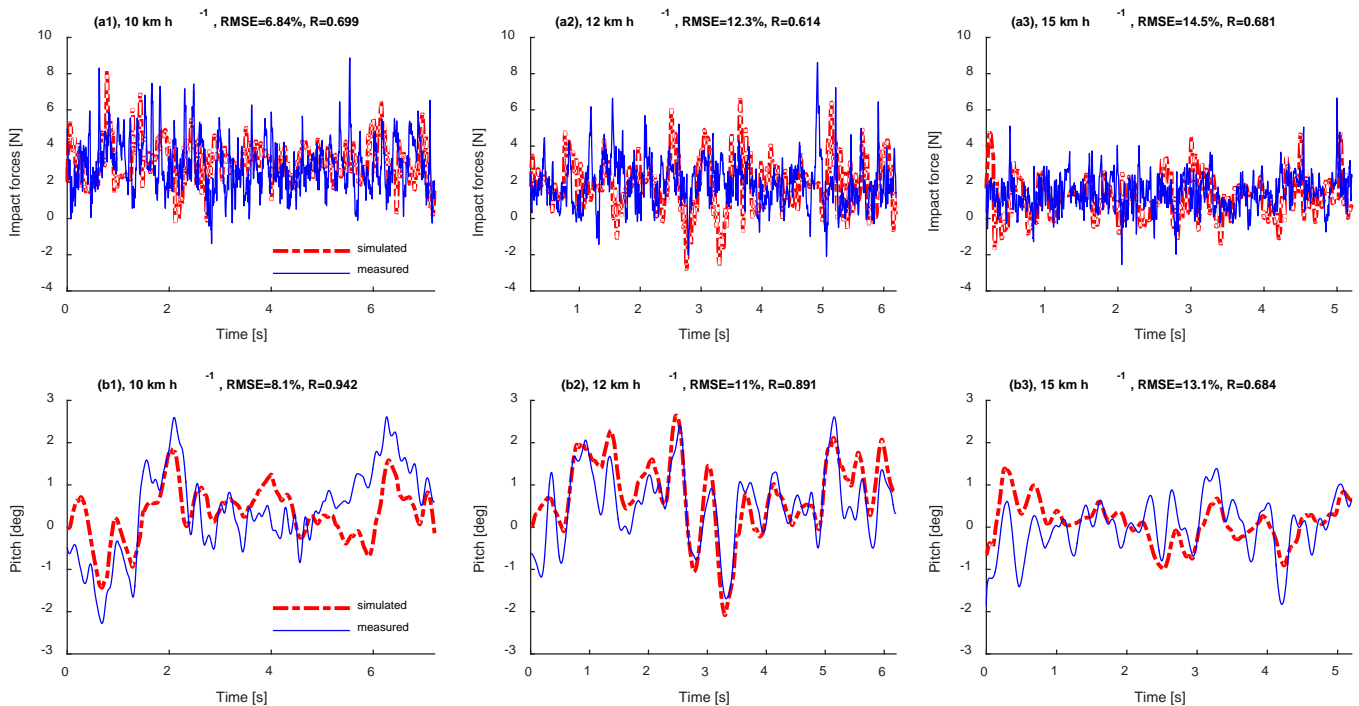


Figure 3.8. The measured and simulated profile impact forces and pitch angles at the speeds of 10 km h<sup>-1</sup> (a1 and b1), 12 km h<sup>-1</sup> (a2 and b2) and 15 km h<sup>-1</sup> (a3 and b3).

The PSDs and the corresponding coherence functions of the measured and simulated impact forces are presented in Figure 3.9. The frequency analyses showed that most of the spatial frequencies

in all data sets were up to  $10 \text{ cycle m}^{-1}$ . The PSDs of the measured and simulated impact forces at  $10 \text{ km h}^{-1}$ ,  $12 \text{ km h}^{-1}$  and  $15 \text{ km h}^{-1}$  speed (Figure 3.9a1, a2 and a3) resulted in a coherence (Figure 3.9b1, b2 and b3) with the maximum values of 0.996, 0.987 and 0.991, respectively. The mean values of coherence at the speeds of  $10 \text{ km h}^{-1}$ ,  $12 \text{ km h}^{-1}$  and  $15 \text{ km h}^{-1}$  were equal to 0.69, 0.672 and 0.67, respectively. These are all above the desired threshold of 0.5 for the coherence. Furthermore, the 60<sup>th</sup> percentile analyses of the coherence revealed the values of 0.643 at  $10 \text{ km h}^{-1}$ , 0.61 at  $12 \text{ km h}^{-1}$  and 0.67 at  $15 \text{ km h}^{-1}$ . This means that 60% of the values in all three data sets of the coherence varied above the desired threshold of 0.5.

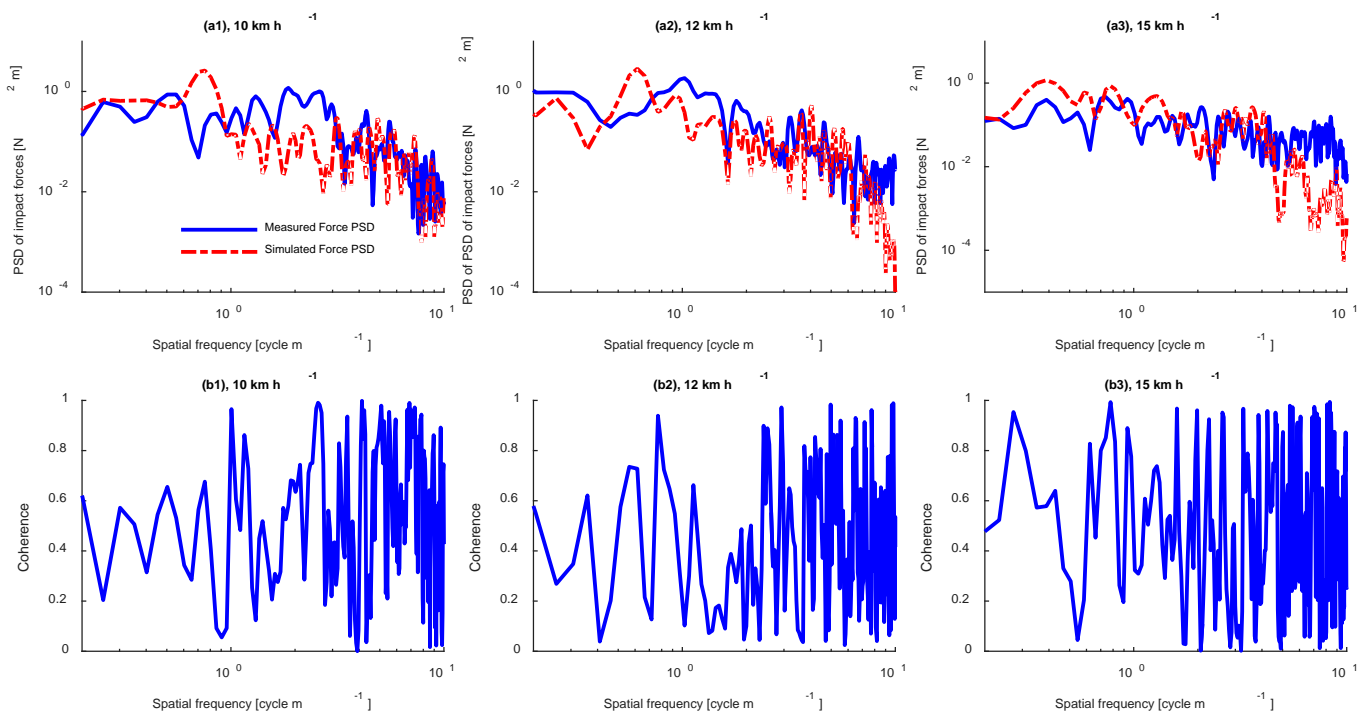


Figure 3.9. PSD of the measured and simulated impact forces (a1, a2 and a3) and the corresponding coherence function (b1, b2 and b3) for the travelling speed of  $10 \text{ km h}^{-1}$ ,  $12 \text{ km h}^{-1}$  and  $15 \text{ km h}^{-1}$ , respectively.

### 3.4.2 Performance of the semi-active MR damper with the applied hysteresis models

Figure 3.10 illustrates the simulated performance, in terms of forces and pitch angles, of the three-hysteresis models characterising the behaviour of the semi-active MR damper system and the coupler model with the rubber packer wheel as a passive system. The calculated MSD (Eq. 3.16) and MDP (Eq. 3.17) for the three-hysteresis models are given in the Table 3.3.

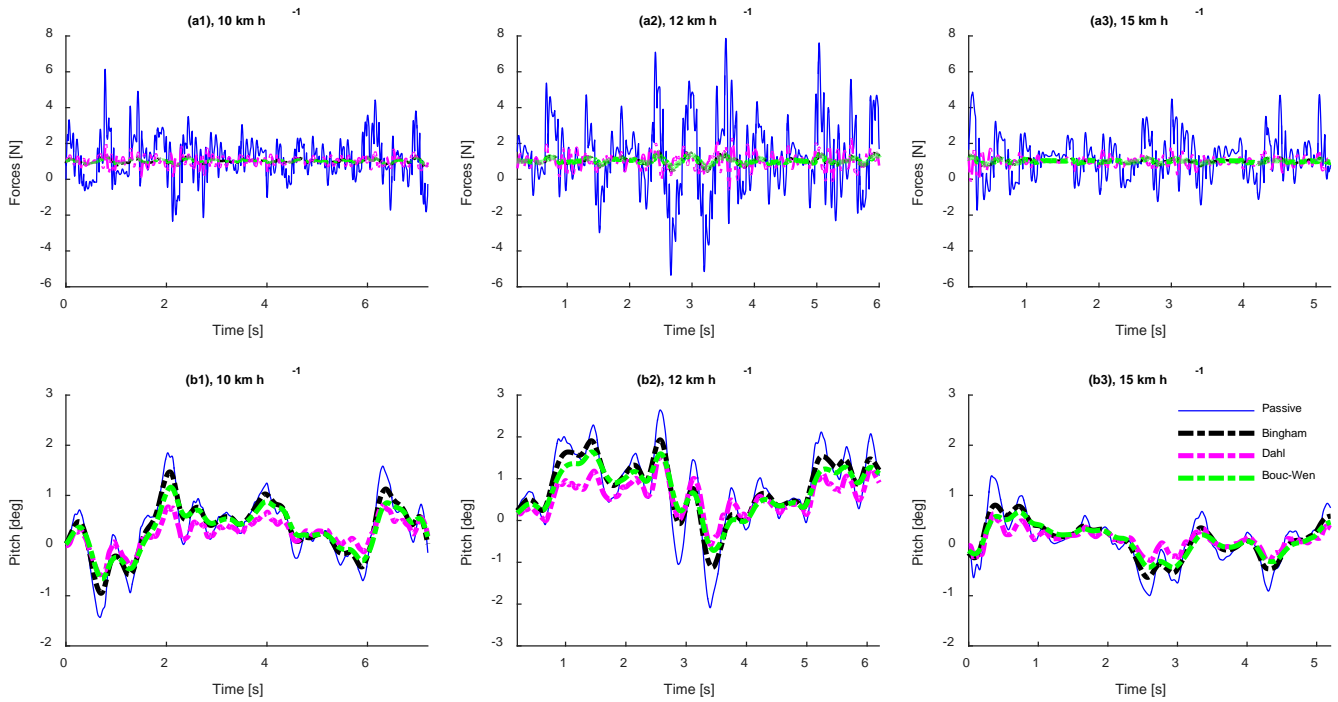


Figure 3.10. Model responses in terms of the (a1, a2 and a3) impact and damped forces and the (b1, b2 and b3) pitch angles for the speed of 10 km h<sup>-1</sup>, 12 km h<sup>-1</sup> and 15 km h<sup>-1</sup>, respectively.

Table 3.3 reveals that all the hysteresis models with the Bingham, Dahl and Bouc-Wen models for the semi-active MR damper outperformed the passive suspension system model. The Bouc-Wen model offered significantly more advantage with a higher percentage of reduction in the amplitude of both the simulated forces (Figure 3.10a1, a2 and a3) and the resulted pitch angles (Figure 3.10b1, b2 and b3) for all three traveling speed (10 km h<sup>-1</sup>, 12 km h<sup>-1</sup> and 15 km h<sup>-1</sup>, respectively) over the other two models. Moreover, a decrease in the amplitude of the forces and the pitch angles at the speed of 10 km h<sup>-1</sup> and 12 km h<sup>-1</sup> was higher in the Bingham model than that in the Dahl model. An interesting result was that the Dahl model performed better in reducing both the forces and the pitch angles amplitude at 15 km h<sup>-1</sup> speed than the Bingham model.

**Table 3.3.** Analysis of the MSD and MDP obtained from the models responses.

Control method	Pitch angle						Impact force					
	Mean Squared			Mean Deviation			Mean Squared			Mean Deviation		
	Deviation (MSD)			Percentage (MDP), [%]			Deviation (MSD)			Percentage (MDP), [%]		
	10	12	15	10	12	15 km	10	12	15	10	12	15 km
km h <sup>-1</sup>	km h <sup>-1</sup>	km h <sup>-1</sup>	km h <sup>-1</sup>	km h <sup>-1</sup>	h <sup>-1</sup>	km	km h <sup>-1</sup>	km h <sup>-1</sup>	km h <sup>-1</sup>	km h <sup>-1</sup>	h <sup>-1</sup>	
1	1	1	1	1	1	h <sup>-1</sup>	1	1	1	1	1	
Bingham	0.143	0.353	0.12	51.2	54.5	25.6	1.12	3.55	2.11	56.9	64	37.8
Dahl	0.14	0.322	0.104	35.7	43.7	28.29	1.16	3.68	2.18	51.12	59.6	38.9
Bouc-Wen	0.189	0.437	0.184	52.3	58.2	38.1	1.18	3.81	2.20	54.1	63.3	41.2

In addition to the analyses of the model performances in the time domain, a qualitative analysis of the forces in the frequency domain was carried out to detect if the forces spectral density confirmed the results of the model responses in the time domain. The computed spectral densities of the forces from all models are presented in Figure 3.11. It can be easily observed that the Bouc-Wen model decreased the values of spectral density in a greater magnitude compared to the Dahl and Bingham models for all three speeds (Figure 3.11a, b and c). In addition, the Bingham model reduced the magnitude of the forces spectral density for 10 km h<sup>-1</sup> and 12 km h<sup>-1</sup> speed more than the Dahl model (Figure 3.11a and b). Conversely, this figure was higher for the Dahl model at the speed of 15 km h<sup>-1</sup> than the Bingham model (Figure 3.11c).



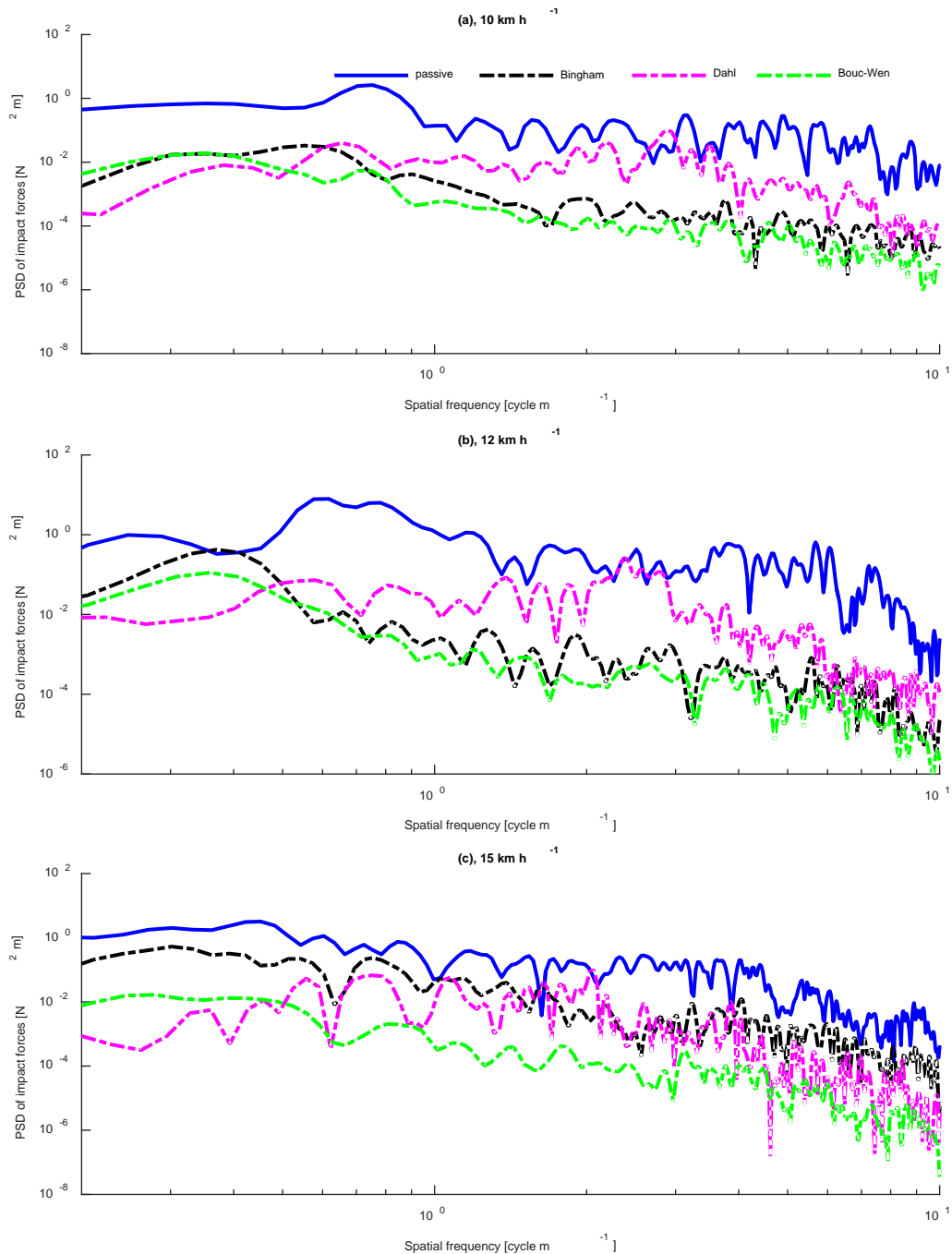


Figure 3.11. PSDs of the forces at  $10 \text{ km h}^{-1}$  (a),  $12 \text{ km h}^{-1}$  (b) and  $15 \text{ km h}^{-1}$  (c) for the passive system and the semi-active MR damper system with the Bingham, Dahl and Bouc-Wen models.

Taking into account the results of both time and frequency domain analyses of the hysteresis models (Bingham, Dahl and Bouc-Wen) performances, the Bouc-Wen model could be more powerful compared to other two models since it takes into account more properties and behaviour of hysteresis effects. Besides our findings, researches carried out by Eshkabilov (2016) and Şahin et al. (2010) verify that the Bouc-Wen model, in terms of better and enhanced control over the useful

characteristics of non-linear features of the MR dampers, performs better than other existing hysteresis models.

### 3.5 Conclusions

The mathematical modelling and simulation of the vertical motion dynamics of the no-till direct seeder coulter assembly with the packer wheel as a passive system and with the semi-active MR damper system were presented. Furthermore, the improvement, in terms of reducing the amplitude of the impact forces and the pitch angles (vertical displacements), in the performance of the coulter assembly with a semi-active MR damper were demonstrated.

The analyses of the RMS errors and the correlation coefficient between the measured and the simulated the impact forces on the packer wheel and the pitch angles of coulter assembly indicated the acceptable performance of the developed coulter assembly model, with the packer wheel as a passive system. The comparative evaluation of the performance of the hysteresis models for the semi-active MR damper against the passive system model demonstrated that the Bouc-Wen model had more adequacy of the MR damper for designing the semi-active suspension system for coulter assembly with the highest reduction in the amplitude, of both the forces and the pitch angles, compared to the other models. Using the defined choice of model and control strategy for the semi-active MR damper, the vertical motion dynamics of the seeder coulter assembly, in terms of vertical displacements and its affecting forces, can be optimised significantly. This would be the main principal in the next steps of our research, where the semi-active MR damper will be implemented into the coulter assembly by defining the optimal values of its performance parameters. The dynamic performance of the coulter assembly with the semi-active MR damper, in terms of precise seeding depth, will be evaluated and compared to the current machine performance without a semi-active MR damper.

### Acknowledgement

The financial support of GA nr 213-2723/001–001–EM Action2 TIMUR (Training of Individuals through Mobility to EU from the Uzbek Republic) project is gratefully acknowledged. The authors would like to thank Ch. Gall from AMAZONEN-WERKE H. Dreyer GmbH & Co.KG (Osnabrück, Germany) and Ch. Schwarze for providing the machine and assisting during the field experiments. The authors also grateful to Dr. Horst Schrogl from Hottinger Baldwin Messtechnik GmbH

(Darmstadt, Germany) for providing the data acquisition system. The project is conducted at the Max-Eyth Endowed Chair (Instrumentation & Test Engineering) at Hohenheim University (Stuttgart, Germany), which is partly grant funded by the Deutsche Landwirtschafts-Gesellschaft (DLG) e.V.

## References

- Abo Al-Kheer, A., Eid, M., Aoues, Y., El-Hami, A., Kharmanda, M.G., Mouazen, A.M., 2011. Theoretical analysis of the spatial variability in tillage forces for fatigue analysis of tillage machines. *J. Terramechanics* 48, 285–295. doi:10.1016/j.jterra.2011.05.002
- Anthonis, J., Mouazen, A.M., Saeys, W., Ramon, H., 2004. An Automatic Depth Control System for Online Measurement of Spatial Variation in Soil Compaction, Part 3: Design of Depth Control System. *Biosyst. Eng.* 89, 59–67. doi:10.1016/j.biosystemseng.2004.06.013
- Braz-Cesar, M.T., Barros, R.C., 2010. Semi-active Vibration Control of Buildings using MR Dampers: Numerical and Experimental Verification . *in: 14th European Conference on Earthquake Engineering. Ohrid, Republic of Macedonia.*
- Burce, M.E.C., Kataoka, T., Okamoto, H., 2013. Seeding Depth Regulation Controlled by Independent Furrow Openers for Zero Tillage Systems - Part 1: Appropriate Furrow Opener. *Eng. Agric. Environ. Food* 6, 1–6. doi:http://dx.doi.org/10.1016/S1881-8366(13)80012-2
- Dahl, P., 1968. A solid friction model, *Aerospace Corporation El Segundo, CA.* doi:TOR-0158(3107-18)-1
- Eshkabilov, S.L., 2016. Modeling and Simulation of Non-Linear and Hysteresis Behavior of Magneto-Rheological Dampers in the Example of Quarter-Car Model. *Eng. Math.* 1, 19–38. doi:10.11648/j.engmath.20160101.12
- Guglielmino, E., Sireteanu, T., Stammers, C.W., Gheorghe, G., Giuclea, M., 2008. Semi-active suspension control. *Springer.* doi:10.1007/978-1-84800-231-9
- Hasimu, A., Chen, Y., 2014. Soil disturbance and draft force of selected seed openers. *Soil Tillage Res.* 140, 48–54. doi:10.1016/j.still.2014.02.011
- Hilton, J., John, N., Field, L., 2011. Estimation of signal coherence threshold and concealed spectral lines applied to detection of turbofan engine combustion noise. *J. Acoust. Soc. Am.* 129. doi:10.1121/1.3546097
- Inman, D.J., 2014. Engineering Vibration, 4th ed, *Upper Saddle River.* doi:10.2307/23499350
- Ismoilov, A., Sellgren, U., Andersson, K., Löfgren, B., 2015. A comparison of novel chassis suspended machines for sustainable forestry. *J. Terramechanics* 58, 59–68. doi:10.1016/j.jterra.2015.01.002

- Lawrance, N.S., 1969. A method of Analyzing Dynamic Responses of A Semi-mounted Farm Implement. *The Ohio State University*.
- Lines, J.A., Murphy, K., 1991. The stiffness of agricultural tractor tyres. *J. Terramechanics* 28, 49–64. doi:10.1016/0022-4898(91)90006-R
- Morrison, J.E., 1987. Interactive Planter Depth Control and Pneumatic Downpressure System. *Power Mach. Div. ASAE* 31(1), 14–18.
- Morrison, J.E., Gerik, T.J., 1985. Planter Depth Control : II . Empirical Testing and Plant Responses. *Trans. ASAE* 28 (6), 1744–1748.
- Ngwangwa, H.M., Heyns, P.S., 2014. Application of an ANN-based methodology for road surface condition identification on mining vehicles and roads. *J. Terramechanics* 53, 59–74. doi:10.1016/j.jterra.2014.03.006
- Paraforos, D.S., Reutemann, M., Sharipov, G., Werner, R., Griepentrog, H.W., 2017. Total station data assessment using an industrial robotic arm for dynamic 3D in-field positioning with sub-centimetre accuracy. *Comput. Electron. Agric.* doi:10.1016/j.compag.2017.03.009
- Rashid, M.M., Rahim, N.A., Hussain, M.A., Rahman, M.A., 2011. Analysis and experimental study of magnetorheological-based damper for semiactive suspension system using fuzzy hybrids. *IEEE Trans. Ind. Appl.* 47, 1051–1059. doi:10.1109/TIA.2010.2103292
- Şahin, İ., Engin, T., Çeşmeci, Ş., 2010. Comparison of some existing parametric models for magnetorheological fluid dampers. *Smart Mater. Struct.* 19, 35012. doi:10.1088/0964-1726/19/3/035012
- Sapiński, B., Filuś, J., 2003. Analysis of parametric models of MR linear damper. *J. Theor. Appl. Mech.* 41, 215–240.
- Shahgoli, G., Fielke, J., Saunders, C., Desbiolles, J., 2010. Simulation of the dynamic behaviour of a tractor-oscillating subsoiler system. *Biosyst. Eng.* 106, 147–155. doi:10.1016/j.biosystemseng.2010.03.002
- Sharipov, G., Paraforos, D., Griepentrog, H., 2017. Modelling and simulation of a no-till seeder vertical motion dynamics for precise seeding depth, in: *Precision Agriculture '17*.
- Sharipov, G., Paraforos, D.S., Pulatov, A., Griepentrog, H.W., 2017. Dynamic performance of a no-till seeding assembly. *Biosyst. Eng.* 158, 64–75. doi:10.1016/j.biosystemseng.2017.03.016
- Suomi, P., Oksanen, T., 2015. Automatic working depth control for seed drill using ISO 11783 remote control messages. *Comput. Electron. Agric.* 116, 30–35. doi:10.1016/j.compag.2015.05.016
- Weatherly, E.T., Bowers, C.G., 1997. Automatic depth control of a seed planter based on soil drying front sensing. *Power Mach. Div. ASAE* 40, 295–305.

# CHAPTER 4

## Paper C

### **Implementation of a magnetorheological damper on a no-till seeding assembly for optimising seeding depth<sup>3</sup>**

Galibjon M. Sharipov\*, Dimitris S. Paraforos, Hans W. Griepentrog

#### **Abstract**

No-till seeding requires a seeder that can effectively cope with the untilled soil and place the seeds at an optimum depth in order to achieve a reliable germination and rapid plant emergence. This aim is more challenging due to the inappropriate response of the machine dynamics to harsh soil conditions, such as the compacted soil undulations and the presence of the stubble. In this paper, a seeder main frame carrying a seed dose mechanism and two no-till seeding assemblies was developed and designed with multiple sensors, to capture the dynamics of the assemblies together with the corresponding surface profile. A magnetorheological (MR) damper was implemented into one of the seeding assemblies to optimise its dynamics for better seed placement. A number of strain gauges were used to measure the dynamics of the seeding assemblies, like vertical and impact forces during seeding operation at a travelling speed of 10 km h<sup>-1</sup>. The accuracy of the surface profile sensing system was validated by obtaining the profile of trapezoidal bumps with a georeferenced dimensions resulting in a root mean squared error of 9.6 mm and 9.9 mm for the damped and undamped seeding assembly, respectively.

Experiments were performed seeding wheat (*Triticum aestivum L.*) operation with a target depth of 40 mm with different damping parameters set on the MR damper by feeding its coil with different current values. The position of each single seed within nine 2 m sections was georeferenced using a total station, to calculate the seeding depth for both seeding assemblies. The seeding assembly with

---

<sup>3</sup> The publication of Chapter 4 is done with the consent of the Elsevier Verlag. The original publication was in: Journal of Computer and Electronics in Agriculture, Vol. 150, pp. 165 – 475. It can be found under the following link: <http://doi.org/10.1016/j.compag.2018.05.024>

the MR damper, excited with 0.5 A, resulted in a better seeding depth variation with a mean value of 39.8 mm, standard deviation of 5.8 mm and 95<sup>th</sup> percentile of 49.8 mm over that of other current values applied on the MR damped and the original seeding assembly. The dynamics were improved with a reduction of 21.34% and 67.69% in the amplitude of the vertical and impact forces, respectively. The seeding depth error compared to the target depth for the damped seeding assembly (at 0.5 A) was less than 11.9 mm for 95% of the samples, while this figure was equal to 21.3 mm for the undamped seeding assembly.

**Keywords:** MR damper, seeding assembly, seeding depth variation, vertical and impact forces

### Nomenclature

$a, b, c$  generic expressions for the translations along  $x, y, z$ - axes, respectively, m

$F_{und,i}$  undamped forces, N

$F_{d,i}$  damped forces, N

$R_{wheel}$  radius of the packer wheel, 0.2 m

$T_p^f$  transformation matrix from the coordinate system of the control prism to the coordinate system of the seeder main frame

$T_f^d$  transformation matrix from the coordinate system of the main frame to the coordinate system of the impact point of the packer wheel of the seeding assembly with the MR damper

$T_f^{au}$  transformation matrix from the coordinate system of the main frame to the coordinate system of the impact point of the packer wheel of the undamped seeding assembly

$x_p, y_p, z_p$  coordinate system of the total station

$x_f, y_f, z_f$  coordinate system of the seeder main frame

$x_{a_d}, y_{a_d}, z_{a_d}$  coordinate system of the ground impact point of the seeding assembly with the MR damper

$x_{a_u}, y_{a_u}, z_{a_u}$  coordinate system of the ground impact point of the undamped seeding assembly

$z_{el}$  measured elevation profile, m

$z_b$  measured bump profile, m

$\alpha$  constant angle between the original assembly arm and the main frame, 0.392 rad

$\omega$  generic expression for the rotation angle over the  $y$ - axis, rad

$\delta$  distance from the control prism to the main frame, 0.21 m

$\eta$  vertical distance from the main frame to the rotating square rod, 0.17 m

$\theta_d$  pitch angle of the seeding assembly with the MR damper, rad

$\theta_u$  pitch angle of the undamped seeding assembly, rad

$\theta_f$  pitch angle of the seeder main frame, rad

$\xi$  distance from the control prism to the laser pointer, 0.39 m

$\varrho$  length of the plate, 0.07 m

$\tau$  distance from the rotating square rod of the main frame to the packer wheel, 1.3 m

$v$  horizontal distance from the main frame to the rotating square rod of the main frame, 1.17 m

$\chi$  measured distance by the laser pointer on the plate, m

#### 4.1 Introduction

The aim in no-till seeding is to disturb the soil as less as possible, to preserve the surface residues, and to place the seeds at a proper depth (Derpsch et al., 2014), which will result in a reliable seed germination and plant emergence. However, harsh soil conditions, like soil undulation and crop residues, increase the difficulty in achieving a constant seeding depth. By measuring the forces that are developed at the interface of the coulter tine, and the vertical movements of the coulter during a seeding operation, the dynamic response of the seeder to the untilled soil undulations and the existing stubble can be determined (Sharipov et al., 2017a; Hasimu and Chen, 2014). Taking into account these forces when controlling the vertical displacement of the coulter and optimising the dynamics, the dynamic performance of the seeder can be significantly improved in order to have a better seed placement. Optimising the dynamics of the seeding assembly by implementing a semi-active magnetorheological (MR) damper, which could reduce the amplitude of those forces leading, thus, to a decrease in vertical displacements of the seeding assembly, would result in a better seed placement. The soil reaction forces resulted from the profile undulations and soil resistance, which are effected by the soil physical properties, influence the mean seeding depth across the coulter width (Fountas et al., 2013). Since the reaction forces describe the dynamics of the seeding component of the seeder, the responses of the seeder to the profile undulations can be expressed by the developed forces (Loghin et al., 2012). In our study, due to the focus on the vertical dynamics of the seeder seeding assemblies, the vertical components of the reaction forces were determined by the vertical and impact forces acting on the coulter tine and the packer wheel, respectively.

Since no-tillage appeared as a part of conservation farming systems, in where the proper seed placement was required while placing the seeds into undisturbed soil (Koller, 2003), many researchers worked on controlling the seeding mechanism for achieving an optimal seeding depth. An early

investigation by Lawrance (1969) introduced an analysis of the dynamic response of a semi-mounted seeding implement to the profile undulations and adjusting the seeding depth based on the dynamic responses. This was followed by Morrison (1978) and (1988) where an automatic seeding depth control was achieved by adjusting the downforces with a hydraulic down pressure system for no-till planters and grain drills. In addition, Morrison and Gerik (1985) presented a depth control for individual furrow-opener units on planters for conservation farming. An advanced control technique for seeding depth was developed and a seeder performance for accuracy and speed response was optimised by Weatherly and Bowers (1997). Burce et al. (2013) adjusted a conventional seeder configuration to a zero tillage and evaluated its performance by implementing an active control system on independent furrow-openers. An automatic control system to assess the performance of a seed drill with disc coulters was developed by Suomi and Oksanen (2015). However, there have been very limited studies on developing a control model of vertical movements of a no-till direct seeder with a semi-active MR damper using the corresponding actual surface profile and the measured reaction forces.

Semi active MR dampers, which are suspensions of magnetically responsive particles in a magnetorheological fluids (Zhu et al., 2012), have rapidly grown in vehicle and civil engineering due to their advantages in design and control. The MR dampers can offer unique dynamic features such as fast response, low and high force capacity, low power consumption, and a simple interface between the electronic input and the mechanical output (Ahamed et al, 2016; Eshkabilov, 2016). Other advantages of the MR dampers are that they produce high yield stress up to 100 kPa, depended on the magnetic field stress, and are very stable within a wide range of temperature (40-150 °C). Despite their aforementioned advantages, there has been no application of an MR damper in no-till seeders aiming to optimise the dynamic responses of the seeder, in terms of a better performance in seed placement.

A previous work by Sharipov et al. (2017b) resulted in a correlation value of 0.6 between the seeder performance, in terms of seeding depth variation, and the dynamic response of the seeder to harsh soil conditions. This value can be regarded as sufficient for this type of complex systems with high in-field dynamics. Data fusion of modern sensors, such as highly accurate robotic total stations, whose accuracy has been tested under realistic conditions (Paraforos et al., 2017), inertial measurement units (IMU), and laser pointers, could provide the means to assess the seeder dynamic performance together with the corresponding seeding depth. Based on the analysis of the correlation between the seeder dynamic response (forces) and the seeding depth variation, the performance of a seeding assembly with a semi-active MR damper was modelled and simulated in our previous study (Sharipov et al., 2017a). The simulation analyses demonstrated significant reduction in the amplitude



of the developed forces which could result in a reduced seeding depth variation. Consequently, the next step forward would be the implementation of the semi-active MR damper into a seeding assembly.

The aim of this paper is to optimise the performance of the seeding assembly, in terms of better seed placement, by implementing an MR damper. The contribution of the present work is the application of an MR damper in no-till seeders, which can reduce the amplitude of the reaction forces resulting in a better performance in seed placement. The seeding depth variation when supplying the MR damper with different supply currents should be compared since an important technical objective is to define the optimum damping parameter (current value) for the MR damper that the seeding assembly achieves its best performance. The dynamics improvement, in terms of amplitude reduction of the vertical and impact forces resulted from the original assembly compared to the produced damped forces by the MR damped implemented assembly should be assessed. In order to validate the performance improvement of the seeding assembly with the MR damper, this should be compared to that of the original seeding assembly under the same operating conditions.

## 4.2 Materials and Methods

### 4.2.1 Developed no-till seeding prototype

A machine prototype was developed comprising a metal frame that carried a Green Drill 200 seed dosing mechanism and two ConTeC Schare no-till seeding assemblies (both from AMAZONEN-Werke H. Dreyer GmbH & Co. KG, Hasbergen, Germany) (Fig. 4.1a). The frame had two side-wheels in a parallelogram assemblage while the height from the ground could be manually configured. The seed dosing mechanism consisted of a 200 l volume hopper and a seed shaft located inside the metering unit below the hopper. The seed shaft was driven by an electric motor powered by the tractor and could be equipped with different seed-metering wheels depending on the seed type and application rates. In our case, a seed-metering wheel for wheat (*Triticum aestivum* L.) was employed. A dedicated in-cab control terminal was responsible for configuring the seed rate, the speed of the seed shaft and the power to the motor. The two seeding assemblies had a 0.25 m inter-row distance and were attached to a rotating square rod controlled by a hydraulic cylinder. The hydraulic cylinder provided down pressure, which was applied on the two seeding assemblies with a value of 6.89 MPa.

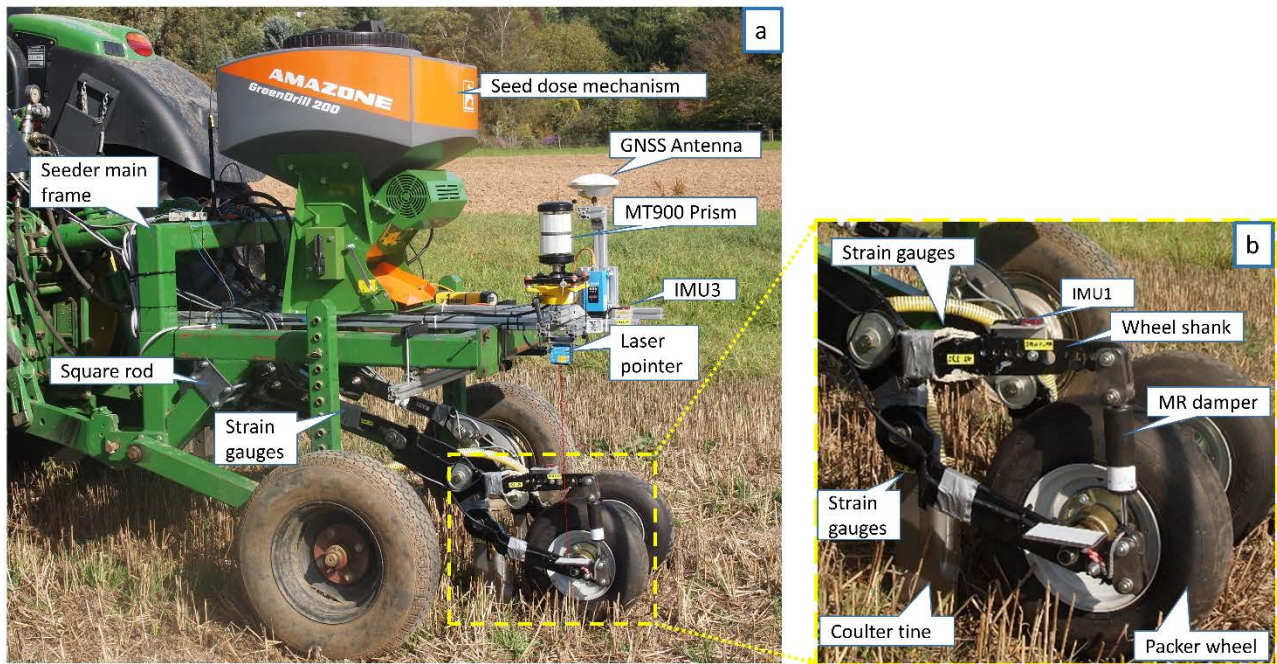


Figure 4.1. (a) The developed prototype with the seed-metering system, the two no-till seeding assemblies and the utilized sensors, and (b) the implemented MR damper in-between the wheel shank and the packer wheel.

To determine the traversed field surface profile of both seeding assemblies and to capture the developed machine dynamics, such as forces and tilting information, all necessary sensors were installed on the seeder main frame and the two seeding assemblies (Fig. 4.1a and b). To produce the surface profiles of the packer wheels on the ground impact point, the in-field absolute geo-referenced position of the seeder main frame was acquired using an SPS930 total station (Trimble, Sunnyvale, CA, USA) tracking a Trimble MT900 machine control prism fixed on the seeder main frame. In addition, an AgGPS 542 RTK-GNSS (Trimble, Sunnyvale, USA) was used to indicate in-field position of the seeder. A DT50 laser range finder (SICK AG, Waldkirch, Germany) detected the displacement of the seeding assembly with the MR damper relative to the main frame. Three VN-100 inertial measurement units (IMUs) (VectorNav, Dallas, TX, USA), one on the seeder main frame, and the other two fixed to the seeding assemblies, were used to gather real-time tilt information (roll-pitch-yaw) of the seeder main frame and the seeding assemblies, respectively. To determine the vertical and profile impact forces, the strains resulted from the loads on the coulters and the packer wheels were recorded using six linear 350 Ohm DY41-1.5 strain gauges (HBM GmbH, Darmstadt, Germany) in a full-bridge configuration, attached at the critical points on the coulters assemblies. More details about the sensors and the data acquisition system can be found in Sharipov et al. (2017b).

### 4.2.2 Semi-active MR damper specifications

To reduce the effect of the vertical and profile impact forces that are the main reason of excessive vertical movements of the seeding assembly, a RD-8040-1 MR damper (LORD, Baltimore, USA) was implemented on one seeding assembly between the wheel shank and the packer wheel. This was performed using an extra shank and a bearing system as indicated in Figure 4.1b. The technical properties of the MR damper are given in Table 4.1. The MR damper consists of a cylinder, a piston, an excitation coil and the MR fluid which is flowing from a high-pressure chamber to a low-pressure chamber in the piston head. A magnetic field in the flow path, which is a function of the excitation current, is applied using a copper coil that is wound around the piston body. The leads of the coil are taken out through the piston rod to provide the coil with the variable current, in order to generate the variable magnetic field, which in turn produces the variable damping effect.

**Table 4.1.** Technical properties of RD-8040-1 MR damper

Property	Value	Unit
Extended length	208	mm
Compressed length	153	mm
Body diameter	42.1	mm
Shaft diameter	10	mm
Input voltage (DC)	12	V
Input Current		
Continuous	1	A
Intermittent	2	A
Coil resistance		
Ambient temperature	5	$\Omega$
At 71 °C	7	$\Omega$
Force (peak to peak)	> 2447 (50 mm sec <sup>-1</sup> at 1 A) < 667 (200 mm sec <sup>-1</sup> at 0 A)	N N
Operating temperature	71	°C
Response time	< 15	ms

During the experiments, the variable damping ratio was controlled by the changes in the currents applied as the magnetic field in the flow path of the MR fluid using a controlling device from the damper manufacturer (Wonder box, LORD, Baltimore, USA). The device provided closed loop current control to compensate for changing electrical loads up to the physical limits of the power supply. More detailed information about the control strategy and the performance of the MR damper can be found in Sharipov et al. (2017a).

### 4.2.3 Validation of the surface profile sensing system

The developed sensor system and the methodology for measuring the surface profiles was tested by traversing the two seeding assemblies over wooden trapezoidal bumps. Measuring the profile of trapezoidal bumps is a common methodology for validating profile measuring systems (Paraforos et al., 2016; Sharipov et al., 2017b). In order to have the bump dimensions (Fig. 4.2) in the same coordinate system as the measured profiles, and to ease post-processing, the profiles of the bumps were acquired using the total station and the target prism. The bumps were firmly attached on the terrain using a metal pin, to avoid sliding motion when the wheel of the seeding assembly was traversing them.

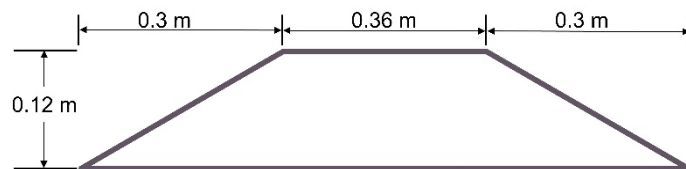


Figure 4.2. A descriptive dimensions of the trapezoidal bump.

The accuracy of the developed sensor-frame was evaluated along the length of the trapezoidal bumps, based on the Root-Mean-Squared (RMS) error between the elevation profile and the trapezoidal bumps profile. The RMS error was calculated using the following equation:

$$RMS_{error} = \sqrt{\frac{\sum_{i=1}^n (z_{el,i} - z_{b,i})^2}{n}} \quad (4.1)$$

where  $z_{el,i}$  is the elevation profile and  $z_{b,i}$  is the bump profile for the  $i$ th point, and  $n$  is the number of the measured points for each profile.

## 4.2.4 Experiments

### 4.2.4.1 Seeder dynamics and surface profile measurements

Field experiments while seeding wheat were performed to acquire the surface profiles and the machine dynamic parameters, such as tilting information, vertical displacements and developed forces (vertical, draught and profile impact forces arising at the interaction points of the coulter and the packer wheel with the soil). Six trials with six different current input levels 0 A, 0.1 A, 0.3 A, 0.5 A, 0.7 A and 1 A applied on the coil of the MR damper, were carried out with a constant operation

speed of  $10 \text{ km h}^{-1}$  (yellow coloured paths in Figure 4.3). For all dynamic measurements, the target seeding depth was set to 40 mm.

Nine sections of 2 m length each (green coloured S1-S9 sections in Figure 4.3), were selected to measure the seed positions, in order to examine the dynamics of both seeding assemblies together with the corresponding seeding depth. In these nine sections, after performing the seeding operation, a measurement was set up to geo-reference the position of every single seed and thus, to extract the absolute seeding depth for both seeding assemblies with and without the MR damper. Regarding the damped seeding assembly, the sections from S1 to S6 denote the paths of the seeder with a current input of 0 A, 0.1 A, 0.3 A, 0.5 A, 0.7 A and 1 A, respectively. The other three sections S7-S9 were the repetitions of the sections S2-S4 (0.1 A, 0.3 A and 0.5 A), respectively, and belonged to the same row. The repetition of only S2-S4 sections was carried out due to the interest in the performance of seeding assembly with the MR damper at 0.1 A, 0.3 A and 0.5 A, based on the simulation results from our previous work (Sharipov et al., 2017a). For the undamped seeding assembly, all nine sections were considered as repetitions of the original seeding assembly without an MR damper.

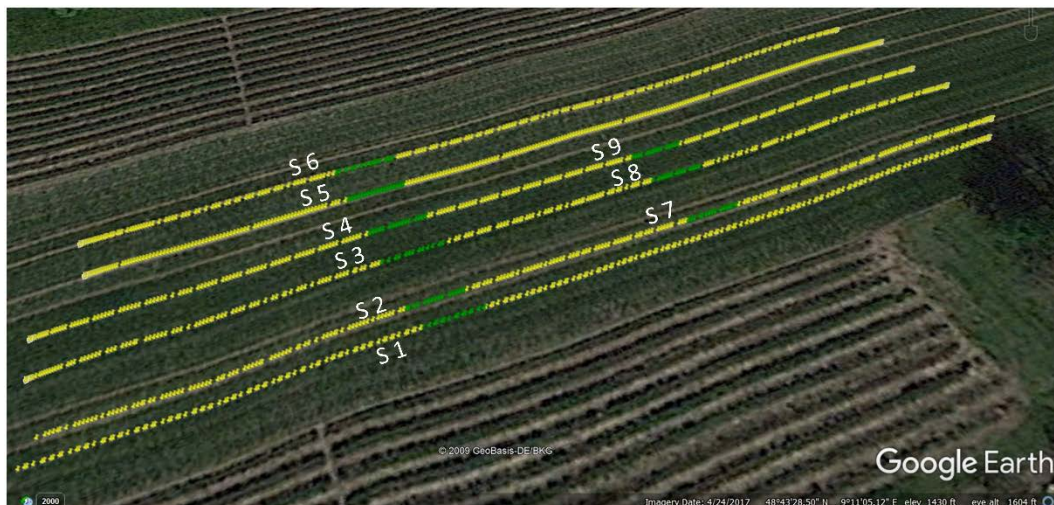


Figure 4.3. Satellite image of the field where the measurements were performed. The yellow dots indicate the position of the GNSS antenna that was attached on the sensor-frame (six paths). For sections S1 to S9 (green coloured) the positions of the seeds were geo-referenced (using the total station) for both examined seeding assemblies (damped and undamped). For the seeding assembly with the MR damper at the sections S1, S2, S3, S4, S5 and S6 the MR damper was supplied with a constant current of 0 A, 0.1 A, 0.3 A, 0.5 A, 0.7 A and 1 A, respectively. The sections S7, S8 and S9 are the replicates of the sections S2, S3 and S4.

The 300 Hz sampling rate of the strain gauges data allowed to calculate the vertical forces and the surface impact forces around every 9 mm. The IMUs and the total station outputted data with a



frequency of 50 Hz and 20 Hz, respectively. The laser pointer DT50 on the damped assembly produced data with a frequency of 62 Hz, which made possible to obtain the vertical displacements every 44 mm (considering the 10 km h<sup>-1</sup> driving speed). However, the laser pointer DT500 was not employed, due to its very low sampling rate. Instead, the vertical displacement of the seeding assembly without the MR damper was extracted using IMUs data. Due to the different sampling rates of the sensors, the measurement data was non-concurrent. Therefore, the measurement values in concurrent time instances were determined using the interpolation method based on their individual timestamps.

#### 4.2.4.2 Georeferenced seed positions

Before performing the seeding operation, the seeding dose mechanism of the seeder was calibrated using the in-cab terminal. Considering the constant operation speed of 10 km h<sup>-1</sup>, a seeding rate was set to 5.2 kg ha<sup>-1</sup>, which corresponded to around 284.8 seeds m<sup>-2</sup>. In each section (Fig. 4.3, sections S1-S9), two parallel 2 m furrows that were traversed by the seeding assemblies with and without the MR damper were carefully opened by hand without disturbing the seeds position on the seedbed, to reveal seeds in each furrow. Subsequently, 40 seeds in each furrow with a seed-to-seed distance of 5 cm were selected to georeference their position. The total station tracking a MT1000-G prism (Trimble, Sunnyvale, CA, USA) on a 2 m pole, provided every seed georeferenced 3D position with the accuracy of  $\pm 2$  mm + 2 ppm in the same coordinate system as the acquired surface profile (Fig. 4.4).



Figure 4.4. Measurement for geo-referenced seed positions.

#### 4.2.4.3 *Site characteristics*

All field experiments were carried out at the agricultural research station of the University of Hohenheim (48°43'27.34" N, 9°11'07.68" E). The soil at the field was a loess-derived stagnic luvisol with silty loam-texture (pH 7.0, organic carbon content 12.1 g kg<sup>-1</sup>) (Poll et al., 2013). The pre-crop in the field from the previous year was also wheat. The measured stubble density was 186 plant-stems per m<sup>2</sup> with an average height of 0.164 m. Soil samples were taken at twelve points of the field with 0.2 m depth to define an average bulk density and gravimetric moisture of the soil. The average bulk density and the moisture content were 1.16 g cm<sup>3</sup> and 21%, respectively.

### 4.3 Theory

#### 4.3.1 Determination of forces and surface profiles

The recorded strains at the three points of the seeding assembly were used to calculate the vertical forces and draught forces acting on the point of coulter interacting with soil, and the profile impact forces at the impact point of the packer wheel. The detailed formulas of calculating all these forces are given in Sharipov et al. (2017b). To extract the surface profiles, the required transformations from the prism, tracked by the total station, to the ground impact point of the packer wheels were performed (Fig. 4.5). Due to the additional degree of movement freedom resulted from the extra shank of the damped seeding assembly (Fig. 4.5a and b), the transformation method for the damped seeding assembly was unlike that for the undamped one (Fig. 4.5c and d).

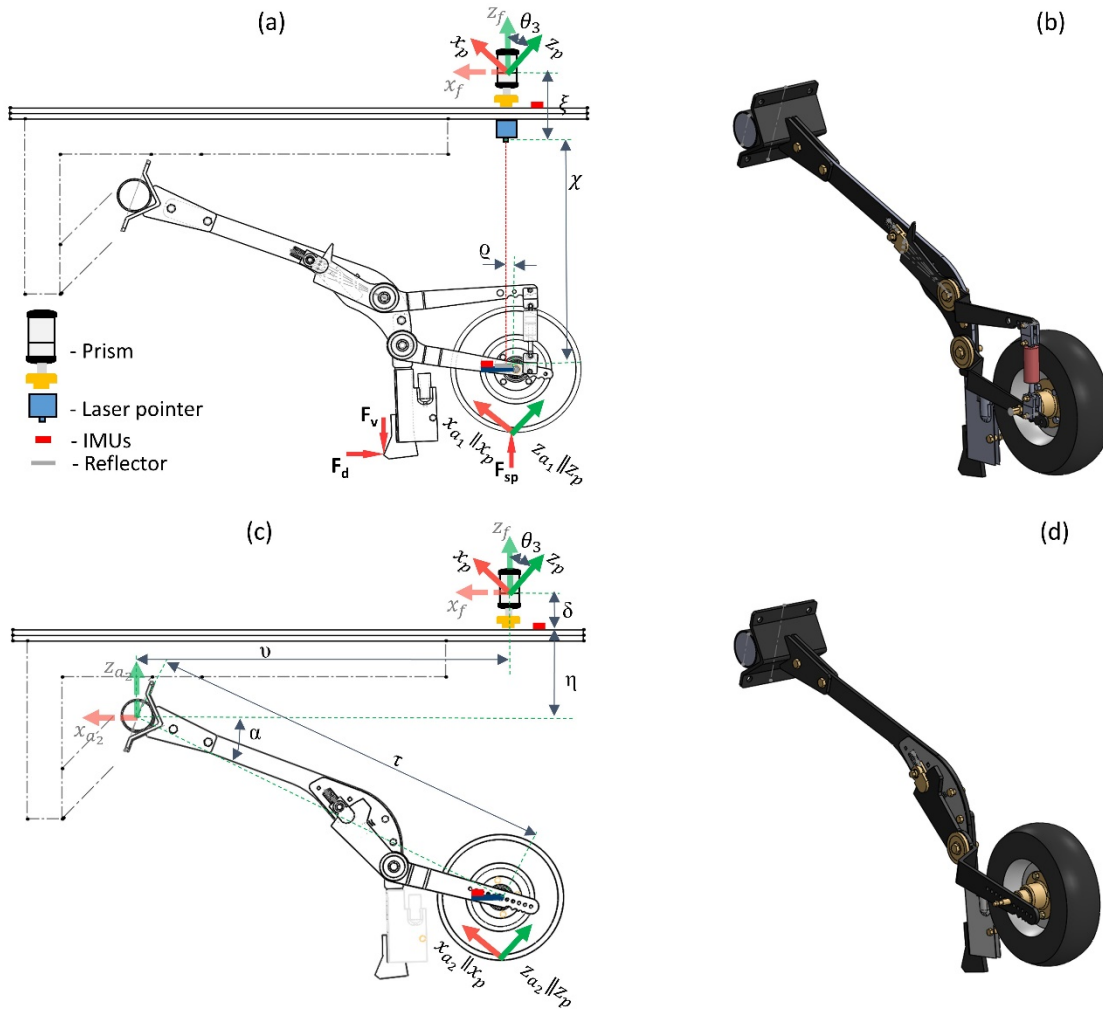


Figure 4.5. Schematic and 3D view of the (a and b) damped and (c and d) undamped seeding assemblies and the seeder main frame. The dimensions for the necessary transformations to calculate the traversed surface profiles are also indicated.

Since only the vertical position of the seeding assemblies relative to the surface profile was the focus of the study, only the rotations on the  $y$ -axis (pitch) were examined. Nevertheless, the necessary translations were performed along all three axes ( $x, y, z$ ). In the initial step of the transformation, the provided pitch ( $\theta_f$ ) from IMU-3, which was attached on the seeder main frame, was engaged to rotate the coordinate system of the control prism ( $x_p, y_p, z_p$ ) to the coordinate system of the seeder main frame ( $x_f, y_f, z_f$ ):

$$[x_f \ y_f \ z_f \ 1]^T = [T_p^f] \times [x_p \ y_p \ z_p \ 1]^T \quad (4.2)$$



where  $T_p^f = Rot(y_p, \theta_f)$  is the transformation matrix from the coordinate system of the control prism to the coordinate system of the seeder main frame. This required a rotation over the  $y_p$ - axis with an angle of  $\theta_f$ .

The transformation from the coordinate system of the main frame to the coordinate system of the impact point of the packer wheel ( $x_{a_d}, y_{a_d}, z_{a_d}$ ) of the seeding assembly with the MR damper was implemented as follows:

$$[x_{a_d} \ y_{a_d} \ z_{a_d} \ 1]^T = [T_f^{a_d}] \times [x_f \ y_f \ z_f \ 1]^T \quad (4.3)$$

where  $T_f^{a_1}$  is the transformation matrix resulted from the translations using the known dimensions  $\xi$ ,  $R_{wheel}$ ,  $\varrho$  and the vertical displacement  $\chi$  of the seeding assemblies detected by the laser pointer and the rotations with the pitch information from both IMU-3 ( $\theta_f$ ) and IMU-1 ( $\theta_d$ ). The following equation can be employed for the sequence of all required rotations and translations:

$$\begin{aligned} T_f^{a_d} &= Trans(z_f, -\xi - \chi) \cdot Rot(y_f, -\theta_f) \cdot Rot(y_{a_d}, \theta_d) \cdot Trans(x_{a_d}, -\varrho) \cdot \\ &Trans(x_{a_d}, -R_{wheel}) \cdot Rot(y_{a_d}, -\theta_d) = \begin{bmatrix} 1 & 0 & 0 & 0 \\ 0 & 1 & 0 & 0 \\ 0 & 0 & 1 & -\xi - \chi \\ 0 & 0 & 0 & 1 \end{bmatrix} \cdot \begin{bmatrix} \cos(-\theta_f) & 0 & -\sin(-\theta_f) & 0 \\ 0 & 1 & 0 & 0 \\ \sin(-\theta_f) & 0 & \cos(-\theta_f) & 0 \\ 0 & 0 & 0 & 1 \end{bmatrix} \cdot \\ &\begin{bmatrix} \cos(\theta_d) & 0 & -\sin(\theta_d) & 0 \\ 0 & 1 & 0 & 0 \\ \sin(\theta_d) & 0 & \cos(\theta_d) & 0 \\ 0 & 0 & 0 & 1 \end{bmatrix} \cdot \begin{bmatrix} 1 & 0 & 0 & -\varrho \\ 0 & 1 & 0 & 0 \\ 0 & 0 & 1 & 0 \\ 0 & 0 & 0 & 1 \end{bmatrix} \cdot \begin{bmatrix} 1 & 0 & 0 & -R_{wheel} \\ 0 & 1 & 0 & 0 \\ 0 & 0 & 1 & 0 \\ 0 & 0 & 0 & 1 \end{bmatrix} \cdot \\ &\begin{bmatrix} \cos(-\theta_d) & 0 & -\sin(-\theta_d) & 0 \\ 0 & 1 & 0 & 0 \\ \sin(-\theta_d) & 0 & \cos(-\theta_d) & 0 \\ 0 & 0 & 0 & 1 \end{bmatrix} \end{aligned} \quad (4.4)$$

Regarding the undamped seeding assembly the main frame coordinate system was shifted to the ground impact point ( $x_{a_u}, y_{a_u}, z_{a_u}$ ) of the packer wheel using the following equation:

$$[x_{a_{u2}} \ y_{a_{u2}} \ z_{a_{u2}} \ 1]^T = [T_f^{a_u}] \times [x_f \ y_f \ z_f \ 1]^T \quad (4.5)$$

where  $T_f^{a_u}$  is the final transformation matrix produced by the translations using the known dimensions  $\delta$ ,  $\eta$ ,  $\nu$ ,  $\tau$ , and  $R_{wheel}$ , and the rotations with the pitch information from IMU-3 ( $\theta_f$ ) and IMU-2 ( $\theta_u$ ), and the constant angle  $\alpha$  between the original assembly arm and the main frame. All the required rotations and translations required for (4.5) can be expressed as follows:

$$\begin{aligned} T_f^{a_u} &= Trans(z_f, -\delta - \eta) \cdot Trans(x_f, \nu) \cdot Rot(y_f, -\theta_f) \cdot Rot(y_{a_u}, \theta_u) \cdot Rot(y_f, -\alpha) \cdot \\ &Trans(x_{a_u}, -\tau) \cdot Trans(x_{a_u}, -R_{wheel}) \cdot Rot(y_f, \alpha) \cdot Rot(y_{a_u}, -\theta_u) = \begin{bmatrix} 1 & 0 & 0 & 0 \\ 0 & 1 & 0 & 0 \\ 0 & 0 & 1 & c - \delta - \eta \\ 0 & 0 & 0 & 1 \end{bmatrix} \cdot \end{aligned}$$

$$\begin{aligned}
& \begin{bmatrix} 1 & 0 & 0 & v \\ 0 & 1 & 0 & 0 \\ 0 & 0 & 1 & 0 \\ 0 & 0 & 0 & 1 \end{bmatrix} \cdot \begin{bmatrix} \cos(\omega - \theta_f) & 0 & -\sin(\omega - \theta_f) & 0 \\ 0 & 1 & 0 & 0 \\ \sin(-\theta_f) & 0 & \cos(-\theta_f) & 0 \\ 0 & 0 & 0 & 1 \end{bmatrix} \cdot \begin{bmatrix} \cos(\theta_u) & 0 & -\sin(\theta_u) & 0 \\ 0 & 1 & 0 & 0 \\ \sin(\theta_u) & 0 & \cos(\theta_u) & 0 \\ 0 & 0 & 0 & 1 \end{bmatrix} \cdot \\
& \begin{bmatrix} \cos(-\alpha) & 0 & -\sin(-\alpha) & 0 \\ 0 & 1 & 0 & 0 \\ \sin(-\alpha) & 0 & \cos(-\alpha) & 0 \\ 0 & 0 & 0 & 1 \end{bmatrix} \cdot \begin{bmatrix} 1 & 0 & 0 & -\tau \\ 0 & 1 & 0 & 0 \\ 0 & 0 & 1 & 0 \\ 0 & 0 & 0 & 1 \end{bmatrix} \cdot \begin{bmatrix} 1 & 0 & 0 & -R_{wheel} \\ 0 & 1 & 0 & 0 \\ 0 & 0 & 1 & 0 \\ 0 & 0 & 0 & 1 \end{bmatrix} \cdot \\
& \begin{bmatrix} \cos(\alpha) & 0 & -\sin(\alpha) & 0 \\ 0 & 1 & 0 & 0 \\ \sin(\alpha) & 0 & \cos(\alpha) & 0 \\ 0 & 0 & 0 & 1 \end{bmatrix} \cdot \begin{bmatrix} \cos(-\theta_u) & 0 & -\sin(-\theta_u) & 0 \\ 0 & 1 & 0 & 0 \\ \sin(-\theta_u) & 0 & \cos(-\theta_u) & 0 \\ 0 & 0 & 0 & 1 \end{bmatrix} \quad (4.6)
\end{aligned}$$

### 4.3.2 Dynamics assessment criteria

In order to make a quantitative evaluation of the differences between the vertical and the impact forces from the seeding assemblies with and without the MR damper, the mean squared deviation (MSD) and mean deviation percentage (MDP) performance criteria were analysed. The MSD measured the average of the squared deviations of the damped vertical and impact forces from that of undamped ones. The MDP evaluated the improvement percentage, i.e. the decrease in the amplitude of the damped forces compared to that of the undamped ones. The expressions of the MSD and MDP were expressed as

$$MSD = \frac{1}{N} \sum_{i=1}^N (F_{und,i} - F_{d,i})^2 \quad (4.7)$$

$$MDP = \frac{1}{N} \sum_{i=1}^N \left| \frac{F_{und,i} - F_{d,i}}{F_{und,i}} \right| \times 100\% \quad (4.8)$$

where  $F_{und,i}$  is the undamped forces (vertical and impact force) obtained from the original seeding assembly and  $F_{d,i}$  is the damped forces from the seeding assembly with the MR damper for distance instance  $i$ .

## 4.4 Results and discussion

### 4.4.1 Profile sensing system validation

The elevation profiles of the seeding assemblies traversing the trapezoidal bumps were calculated by implementing the Eqs. (4.4) and (4.6). In Fig. 4.6, the profile of the trapezoidal bumps and the obtained profiles of seeding assemblies for the speed of 10 km h<sup>-1</sup> are presented. Using Eq. (4.1),

the RMS errors between the elevation profiles and the profiles of the bumps profile were evaluated. The profile of the seeding assembly with the MR damper as it was compared to the profiles of the bumps indicated an RMS error of 9.6 mm and a maximum absolute error of 12.4 mm. These figures were equal to 9.9 mm and 13.2 mm for the profile of the undamped seeding assembly. Taking into account the resulted errors and the packer wheel diameter of 400 mm, the accuracy of the sensor system was regarded as adequate for measuring the field surface profiles.

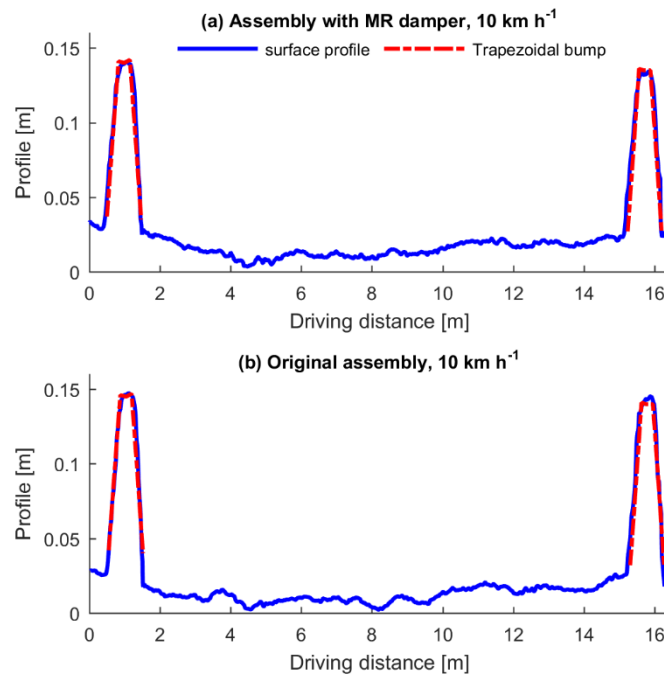


Figure 4.6. Elevation profiles of the two seeding assemblies (a) with the MR damper and (b) the original one (undamped) traversing two trapezoidal bumps with a travelling speed of  $10 \text{ km h}^{-1}$ .

#### 4.4.2 Performance of the seeding assemblies

In order to detect the current value to the MR damper that gave the best results in terms of seeding depth, the latter was evaluated for all six 2 m S1-S6 sections (Fig. 4.3). The georeferenced seed positions together with the corresponding surface profile, as these were determined using Eq. (4.3) and (4.5), are illustrated in Fig. 4.7a1-a6. The calculated seeding depths of the measured seeds position are represented in Fig. 4.7b1-b6.

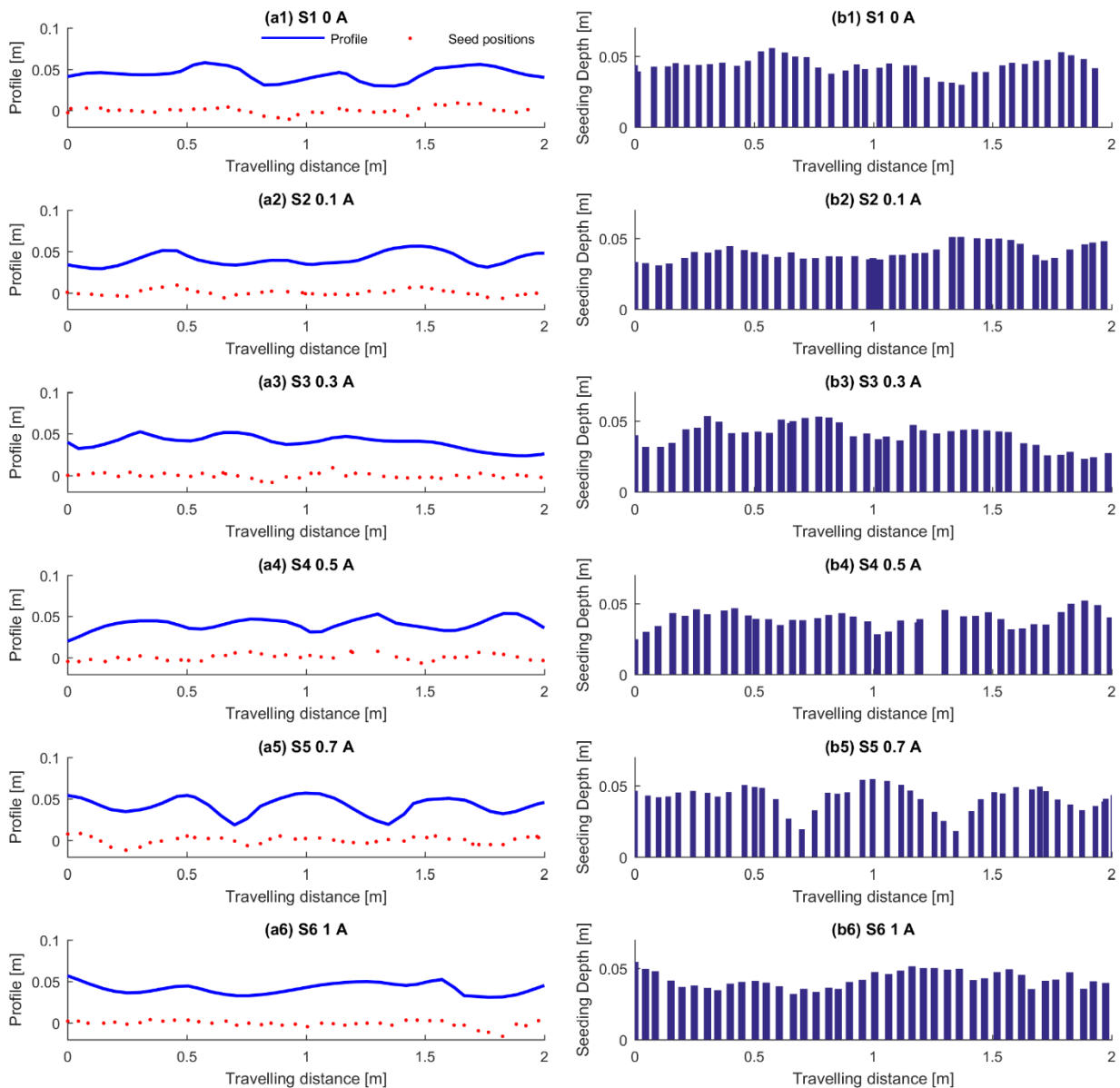


Figure 4.7. (a1-a6) Seed positions with the corresponding surface profile of the seeding assembly with the MR damper and (b1-b6) the resulted seeding depths of the measured seeds.

The summary statistics of all damped seeding depth variations resulted from the performances of the seeding assembly with MR damper are presented in Table 4.2. Comparing the mean values of the damped seeding depth datasets at 0 A, 0.1 A, 0.3 A, 0.5 A, 0.7 A and 1 A to the target seeding depth, a discrepancy of 3.8 mm, 7 mm, 3 mm, 2 mm, 4 mm and 3.1 mm, respectively, was noticed. The smallest discrepancy with the value of 2 mm belonged to section S4 where the MR damper was supplied with 0.5 A on the coil. In section S4, the standard deviation with a value of 5.6 mm was also the smallest one compared to that of all other datasets. Furthermore, the 95% samples of the dataset

at 0.5 A varied below the value of 49.2 mm, which was the closest one to the target seeding depth among all datasets.

**Table 4.2.** Statistics of the damped seeding depth variations.

Type/Unit	Damped (mm)					
Section/Current	S1 - 0 A	S2 - 0.1 A	S3 - 0.3 A	S4 - 0.5 A	S5 - 0.7 A	S6 - 1 A
Mean value	43.8	40.7	40.3	39.8	44	43.1
St. deviation	5.7	5.6	8.4	5.6	8.3	5.9
95 <sup>th</sup> percentile	53.2	50.5	52.6	49.2	53.5	51.7
Min	29.9	31	23.4	24.7	18.3	32.1
Max	55.9	51.1	53.4	52	54.7	54.6

In addition to the above-given statistical analyses, the box plots for all the datasets of the damped seeding depth were produced using MATLAB's *boxplot* function (Fig. 4.8), to display the distribution of each dataset. In these box plots, the central rectangle spans from the 25<sup>th</sup> percentile up to the 75<sup>th</sup> percentile while the segment inside the rectangle shows the median. The "whiskers" above and below the box extend to the most extreme data values (approximately  $\pm 2.7\sigma$  when data follow a Gaussian distribution) of the damped seeding depth variations. The red crosses illustrate the outliers. From Figure 4.8 it can be seen that the smaller variation belonged to the datasets of the sections S1 (0 A), S4 (0.5 A) and S5 (0.7 A) with a 25<sup>th</sup> percentile of 41.5 mm, 36.2 mm and 39.9 mm, and a 75<sup>th</sup> percentile of 46.8 mm, 43.2 mm and 46.5 mm, respectively. Conversely, the section S2 (0.1 A), S3 (0.3 A) and S6 (0.7 A) indicated the higher variation with a 25<sup>th</sup> percentile of 36.2 mm, 34.3 mm and 37.9 mm, and a 75<sup>th</sup> percentile of 45.9 mm, 45.2 mm and 48.9 mm, respectively. Compared to the median of all datasets, the median of the dataset from the sections S2 (0.1 A) and S4 (0.5 A) with a value of 39.8 mm and 39.5 mm, respectively, were the closest ones to the target seeding depth. Based on these analyses, section S4 (0.5 A) can be regarded as where the seeding assembly with the MR damper outperformed.

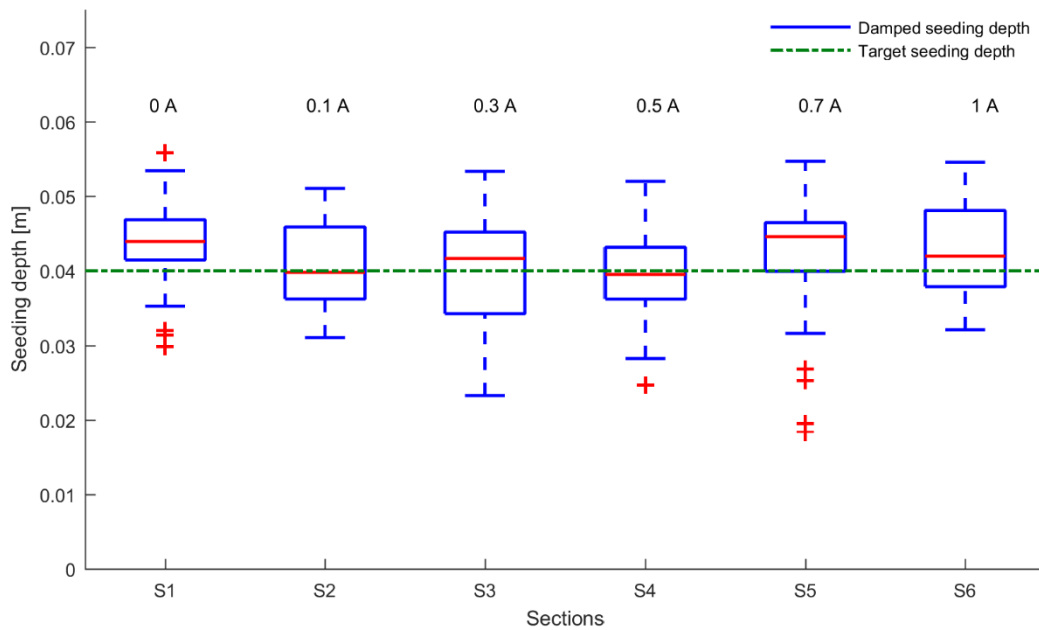


Figure 4.8. Boxplots for all the datasets of the damped seeding depth variations with the operation speed of  $10 \text{ km h}^{-1}$ . The target seeding depth of 40 mm for the performed experiments is also indicated.

The statistics of the defined datasets of the damped seeding depth variation in section S4 were compared with its replicate in section S9, to check if they confirm each other. The comparison confirmed that there were negligible discrepancies with the values of 0.3 mm, 0.1 mm and 1.4 mm between the mean values, standard deviations and the 95<sup>th</sup> percentiles, respectively (Table 4.3). This means that in both measurements, the variation of the seeding depth was evenly close to the target seeding depth value. From all above-highlighted statistical and boxplots analyses, it can be concluded that the seeding assembly with the MR damper at 0.5 A offered a more precise seeding depth over the other values of current applied on the coil of the MR damper.

The next step was to compare the defined best-damped seeding depth variations in S4 with the best of all undamped seeding depth variations among sections from S1 to S6. Therefore, the statistical analyses of the undamped seeding depth variations in all sections are presented in Table 4.3. The comparison analyses indicated that the mean values of all undamped seeding depth variations in sections S1, S2, S3, S4, S5 and S6 were noticeably higher with a difference of 4.7 mm, 4.2 mm, 3.6 mm, 4.4 mm, 5.4 mm and 5.1 mm, respectively, than the mean value of the damped seeding depth variation in section S4 (0.5 A). The 95<sup>th</sup> percentile with a difference of 4.2 mm, 0.8 mm, 8.8 mm, 14 mm, 18.9 mm and 12 mm, for sections S1-S6, respectively, followed this pattern. The standard deviation of the undamped seeding depth variation in sections S1 and S2 with a discrepancy of 0.1

and 1 mm were quite similar to the standard deviation of the damped seeding depth variation in S4. However, these figures with a difference of 4.6 mm, 7.8 mm and 3.1 mm for the sections S4, S5 and S6, respectively, were much higher than that of the damped seeding depth variation in S4. It has to be noticed that in our previous work (Sharipov et al., 2017b) the georeferenced seeding depth variation, resulted from the original (undamped) seeding assembly, was compared to the ground truth depth measured from seedlings as this is a common seeding depth measurement (Burge et al., 2011). This comparison showed a negligible difference between the mean values, standard deviations and 95<sup>th</sup> percentiles for the two methodologies.

**Table 4.3.** Comparison of statistics between the damped seeding depth variation at 0.5 A (S4) with its replicate (S9) and all the undamped seeding depth variations. In all cases the target seeding depth was 40 mm.

Type	Damped (0.5 A) (mm)		Undamped (mm)					
	S4	S9 (S4 rep)	S1	S2	S3	S4	S5	S6
Sections	S4	S9 (S4 rep)	S1	S2	S3	S4	S5	S6
Mean value	39.8	40.1	44.5	44.0	43.4	44.2	45.2	44.9
St. deviation	5.8	5.7	5.6	4.8	9.4	9.7	13.6	8.9
95th percentile	49.2	47.8	53.5	50.1	58	63.2	68.1	61.2
Min	24.7	28.2	21	21.6	23.6	27.1	14.8	26.5
Max	52.0	52.1	54.8	54.9	61.2	65.3	71.1	64.6

The boxplots for the damped seeding depth variation in S4 with its replicate and the undamped seeding depth variations in all sections are presented in Fig. 4.9. Based on the 25<sup>th</sup> percentile with values 35.6, 37.7, 37.0, 40.2 mm and the 75<sup>th</sup> percentiles with values 50.4, 51.6, 53.2, 49.7 mm for section S3, S4, S5 and S6, respectively, the original seeding assembly resulted in significantly higher variation in the seeding depth than the assembly with the MR damper. The variations of the seeding depth in sections S1 and S2 were similar to that of the damped one at 0.5 A. However, the median values of all datasets (44.8, 44.3, 43.6, 41.3, 45.8 and 45.4 mm for sections S1-S6, respectively) for the undamped seed depth variations were higher than the median value (39.5 mm) of the damped seeding depth in S4.

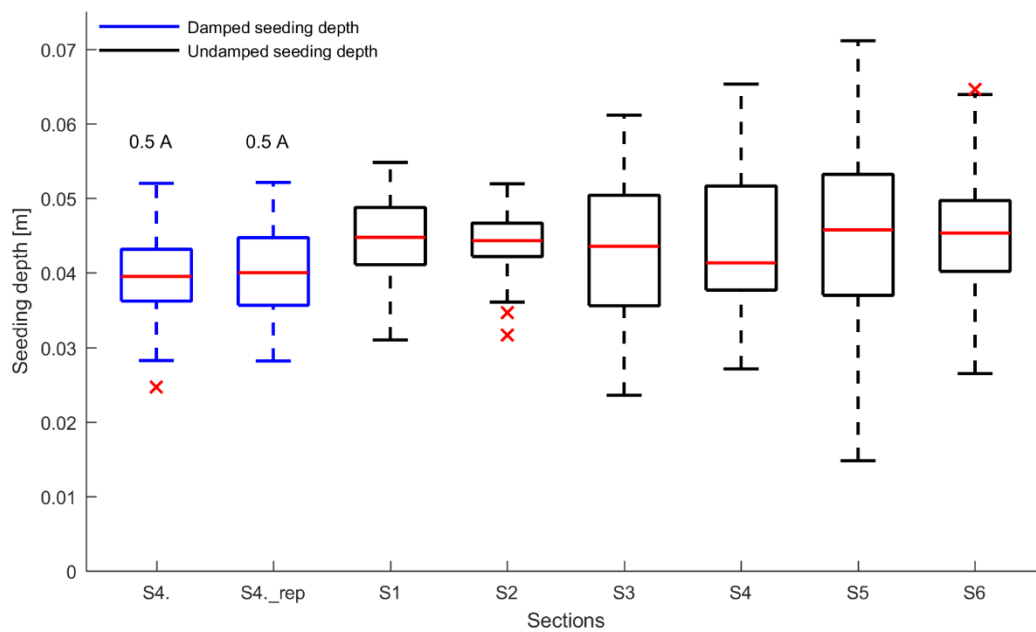


Figure 4.9. Boxplots of the damped seeding depths in S4 (0.5 A) and all undamped seeding depths with the operation speed of  $10 \text{ km h}^{-1}$ .

#### 4.4.3 Assessment of improvements in dynamics

The vertical and impact forces of the seeding assembly with the MR damper were compared to those of the undamped seeding assembly using the Eqs. (4.7) and (4.8). Since the seeding assembly with the MR damper at 0.5 A outperformed those of any other currents applied on the coil and the original seeding assembly, the assessment of the dynamics, in terms of the reduction in the amplitude of the both damped and undamped vertical and impact forces were carried out for the section S4 (0.5 A). Both damped and undamped vertical and impact forces were extracted from the measured strain data, and can be seen in Fig. 4.10a and b, respectively. The MSD between the damped and undamped vertical forces was equal to 5.62 N, while the MDP indicated 21.34% of reduction in the amplitude of the vertical forces. These figures were more significant with the values of 6.84 N and 67.69% for the impact forces. In addition, the amplitude reduction of the impact forces were compared to that of simulation results obtained in previous work by Sharipov et al. (2017a). The comparison confirmed the validity of the simulation results with a difference of 3.16 N and 11% between the MSD and MDP values, respectively.



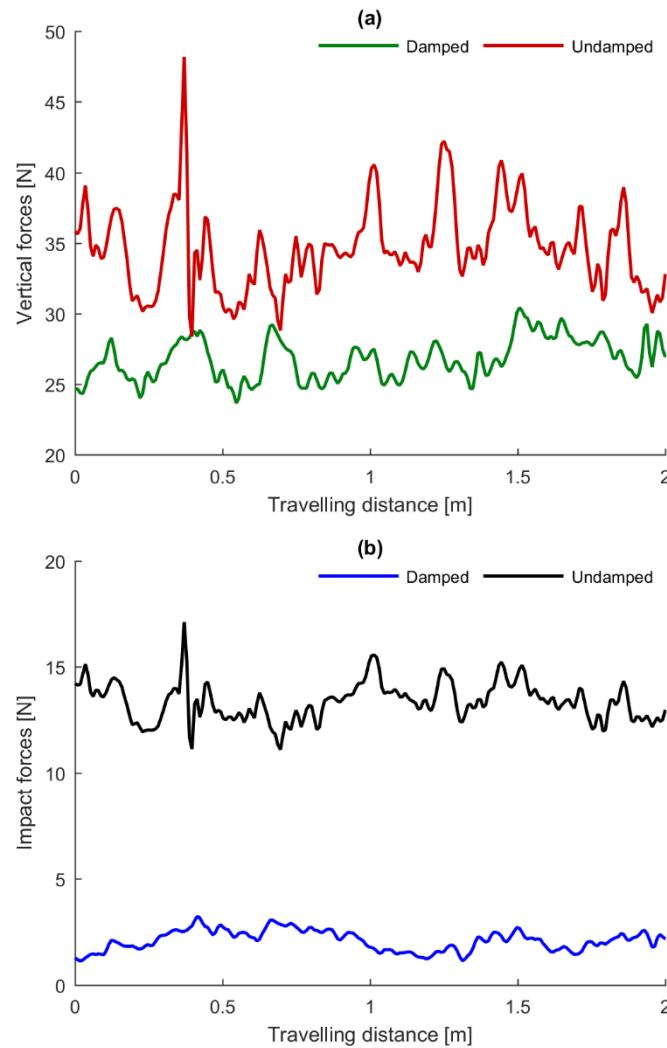


Figure 4.10. (a) vertical and (b) impact forces of both seeding assemblies from the performance with the operation speed of  $10 \text{ km h}^{-1}$ .

Beside the analysis of the dynamic performance of the assemblies in the time domain, a qualitative analysis for both damped and undamped forces in the frequency domain was carried out to detect if the forces' spectral density confirmed the results of the dynamic performances of the assemblies in the time domain. The computed spectral density for both the damped and undamped vertical and impact forces are presented in Fig. 4.11 a and b, respectively. It can be observed that the spectral density magnitude of the damped vertical forces was lower than the magnitude of the undamped forces. This figure for the damped and undamped impact forces was followed by the same pattern, but with a more significant decrease in the magnitude of the spectral density. Taking into account the results for both time and frequency domain, the MR damper implemented assembly could be more effective in optimizing the dynamics of the seeder, in terms of the vertical and impact forces

that are responsible for the seeding depth variation, for better seed placement than the original undamped seeding assembly.

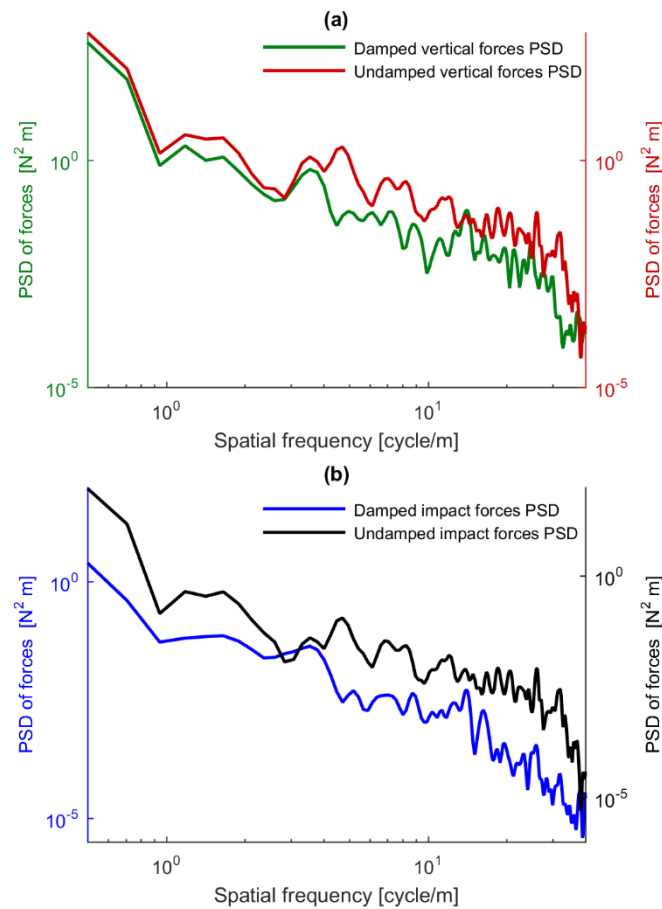


Figure 4.11. PSDs of the (a) vertical and the (b) impact forces for both the damped (with 0.5 A for the MR dumper) and undamped seeding assemblies.

#### 4.4.4 Estimation of seeding depth variations

All above-given analyses showed that the damped seeding depth at 0.5 A was more precise, in terms of seeding depth, compared to the undamped seeding depth. Therefore, a normalized error in the variation of the damped seeding depth in S4 (0.5 A) and the undamped seeding depth in the same section compared to the target seeding depth (40 mm) together with the probability distribution function was assessed, as illustrated in Fig. 4.12a and b. The histograms for the variation in the error of the damped and undamped seeding depth were best fitted by the exponential distribution with mean parameter equal to 4.4 and 8.12, respectively. It can be noticed that the 95<sup>th</sup> percentile of the damped seeding depth was lower than 11.9 mm. This figure for the undamped seeding depth was equal to 21.3 mm.

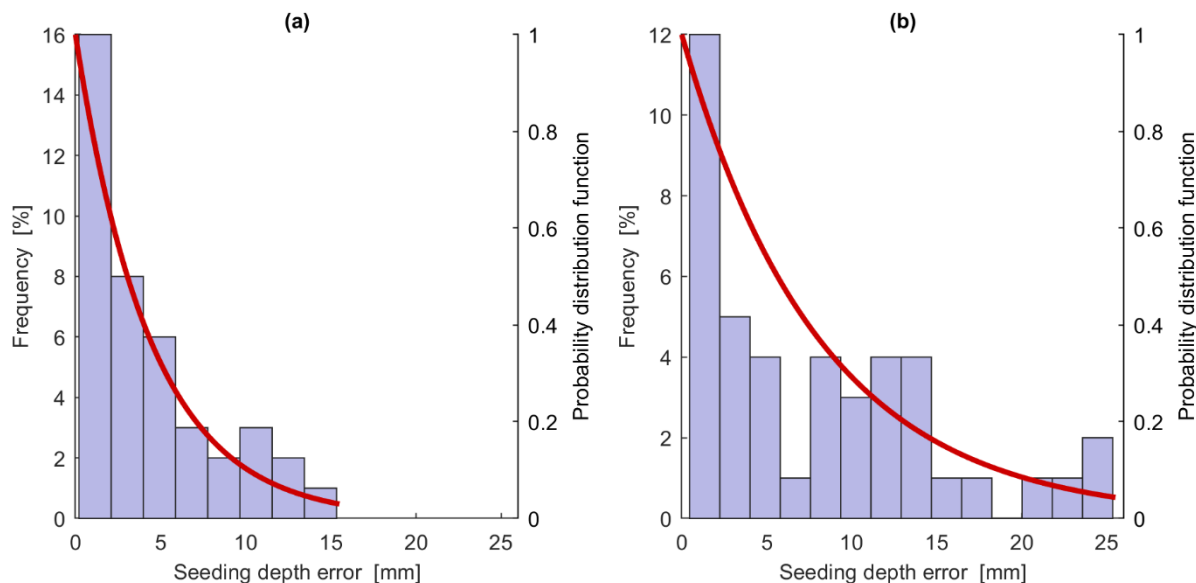


Figure 4.12. Histogram (blue bars) and cumulative distribution function (red line) of the errors in the (a) damped and (b) undamped seeding depth variation in section S4 compared to the target depth of 40 mm.

#### 4.5 Conclusions

A no-till seeder was constructed consisting of an automatic seed dose mechanism and two seeding assemblies with and without semi-active MR damper. The developed profile sensing system indicated sufficient accuracy for obtaining the field surface profiles during seeding operation in absolute georeferenced coordinates. The performances as seeding depth variation and the dynamics of both seeding assemblies were evaluated. Compared to the dynamics of the original seeding assembly, the seeding assembly dynamics with the MR damper supplied with 0.5 A were improved with a reduction of 21.34% and 67.69% in the amplitude of the vertical and impact forces, respectively. The seeding assembly with the MR damper excited at 0.5 A resulted in a lower variation in seeding depth than that of the other values of current applied on the coil of the MR damper. Furthermore, the variation of the damped seeding depth compared to the target seeding depth had an absolute error of 11.9 mm for 95% of its samples. This error with a value of 21.3 mm was considerably higher for the undamped seeding depth variation. In comparison with the original seeding assembly, the MR implemented seeding assembly has manifested the following advantages:

- The damped seeding depth variation assessed with the standard deviation, 25<sup>th</sup>, 75<sup>th</sup>, 95<sup>th</sup> percentiles and min/max values was significantly lower than the undamped seeding depth variation.

- The closeness of the mean seeding depth to the target depth, means that the variation of the damped seeding depth occurred close to the value of the target seeding.
- The seeding assembly with the MR damper was more powerful in optimizing the dynamics of the seeder, in terms of reducing the amplitude of the vertical and impact forces that are responsible for the seeding depth variation.

Using the defined semi-active MR damper, the vertical motion dynamics of the seeding assembly, in terms of the affecting forces can be significantly optimized for better seeding depth. Future studies should be focused on developing different control techniques, such as real time adaptive PID and fuzzy hybrid controller in association with the MR damper models, to improve its dynamic performance for different soil conditions.

### Acknowledgements

The financial support of GA nr 213-2723/001–001–EM Action2 TIMUR (Training of Individuals through Mobility to EU from the Uzbek Republic) project is gratefully acknowledged. The authors are very thankful to Dr. R. Resch and Ch. Gall from AMAZONEN-WERKE H. Dreyer GmbH & Co.KG (Osnabrück, Germany) for providing the seed dose mechanism and the seeding assemblies and to Ch. Schwarze for the assistance building the seeder main frame and performing the field experiments. The authors are also grateful to Dr. Horst Schrogl from Hottinger-Baldwin Messtechnik GmbH (Darmstadt, Germany) for providing the data acquisition system. The project is conducted at the Max-Eyth Endowed Chair (Technology in Crop Production) at Hohenheim University (Stuttgart, Germany), which is partly grant funded by the Deutsche Landwirtschafts-Gesellschaft (DLG) e.V.

### References

- Ahamed, R., Ferdous, M.M., Li, Y., 2016. Advancement in energy harvesting magneto-rheological fluid damper: A review. *Korea Aust. Rheol. J.* 28, 355–379. doi:10.1007/s13367-016-0035-2
- Burce, M.E., Kataoka, T., Okamoto, H., Shibata, Y., 2011. Precise Seed Placement Control System for Various Terrain Surfaces. *ASABE 7004*.
- Burce, M.E.C., Kataoka, T., Okamoto, H., 2013. Seeding Depth Regulation Controlled by Independent Furrow Openers for Zero Tillage Systems - Part 1: Appropriate Furrow Opener. *Eng. Agric. Environ. Food* 6, 1–6. doi:http://dx.doi.org/10.1016/S1881-8366(13)80012-2
- Derpsch, R., Franzluebbbers, A.J., Duiker, S.W., Reicosky, D.C., Koeller, K., Friedrich, T., Sturny,

- W.G., S??, J.C.M., Weiss, K., 2014. Why do we need to standardize no-tillage research? *Soil Tillage Res.* 137, 16–22. doi:10.1016/j.still.2013.10.002
- Eshkabilov, S.L., 2016. Modeling and Simulation of Non-Linear and Hysteresis Behavior of Magneto-Rheological Dampers in the Example of Quarter-Car Model. *Eng. Math.* 1, 19–38. doi:10.11648/j.engmath.20160101.12
- Fountas, S., Paraforos, D., Cavalaris, C., Karamoutis, C., Gemtos, T.A., Abu-Khalaf, N., Tagarakis, A., 2013. A five-point penetrometer with GPS for measuring soil compaction variability. *Comput. Electron. Agric.* 96, 109–116. doi:10.1016/j.compag.2013.04.018
- Hasimu, A., Chen, Y., 2014. Soil disturbance and draft force of selected seed openers. *Soil Tillage Res.* 140, 48–54. doi:10.1016/j.still.2014.02.011
- Koller, K., 2003. Techniques of soil tillage, in: *Soil Tillage in Agroecosystems*. CRC Press, Boca Raton, FL, pp. 1–25.
- Lawrance, N.S., 1969. A method of Analyzing Dynamic Responses of A Semi-mounted Farm Implement. *The Ohio State University*.
- Loghin, F., Ene, T.A., Mocanu, V., Căpătină, I., 2012. Dynamic Modeling of Technical System Tractor - Seed Drill. *Agric. Food Eng.* 5 (54), 155–160.
- Morrison, J.E., 1988. Hydraulic Downpressure System Performance for Conservation Planting Machines 31, 19–23.
- Morrison, J.E., 1978. No-Tillage Experimental Planter Performance and Depth Regulation Evaluation 3–6.
- Morrison, J.E., Gerik, T.J., 1985. Planter Depth Control : II . Empirical Testing and Plant Responses. *Trans. ASAE* 28 (6), 1744–1748.
- Paraforos, D.S., Griepentrog, H.W., Vougioukas, S.G., 2016. Country road and field surface profiles acquisition, modelling and synthetic realisation for evaluating fatigue life of agricultural machinery. *J. Terramechanics* 63, 1–12. doi:10.1016/j.jterra.2015.10.001
- Paraforos, D.S., Reutemann, M., Sharipov, G., Werner, R., Griepentrog, H.W., 2017. Total station data assessment using an industrial robotic arm for dynamic 3D in-field positioning with sub-centimetre accuracy. *Comput. Electron. Agric.* doi:10.1016/j.compag.2017.03.009
- Poll, C., Marhan, S., Back, F., Niklaus, P.A., Kandeler, E., 2013. Field-scale manipulation of soil temperature and precipitation change soil CO<sub>2</sub> flux in a temperate agricultural ecosystem. *Agric. Ecosyst. Environ.* 165, 88–97. doi:10.1016/j.agee.2012.12.012
- Sharipov, G.M., Paraforos, D.S., Griepentrog, H.W., 2017a. Modelling and simulation of the dynamic performance of a no-till seeding assembly with a semi-active damper. *Comput. Electron. Agric.* 139, 187–197. doi:10.1016/j.compag.2017.05.010

- Sharipov, G.M., Paraforos, D.S., Pulatov, A., Griepentrog, H.W., 2017b. Dynamic performance of a no-till seeding assembly. *Biosyst. Eng.* 158, 64–75. doi:10.1016/j.biosystemseng.2017.03.016
- Suomi, P., Oksanen, T., 2015. Automatic working depth control for seed drill using ISO 11783 remote control messages. *Comput. Electron. Agric.* 116, 30–35. doi:10.1016/j.compag.2015.05.016
- Weatherly, E.T., Bowers, C.G., 1997. Automatic depth control of a seed planter based on soil drying front sensing. *Power Mach. Div. ASAE* 40, 295–305.
- Zhu, X., Jing, X., Cheng, L., 2012. Magnetorheological fluid dampers: A review on structure design and analysis. *J. Intell. Mater. Syst. Struct.* 23, 839–873. doi:10.1177/1045389X12436735

# CHAPTER 5

## General discussion

### 5.1 Working quality of a no-till seeder

Studying working quality, in terms of variations in seeding depth, related to dynamics of no-till seeder showed that the performance of no-till seeders highly depends on its dynamic behaviour during soil-engaging process as well as the type of furrow opening component (hoe, disc, tine, etc.) of the single seeding assembly. In latest no-till seeding machines, hoe (tine) type furrow opening components have become very common to assemble due to its advantages like well-guided depth, no hair pinning effect of residues, reasonable penetration forces, less disturbance of soil, etc. Therefore, in the present work, the AMAZONEN no-till direct seeder containing 12-tine type seeding assembly was chosen to evaluate its working quality under realistic high-capacity performance. Under working conditions, the maximum width is 3 m resulted from the inter-row distance of 0.25 m between the assemblies. The seeding assemblies are attached to a rigid mainframe, which is supported by two big side-wheels and a downforce is applied to them by a hydraulic cylinder. Rubber rollers in-between the mainframe and the assemblies are used in order to keep the packer wheels of the assemblies on the ground with the aim to maintain a consistent seeding depth during seeding operation. A new methodology was proposed for assessing the dynamic performances of the no-till seeder, in terms of seeder dynamics together with the corresponding geo-referenced seed positions.

The seeder dynamics with the corresponding field surface profile were captured using up-to-date sensor technology. A sensor-frame that carried all the necessary sensors was developed and mounted on the main frame of the seeder. A combination of strains, recorded at the three corresponding points of the seeding assembly using linear strain gauges, was employed to calculate the vertical forces, draught forces and the profile impact forces. A Laser pointer and two IMUs recorded the dynamics parameters, i.e. accelerations, displacements, and tilting information. In particular, data from a

Trimble Total Station, IMUs and laser pointer were engaged to extract the field surface profile in absolute geo-referenced coordinates. All sensor data were stored with a computer clock timestamp, for synchronisation purposes during post-processing.

Measuring profiles on agricultural terrains is challenging because in most occasions the actual soil surface is covered by the crop residue, which is usually left after harvesting. Thus, direct optical methods that are commonly used for profiling (Sayers and Karamihas, 1998) cannot be used for measuring the real soil surface profile. This is why the developed sensor-frame with the packer wheel of the seeding assembly, which rolled on the soil surface, were employed. The size of the packer wheels was adequate to detect the wavelengths of higher spatial frequency that would influence the seeding assembly motion.

The accuracy of the developed sensor frame with a root mean squared (RMS) error of 7.3 mm and 8.7 mm for travelling speed of 2 km h<sup>-1</sup> and 10 km h<sup>-1</sup>, respectively indicated acceptable sufficiency for acquiring the field surface profiles during seeding operation in absolute geo-referenced coordinates. The methodology for measuring the geo-referenced position of each single seed and its combination with the extracted surface profile resulted in determining the absolute seeding depth. The geo-referenced coordinates of seeds position in combination with the geo-referenced surface profile and machine dynamics parameters, offered the possibility to define the reason of seeding depth variation. Other researchers (Choudhary et al., 1985; Tessier et al., 1991; Altikat et al., 2013) evaluated the variations in seeding depth for different no-till seeders on various soil conditions. However, there has been no research on defining the concrete relation, in terms of correlation, between the seeder dynamics and seeding depth variations. The relation between the forces and the variation of seeding depth was introduced by correlating spatial frequency contents of each dataset. The critical frequency ranges, where extreme seeding depth variations occurred, were defined based on coherence values that are above 0.6 of threshold for correlation. Consequently, it was decided to investigate the seeder dynamics by modelling and simulating its performance based on the measured data in order to be able to define a system or mechanism that can reduce the effect of those forces in the defined frequency ranges for better seed placement in no-till seeding.

## **5.2 Simulating the dynamic response of a no-till seeder**

With the aim to assess and optimise the dynamic response of a no-till seeder, a mathematical model was developed to simulate the vertical motion of the seeding assembly. The modelling and simulation of the vertical motion behaviour of the seeding assembly were carried out in two phases. In the first phase, the seeding assembly together with the packer wheel, which was considered as a damped



oscillating mechanism (Inman, 2014), was introduced as a passively controlled system due to spring and damping characteristics of the packer wheel tire. The introduced model used as input the field surface profile and vertical forces on the coulter tine, determined from the measured data to simulate the profile impact forces and vertical movements, in terms of pitch angles of the seeding assembly. The correctness of the model was verified based on the correlation between the simulated and the measured impact forces and pitch angles. The second phase included a semi-active MR (magnetorheological) damper system that was considered to be located in-between the coulter and the packer wheel. This device is mostly applied in the domain of vehicle and civil engineering and provides appealing dynamic features such as fast response, low and high force capacity, low power consumption, and a simple interface between the electronic input and the mechanical output (Balamurugan et al., 2014). It was also proven that the best performance of the MR damper highly depends on selecting an appropriate hysteric control model and damping ratio (Savaresi et al., 2010).

Three hysteresis models, i.e. Bingham, Dahl and Bounc-Wen model, were applied for the semi-active MR damper system behaviour to find out the best performance of the MR damper system, and also if it outperforms the passive system model. The performance criteria evaluation of the hysteresis models for the semi-active MR damper against the passive system model indicated that the Bouc-Wen model gave the best results. It was proved that this model should be used for designing the semi-active suspension system for the coulter assembly as it gave the highest reduction in the amplitude, of both the forces (54.1%) and the pitch angles (52.3%). Using the defined model and control strategy while performing seeding operation with the semi-active MR damper implemented seeding assembly, its vertical motion dynamics, in terms of vertical displacements and its affecting forces, can be significantly optimised for better seed placement.

### **5.3 The effect of the optimised seeder dynamics on seeding depth**

Simulation of the dynamics of the seeding assembly with the semi-active MR damper system proved the impact forces acting on the packer wheel and resulting vertical movements of the seeding assembly to be significantly improved, in terms of reduction in the amplitude values. One of the imperative contributions that the coulter makes to regulating seeding depth is the presence of the packer wheel since it is the only component of the coulter assembly, which is tracking the soil surface undulations. In addition, the packer wheel is responsible to dampen the excessive variation in the forces resulted from the response of the packer wheel to the inherent soil surface undulations (Baker et al., 2006). However, there are often limitations to where the packer wheel can be assembled on the

coulter in relation to where the seeds are eventually placed into the soil. The depth-control capacity of the seeding assembly strongly relies on the behaviour of the packer wheel (Karayel, 2009). Therefore, stability in the vertical motion of the packer wheel that maintains a consistency in seeding depth can be achieved by absorbing the profile impact forces and regulating the vertical movements of the packer wheel in relation to the coulter vertical forces.

With the aim to optimise the performance of the seeding assembly, in terms of better seed placement, a no-till seeding machine prototype was constructed consisting of an automatic seed dose mechanism and two seeding assemblies; one with and one without a semi-active MR damper. A sensor-frame that carried all the necessary sensors to capture the seeding assembly dynamics with the corresponding surface profile was developed. Performing the same procedure for verifying the correctness of the developed sensor system indicated sufficient accuracy in obtaining the field surface profiles during seeding operation in absolute geo-referenced coordinates.

Comparative analysis of the performances of the seeding assembly with the MR damper excited with six different current levels indicated that the seeding assembly achieves its best performance, in terms of significantly less variation in seed depth, when the coil of the MR damper is supplied with 0.5 A. The investigation of the seeding assembly dynamics with and without the MR damper in both time and frequency domain proved the MR damper implemented seeding assembly with the supplied current of 0.5 A to be more effective in optimising the dynamics of the seeder. Furthermore, the variation of the damped seeding depth compared to the target seeding depth resulted in an absolute error of 11.9 mm for 95% of its samples, which is considerably less than the error with a value of 21.3 mm for the undamped seeding depth variation. By designing the seeding assembly with the system that can dampen the effect of the vertical and impact forces, the dynamics of the seeding machine can be significantly optimised for better seeding depth.

## 5.4 Outlook

Analysis of no-till seeder dynamic performance under realistic non-tilled soil conditions demonstrated that the vertical motion stability of the seeder is highly effected by the soil conditions. The instability of the seeding assembly dynamic motion resulted from the response of the seeder to the soil condition causes a high variation in seeding depth (Nielsen et al., 2016). By addressing to frequency content of both the resulted seeding depth variations and the dynamics, as all vertical forces that are responsible for the vertical motion of the seeding assembly, specific frequency ranges of those forces were defined as a major factor of the high seeding depth variation. As a part of future work, by employing the same methodology for acquiring the seeder dynamic response to the soil

condition together with the corresponding soil surface profile, the defined factor could be investigated by testing the seeding assembly with different types of furrow openers. Furthermore, the variation in seeding depth and the wavelength of the seeding assembly vertical movement suffer from the location packer wheels (Baker et al., 2006). Therefore, the effect of the packer wheel position relative to the coulter (furrow opener) on the seeding depth variation could be optimised.

When dealing with the optimisation of the seeder dynamics for better performance, the defined relationship, in terms of the afore-described frequency ranges could be a salient point to put a focus on. Considering those specific frequency ranges, the dynamic performance of the seeder could be simulated by developing different damping systems (passive or active) with many potential design configuration to investigate the improvements in the dynamics of the seeder for better performance. This was proved when the simulation of the motion dynamics of the seeding assembly with MR damper system, based on the real-measured data (i.e. field surface profile and forces), was modelled. Furthermore, the presented methodology for optimising the seeding assembly dynamics, in terms of both the simulation and implementation could be advanced by improving control techniques using real time adaptive PID and fuzzy hybrid controller in association with the MR damper models, to improve its dynamic performance.

## References

- Altikat, S., Celik, A., Gozubuyuk, Z., 2013. Effects of various no-till seeders and stubble conditions on sowing performance and seed emergence of common vetch. *Soil Tillage Res.* 126, 72–77. doi:10.1016/j.still.2012.07.013
- Baker, C.J., Saxton, K.E., Ritchie, W.R., Chamen, W.C.T., Reicosky, D.C., Ribeiro, F., Justice, S.E., Hobbs, P.R., Justice, F.R.S.E., 2006. No-tillage seeding in conservation agriculture, No-Tillage Seeding: *Science and Practice*. doi:10.1079/9781845931162.0000
- Balamurugan, L., Jancirani, J., Eltantawie, M.A., 2014. Generalized magnetorheological (MR) damper model and its application in semi-active control of vehicle suspension system. *Int. J. Automot. Technol.* 15, 419–427. doi:10.1007/s12239-014-0044-4
- Choudhary, M.A., Guo Pei Yu, Baker, C.J., 1985. Seed placement effects on seedling establishment in direct-drilled fields. *Soil Tillage Res.* 6, 79–93. doi:10.1016/0167-1987(85)90008-X
- Inman, D.J., 2014. Engineering Vibration, 4th ed, *Upper Saddle River*. doi:10.2307/23499350
- Karayel, D., 2009. Performance of a modified precision vacuum seeder for no-till sowing of maize and soybean. *Soil Tillage Res.* 104, 121–125. doi:10.1016/j.still.2009.02.001
- Nielsen, S.K., Norremark, M., Green, O., 2016. Sensor and control for consistent seed drill coulter

depth. *Comput. Electron. Agric.* 127, 690–698. doi:10.1016/j.compag.2016.07.029

Savaresi, S.M., Poussot-Vassal, C., Spelta, C., Sename, O., Dugard, L., 2010. Semi-Active Suspension Control Design for Vehicles. *Elsevier Ltd.*

Sayers, M.W., Karamihas, S.M., 1998. The Little Book of. *University of Michigan.*

Tessier, S., Saxton, K.E., Papendick, R.I., Hyde, G.M., 1991. Zero-tillage furrow opener effects on seed environment and wheat emergence. *Soil Tillage Res.* 21, 347–360.

## Summary

Achieving better seeding depth consistency in no-till seeding is a critical performance metric of the seeding machine and is of great importance due to its profound effect on reliable seed germination and seedling emergence resulting in a yield increase. Growing implementation of no-tillage in big size farms requires high-capacity seeding machines with increased operation speed and working width. Thus, the increased capacity of the seeding machine as well as harsh soil conditions like the surface undulations and the presence of previous crop residues make the desired working quality of no-till seeders challenging for both designers and manufacturers.

The aim of this cumulative dissertation was to optimise a no-till seeder dynamics in terms of vertical motion stability for better seed placement under realistic high-capacity performance. To fulfil this aim, an approach to achieve the desired dynamic behaviour of the seeder was carried out based on three phases: (1) evaluation of the seeder dynamic performance by defining the relationship between the seeder dynamics and the corresponding seeding depth variation, (2) modelling and simulation of the seeding assembly motion dynamics to specify a control system (e.g. MR damper system) for dynamics improvement, (3) implementation of the defined system into the seeding assembly and testing of the new seeding assembly prototype.

The present work was the first approach to optimise the dynamic motion behaviour of a no-till seeder by implementing an MR damper system into its seeding assembly for better seed placement under realistic high-capacity working conditions. The AMAZONEN no-till direct seeder was an ideal candidate for this investigation as it contains 12 identical tine type seeding assemblies where the operating depth is defined by the position of the packer wheel. Under working conditions, the maximum width is 3 m resulted from the inter-row distance of 0.25 m between the seeding assemblies. The seeding assemblies are provided with downforces using a hydraulic cylinder in order to keep the packer wheel of the assemblies on the ground and to maintain a consistent seeding depth during seeding operation. Concurrent and geo-referenced sensor data made it possible to acquire the dynamics parameters of the seeder and the corresponding soil surface profiles (the point where the packer wheel touches the ground). This together with the measured 3D geo-referenced position of the seeds gave the opportunity to define the reason of high variations in seeding depth.

A sensor-frame was developed, utilising up-to-date sensor technology, to capture the seeder dynamics and to determine the corresponding soil surface profile. A combination of strains recorded at the three corresponding points of the seeding assembly using linear strain gauges was employed to calculate the vertical forces, draught forces and the profile impact forces. A new methodology was introduced to extract the absolute seeding depth from the combination of the determined surface profile and the measured 3D position of the seeds in absolute coordinates. Geo-referenced coordinates

of seed positions in combination with geo-referenced surface profile and machine dynamics parameters, offered the possibility to define the reason of seeding depth variation. To do that, the relation between the forces (i.e. vertical and profile impact forces) and the variation of seeding depth was defined by correlating the spatial frequency contents of each dataset.

An investigation of the seeder dynamics was carried out by modelling and simulating its performance based on measured data (e.g. determined surface profile and vertical forces) to define a system that can reduce the effect of the forces for better seed placement in no-till seeding. The seeding assembly together with and without a MR (magnetorheological) damper system, which was considered to be located in-between the coulter and the packer wheel, was introduced as a semi-active and passive system. Furthermore, three hysteresis models, such as Bingham, Dahl and Bouc-Wen model, were applied for the semi-active MR damper system behaviour. Among the models, the Bouc-Wen model demonstrated more significant improvements over the passive system model. Analysis of the performance of the semi-active MR damper implemented seeding assembly against the passive system proved the vertical motion dynamics of the assembly, in terms of vertical displacements (52.3%) and its affecting forces (54.1%) to be optimised for better seed placement. Testing the performance of the MR damper implemented seeding assembly compared with that of the original seeding assembly confirmed the potential of the MR damper implemented seeding assembly. The dynamics of the seeding assembly with the MR damper depicted a reduction of 67.69% in the amplitude of the impact forces compared to the original seeding assembly. Consequently, the improvement in the dynamics resulted in better seed placement. The variation of the damped seeding depth, as it was the performance of the seeding assembly with the MR damper, compared to the target seeding depth resulted in an absolute error of 11.9 mm for 95% of its samples, which is considerably less than the error with a value of 21.3 mm for the seeding depth variation resulted from the original seeding assembly. By designing the seeding assembly with the MR damper system, the dynamics of seeding machine can be significantly optimized for better seeding depth consistency.

## Zusammenfassung

Das Erreichen einer gleichmäßigen Saattiefe ist bei der Direktsaat eine kritische Leistungsmetrik der Sämaschine und ist von großer Bedeutung für eine zuverlässige Keimung und ein gleichmäßiges Auflaufen des Saatgutes und der daraus resultierenden Ertragssteigerung. Die wachsende Implementierung von Nicht-Bodenbearbeitung in großen Betrieben erfordert Hochleistungs-Sämaschinen mit erhöhter Arbeitsgeschwindigkeit und großer Arbeitsbreite. So sorgen die erhöhte Kapazität der Sämaschine sowie harte Bodenbedingungen wie Oberflächenunebenheiten und das Vorhandensein von Ernterückständen dafür, dass die gewünschte Arbeitsqualität der Direktsaatmaschinen sowohl für die Konstrukteure als auch für die Hersteller eine Herausforderung darstellt.

Das Ziel dieser kumulativen Dissertation war die Optimierung einer Direktsaat-Dynamik in Bezug auf die vertikale Bewegungsstabilität für eine verbesserte Saatgutplatzierung unter realistischen Bedingungen mit hoher Flächenleistung. Um dieses Ziel zu erreichen, wurde das gewünschte dynamische Verhalten der Sämaschine anhand von drei Phasen evaluiert: (1) Bewertung der dynamischen Leistung der Sämaschine durch definieren der Beziehung zwischen der Sämaschinendynamik und der entsprechenden Variation der Saattiefe, (2) Modellierung und Simulation der Bewegungsdynamik der Säaggregate zur Spezifizierung eines Steuersystems (z.B. MR-Dämpfersystem) zur Dynamikverbesserung, (3) Implementierung des definierten Systems in die Säaggregate und den Test des neuen Prototyps.

Die vorliegende Arbeit war der erste Ansatz zur Optimierung des dynamischen Bewegungsverhaltens einer Direktsaatmaschine durch die Implementierung eines MR-Dämpfungssystems in ein Säaggregat für eine bessere Saatgutablage unter realistischen Arbeitsbedingungen mit hoher Kapazität. Die Direktsaatmaschine AMAZONE war ein idealer Kandidat für diese Untersuchung, da sie 12 identische Zinkenbaugruppen enthält, bei denen die Arbeitstiefe durch die Position des Packerrades definiert wird. Unter Arbeitsbedingungen ist die maximale Breite 3 m, die sich aus dem Reihenabstand von 0,25 m zwischen den Säaggregaten ergibt. Die Säaggregate werden mit Hilfe eines Hydraulikzylinders mit Abtriebskräften versehen, um das Packerrad der Aggregate auf dem Boden zu halten und eine gleichbleibende Saattiefe während des Säbetriebs zu erhalten. Gleichzeitig erfasste und georeferenzierte Sensordaten ermöglichten die Erfassung der Dynamikparameter der Sämaschine und der entsprechenden Bodenoberflächenprofile (der Punkt, an dem das Packerrad den Boden berührt). Zusammen mit der gemessenen georeferenzierten 3D-Position der Samen ergab sich die Möglichkeit, die Ursachen für eine hohe Variation in der Saattiefe zu ermitteln.

Es wurde ein mit modernster Sensortechnologie ausgestatteter Sensorrahmen entwickelt, um die Dynamik der Sämaschine zu erfassen und das entsprechende Bodenoberflächenprofil zu bestimmen. An drei bestimmten Punkten der Säaggregate wurde unter Verwendung von linearen Dehnungsmessstreifen Dehnungen aufgezeichnet, um die vertikalen Kräfte, Zugkräfte und die Profilaufprallkräfte zu berechnen. Eine neue Methodik wurde entwickelt, um die absolute Saattiefe aus der Kombination des ermittelten Oberflächenprofils und der gemessenen 3D-Position der Samen in absoluten Koordinaten zu extrahieren. Die georeferenzierten Koordinaten der Saatgutpositionen in Kombination mit georeferenzierten Oberflächenprofil- und Maschinendynamikparametern boten die Möglichkeit, die Ursache für die Variation der Saattiefe zu bestimmen. Um dies zu tun, wurde die Beziehung zwischen den Kräften (d.h. die vertikalen und Profilaufprallkräften) und der Variation der Saattiefe durch Korrelieren der räumlichen Frequenzinhalte eines jedes Datensatzes bestimmt.

Eine Untersuchung der Sämaschinendynamik wurde durchgeführt, indem ihre Leistung basierend auf gemessenen Daten (z. B. bestimmtem Oberflächenprofil und vertikalen Kräften) modelliert und simuliert wurde, um ein System zu entwickeln, das den Einfluss der Kräfte auf die Samenplatzierung beim pfluglosen Säen verbessern kann. Das Säaggregat mit und ohne MR (magnetorheologisches) Dämpfersystem zwischen dem Sächar und dem Packerrad liegend, wurde als semiaktives und passives System eingeführt. Darüber hinaus wurden drei Hysterese-Modelle wie das Bingham-, Dahl- und Bouc-Wen-Modell für das semiaktive MR-Dämpfersystemverhalten verwendet. Unter den Modellen zeigte das Bouc-Wen-Modell signifikantere Verbesserungen gegenüber dem passiven Systemmodell. Die Analyse der Leistungen der semiaktiven MR-Dämpferimplementierten Impfanordnung gegenüber dem passiven System bewies, dass die vertikale Bewegungsdynamik in Bezug auf vertikale Fehlplatzierung des Samens (52,3%) und ihre beeinflussenden Kräfte (54,1%), um für besseres Saatgut optimiert zu werden Platzierung. Das Testen der Leistung der mit dem MR-Dämpfer implementierten Säanordnung im Vergleich zu der ursprünglichen Säanordnung bestätigte das Potenzial der MR-Dämpferimplementierten Säanordnung. Die Messung des Säaggregates mit dem MR-Dämpfer zeigte eine Reduzierung der Amplitude der Aufprallkräfte um 67,69% im Vergleich zur ursprünglichen Säeinheit. Folglich führte die Verbesserung der Dynamik zu einer besseren Saatgutplatzierung. Die Saattiefe, wie sie bei der Sämaschine mit dem MR-Dämpfer vorlag, wies im Vergleich zur Soll-Saattiefe bei 95% der Stichproben einen absoluten Fehler von 11,9 mm auf, der erheblich geringer ist als der absolute Fehler von 21,3 mm Saattiefe beim Vergleichsaggregat. Durch die Ausstattung der Sämaschine mit dem MR-Dämpfersystem kann die Ablagegenauigkeit in der Saattiefe signifikant optimiert werden.



## Curriculum Vitae

<b>Personal information</b>	
First name(s)	Galibjon
Surname	Sharipov
Address	Aixheimer Str. 20, D-70619, Stuttgart, Germany
E-mail(s)	<a href="mailto:Galibjon.Sharipov@uni-hohenheim.de">Galibjon.Sharipov@uni-hohenheim.de</a> , <a href="mailto:shgolibm@gmail.com">shgolibm@gmail.com</a>
Nationality	Uzbek
Date of birth	23 February 1986
Marital status	Married, 2 child
<b>University degrees</b>	
MSc	Transportation engineering / Tashkent Automobile and Road Construction Institute, Tashkent, Uzbekistan.
<i>10.2008 – 07.2010</i>	Thesis: Beam design and modelling for academic purposes.
BSc	Vehicle engineering / Tashkent Automobile and Road Construction Institute, Tashkent, Uzbekistan.
<i>10.2004 – 07.2008</i>	Thesis: The analysis parameters of road safety.
<b>Work experience</b>	
Research Assistant	Control and Dynamics Lab, Tashkent Automobile and Road Construction Institute, Tashkent, Uzbekistan.
<i>09.2010 – 07.2014</i>	- Dynamics and vibration analysis of vehicles
Laboratory Associate	Electrodynamics of Road Machines, Tashkent Automobile and Road Construction Institute, Tashkent, Uzbekistan.
<i>09.2010 – 07.2014</i>	Teaching courses regarding: - Control in mechatronics (Programming and MATLAB/Simulink) - Digital Control (A/D,D/A, Sensors and Actuators)
<b>Language skills</b>	
Uzbek (native), English (excellent), German (intermediate), Russian (intermediate)	
<b>Journal articles</b>	
J1. <b>Sharipov, G.M.</b> , Paraforos, D.S., Pulatov, A., Griepentrog, H.W., 2017b. Dynamic performance of a no-till seeding assembly. Biosyst. Eng. 158, 64–75. doi:10.1016/j.biosystemseng.2017.03.016	
J2. <b>Sharipov, G.M.</b> , Paraforos, D.S., Griepentrog, H.W., 2017a. Modelling and simulation of the dynamic performance of a no-till seeding assembly with a semi-active damper. Comput. Electron. Agric. 139, 187–197. doi:10.1016/j.compag.2017.05.010	

<p>J3. <b>Sharipov, G.M.</b>, Paraforos, D.S., Griepentrog, H.W., 2018. Implementation of a magnetorheological damper on a no-till seeding assembly for optimising seeding depth. <i>Comput. Electron. Agric.</i> 150, 465–475. doi:10.1016/j.compag.2018.05.024</p> <p>J4. Paraforos, D.S., Reutemann, M., <b>Sharipov, G.</b>, Werner, R., Griepentrog, H.W., 2017. Total station data assessment using an industrial robotic arm for dynamic 3D in-field positioning with sub-centimetre accuracy. <i>Comput. Electron. Agric.</i> doi:10.1016/j.compag.2017.03.009</p>	
<p><b>Conference proceedings</b></p>	
<p>C1. <b>Sharipov, G.</b>, Paraforos, D., Griepentrog, H.W., 2016. Modeling and optimization of a no-till direct seeding machine, in: <i>Lecture Notes in Informatics (LNI), Proceedings - Series of the Gesellschaft Fur Informatik (GI)</i>. Osnabrück, pp. 193–196.</p> <p>C2. <b>Sharipov, G.</b>, Paraforos, D.S., Griepentrog, H.W., 2017. Modelling and simulation of a no-till seeder vertical motion dynamics for precise seeding depth, in: <i>Advances in Animal Biosciences</i>. Cambridge University Press, pp. 455–460. doi:10.1017/S2040470017000590</p> <p>C3. <b>Sharipov, G.M.</b>, Paraforos, D.S., Griepentrog, H.W., Gall, C., 2017. Defining the dynamic performance of a no-till seeder by measuring the geo-referenced seeding depth, in: <i>75th International Conference on Agriculture Engineering: LAND. TECHNIK AgEng 2017</i>. pp. 329–335.</p> <p>C4. Reiser, D., Vázquez-Arellano, M., Izard, M.G., Paraforos, D.S., <b>Sharipov, G.</b>, Griepentrog, H.W., 2017. Clustering of Laser Scanner Perception Points of Maize Plants. <i>Adv. Anim. Biosci.</i> 8, 204–209. doi:10.1017/S204047001700111X</p>	
<p><b>Project participation</b></p>	
<p>10.2012 – 07.2014</p>	<p>TEMPUS EU project: Modernizing higher engineering education in Georgia, Ukraine and Uzbekistan to meet the technology challenge. 530244-TEMPUS-1-2012-1-SE-TEMPUS-JPCR</p>
<p><b>Scholarship Awards</b></p>	
<p>03.2010 – 06.2010</p>	<p>TEMPUS EU scholarship as an exchange student in KTH (Royal Institute of Technology, Sweden).</p>
<p>07.2014 – 07.2017</p>	<p>Erasmus Mundus scholarship: GA nr 213-2723/001–001–EM Action2 TIMUR (Training of Individuals through Mobility to EU from the Uzbek Republic) project</p>
<p><b>Scientific Recognition</b></p>	
<p><i>Reviewer</i></p>	<ul style="list-style-type: none"> <li>- Journal of Computers and Electronics in Agriculture</li> <li>- ECPA 2017 - 11<sup>th</sup> European Conference on Precision Agriculture</li> </ul>
<p><i>Conference organisation</i></p>	<ul style="list-style-type: none"> <li>- Organising Committee Field Robot Event 2016 and 2018</li> </ul>

Galibjon M. Sharipov

Stuttgart-Hohenheim, February 2019

## **Author's declaration**

I hereby declare that this doctoral dissertation is a result of my own work, and that no other than the indicated aids have been used for its completion. All sources of information I exploited have been cited appropriately.

Furthermore, I assure that the work has not been used, neither completely nor in parts, for achieving any other academic degree.

Galibjon M. Sharipov

Stuttgart-Hohenheim, February 2019